Planktondynamik im Südpolarmeer

Numerische Untersuchungen mit einer Hierarchie biologisch-physikalischer Modelle

Dissertation

zur
Erlangung des Grades eines
Doktors der Naturwissenschaften
- Dr. rer. nat. -

dem Fachbereich Biologie/Chemie der
Universität Bremen
vorgelegt von

Inga Hense

18. Dezember 2001

Alfred-Wegener-Institut für Polar- und Meeresforschung, Bremerhaven

1. Gutachter: Dr. habil. U. V. Bathmann
2. Gutachter: Prof. Dr. D. Wolf-Gladrow

Datum der Promotion: 5. Februar 2002

Danksagung

Diese Dissertation entstand am Alfred-Wegener-Institut für Polar- und Meeresforschung (AWI), Bremerhaven unter der Betreuung von Dr. habil. Ulrich Bathmann. Für seine Initiative und und die umfassende Unterstützung möchte ich mich herzlich bedanken. Prof. Dieter Wolf-Gladrow danke ich ebenso herzlich für seine Bereitschaft, die Dissertation zu begutachten und für wertvolle Hinweise gerade zu Beginn der Arbeit. Dr. habil. Aike Beckmann hat die ozeanische Komponente für das wirbelauflösende Modell des ACCs bereitgestellt und damit einen wichtigen Wendepunkt dieser Arbeit markiert. Aike war für viele Fragen zur Beschreibung der mesoskaligen Dynamik mein Ansprechpartner; seine wissenschaftliche Neugier ist ansteckend und auch wenn es häufig schwierig war, aufgeworfene Fragen zu beantworten, hat dieser Gedankenaustausch mir immer Freude bereitet. Ich möchte ihm für seine Unterstützung sehr herzlich danken.

Mein besonderer Dank gilt Dr. Ralph Timmermann, der nicht nur das gekoppelte Eis-Ozean-Modell für Untersuchungen zur Verfügung stellte, sondern mich auch bei der Entwicklung der gekoppelten Modelle und bei der Interpretation der Resultate mit Rat und Tat unterstützte. Konstruktive Kritik und sehr viele neue Ideen haben dazu geführt, daß die Modelle stetig verbessert wurden; viele kritische Fragen zur Wechselwirkung zwischen Hydrographie und Planktondynamik haben mich dazu gezwungen, einige der Hypothesen noch einmal zu überdenken.

Großer Dank gilt auch Chresten Wübber, der dafür sorgte, daß die benutzten CRAYs und das Data Storage Silo zuverlässig liefen und bei Problemen auch im Urlaub nicht davor scheute, diese zu beheben. Dank seines unermüdlichen Einsatzes für die ,,Pflege" der Großrechner konnte eine große Anzahl an Modelläufen reibungsfrei realisiert werden.

Adriene Ferreira Pereira hat mir bei vielen kleinen Dingen geholfen und mich in verschiedenster Weise unterstützt. André L. Belém bin ich dankbar für die Bereitstellung der SeaWIFS-Daten und hilfreiche Diskussionen bezüglich Primärproduktion und Verteilung von Phytoplanktonbiomasse im Südpolarmeer.

Desweiteren danke ich Corinna Dubischar, Sabine Schultes und Jörg Dutz für wertvolle Hinweise und Diskussionsbereitschaft bezüglich Fraßdruck von Mesozooplankton und Schwarmorganismen sowie der Doktoranden-Silikat-Gruppe für die Diskussionsbereitschaft rund um das Thema Silikat.

Christian Dieterich danke ich ebenfalls sehr herzlich für seine Diskussionsbereitschaft und den gegenseitigen Gedankenaustausch.

Der BRIOS-Gruppe danke ich für ihre Aufnahmebereitschaft, Rücksichtnahme, Offenheit und Diskussionsbereitschaft während dieser Zeit.

Wolfgang Cohrs danke ich für seine Hilfe rund um den Computer. René Redler hat für eine vorrübergehend genutzte ein-dimensionale Version Vertikalgeschwindigkeiten und Deckschichttiefen aus FLAME zur Verfügung gestellt. Christine

Klaas danke ich für die Bereitstellung von Fraßraten und anderer Protozooplanktondaten. Die Daten der ECMWF-Analysen/Reanalysen wurden vom DWD und DKRZ zur Verfügung gestellt.

Desweiteren danke ich sehr herzlich dem türkischen Institute for Marine Sciences and Technology, vor allem Erdem Sayin und Mustafa Ozerler sowie dem Goethe Institut Izmir, für ihre Einladung zu dem deutsch-türkischem Seminar “The role of physical, chemical and biological processes in marine ecosystems” in Izmir und überwältigende Gastfreundschaft.

Auch danke ich Melckzedeck K. W. Osore vom Kenya Marine & Fisheries Research Institute aus Mombasa, Kenia für den netten Kontakt und die Möglichkeit, einen Bericht in der ostafrikanischen UNESCO Zeitschrift WINDOWS zu veröffentlichen.

Vielen, auch namentlich nicht genannten Kollegen(innen) der Sektionen Biologische Ozeanographie und Regionale/Globale Kimadynamik danke ich sehr herzlich für ihr Entgegenkommen, hilfreiche Hinweise und angenehme Arbeitsatmosphäre.

Zusammenfassung

Ziel dieser Arbeit ist ein besseres Verständnis der biologischen Prozesse im Südpolarmeer, wobei der Schwerpunkt auf den für regionale und zwischenjährliche Variabilität wichtigen Mechanismen liegt. Zur Untersuchung der Planktondynamik im Südpolarmeer wurde ein gekoppeltes biologisch-physikalischen Modell entwickelt, das die Charakteristika des pelagischen Ökosystems dieser Region widerspiegelt. Das biologische Modell (BIMAP) enthält miteinander gekoppelte Kreisläufe von Silizium, Stickstoff und Eisen; Parametrisierungen der Flüsse zwischen den verschiedenen Kompartimenten orientieren sich eng an Feldmessungen und Laborexperimenten. Simulationen werden mit Nährstoffverteilungen aus dem WOCE-Datensatz initialisiert. Neben Studien in einer vertikal integrierten Version mit vorgegebenen Randbedingungen wird das Modell in einer idealisierten, wirbelauflösenden Konfiguration mit 6 km Auflösung betrieben, die einen Ausschnitt des Antarktischen Zirkumpolarstroms (ACC) widergibt. Das *s-Coordinate Primitive Equation Model* (SPEM) bildet in diesen Simulationen die Ozeankomponente. In einer zirkumpolaren Modellversion, die mit einer gröberen Auflösung das gesamte Südpolarmeer umfaßt, ist zusätzlich ein dynamisch-thermodynamisches Meereismodell enthalten.

Die Simulationsresultate weisen darauf hin, daß die maximale Planktonkonzentration zwar stark von der Wahl des Si:N-Aufnahmeverhältnisses und dem vorgegebenen Jahresgang der Deckschichttiefe abhängt, daß diese Parameter aber nicht genügen, um die beobachteten regionalen Unterschiede in der Planktonkonzentration im Antarktischen Zirkumpolarstrom zu erklären. Im Bereich der Antarktischen Polarfront (APF) führt barokline Instabilität zu mäandrierenden Strömungen und zur Ausbildung mesoskaliger Auf- und Abtriebsgebiete, die sich in einer vertikalen und horizontalen Umverteilung von Nährstoffen und Plankton widerspiegeln. Während niedrige Silikatkonzentrationen nördlich der APF die Bildung reicher Phytoplanktonblüten verhindern, sorgt Eisenlimitierung im südlichen ACC für die Entstehung des aus Beobachtungen bekannten HNLC-Gebietes. Im Bereich der APF dagegen wird durch mesoskalige upwelling-Gebiete und durch die mit der Querfront-Zirkulation verbundene meridionale Umwälzbewegung Eisen aus tieferen Schichten des Ozeans in die euphotische Zone transportiert. Dieses Wasser ist arm an Phytoplankton, so daß die Auftriebsregionen lokale Minima der Phytoplanktonkonzentration darstellen. Erst während sich dieses Wasser entlang der Oberfläche ausbreitet, kann Phytoplankton unter dem Einfluß der solaren Einstrahlung *so* lange wachsen, bis es in einer konvergenten Strömung wieder in lichtärmere Schichten verfrachtet wird. Die maximalen Planktonkonzentrationen findet man daher in den *downwelling*-Gebieten, deren Lage im zonalen Mittel durch die großskalige Bodentopographie bestimmt wird. Wird dagegen der Effekt der Eisenlimitierung vernachlässigt, bildet sich unter dem Einfluß der

großen Silikatkonzentrationen südlich der APF eine ausgedehnte Phytoplanktonblüte, die mit Beobachtungen nicht in Einklang steht.

Änderungen im Aufnahmeverhältnis von Si:N haben keinen Einfluß auf die Horizontalverteilung der Phytoplanktonbiomasse, sondern nur auf die maximale Phytoplanktonkonzentration. Auch der Effekt eines periodischen Auftretens von Schwarmorganismen (Krill, Salpen) konnte als Alternativhypothese für das Entstehen der beobachten Planktonverteilung im ACC verworfen werden.

Bei Untersuchungen der mit der Antarktischen Zirkumpolarwelle assoziierten zwischenjährlichen Variabilität des Ökosystems im Südpolarmeer zeigen sich große regionale Unterschiede in den grundlegenden Wechselwirkungen zwischen den physikalischen Randbedingungen und der Reaktion des Ökosystems: Im pazifischen Sektor (nördliches Amundsen-/Bellingshausenmeer) führen positive Anomalien der winterlichen Deckschichttiefe zu signifikant erhöhtem Eiseneintrag und damit zu erhöhten Phytoplanktonkonzentrationen im folgenden Sommer. Im atlantischen Sektor dagegen bilden Anomalien der Vertikalgeschwindigkeit die primäre Ursache für zwischenjährliche Variabilität des Planktonwachstums. In beiden Sektoren haben mit der Antarktischen Zirkumpolarwelle verknüpfte atmosphärische Anomalien signifikanten Einfluß auf den Aufbau einer Phytoplanktonblüte, jedoch verhindert die Verschiedenheit der hierfür relevanten Mechanismen die Ausbildung eines fortschreitenden zirkumpolaren Signals.

Weitere Gebiete mit hoher zwischenjährlicher Variabilität der sommerlichen Planktonblüte liegen in der Seasonal Ice Zone, z. B. um Maud Rise und in der Coastal and Continental Shelf Zone, wobei die Ronne-Polynya des Sommers 1997/98 als singuläres Ereignis auffällt. Die hohen Planktonkonzentrationen im Rossmeer werden auf anhaltendes *upwelling* vor allem während der Wintermonate, ein frühes Aufbrechen des Meereises in der Ross-Polynya und flache Deckschichten im Sommer zurückgeführt.

Abstract

To investigate plankton dynamics in the Southern Ocean, a coupled biological-physical model has been developed. The biological model (BIMAP) comprises two biogeochemical cycles - silicon and nitrogen - and a prognostic iron compartment to include possible effects of micronutrient limitation. Whereever possible, parameterizations of fluxes between different compartments are derived from measurements.

The model has been run in three different configurations. Sensitivity studies concerning phytoplankton growth rates, half saturation constants and different Si:N-uptake ratios were conducted with a zero-dimensional version of the model. To study the processes leading to observed phytoplankton distribution in the region of the Antarctic Polar Front, the biological model has been coupled to an eddy-resolving version of the s-Coordinate Primitive Equation Model (SPEM). To investigate regional and interannual variability of the ecosystem in the Southern Ocean, model experiments were conducted with a circumpolar version including a dynamic-thermodynamic sea ice-model.

Results from experiments neglecting possible iron limitation indicate that frontal dynamics alone cannot explain the observed enhanced concentrations of phytoplankton biomass near the APF and the minima in the northern and southern ACC. Also, the effect of swarm organisms and heavy grazing in the southern ACC was found to be insufficient to explain the observed low phytoplankton concentration in this HNLC area. Only when iron limitation is taken into account, the model simulates plankton concentrations in close agreement with observations: While in the northern ACC phytoplankton growth is limited by silicate, primary production is limited by iron limitation south of the APF. Near the APF, mesoscale iron upwelling enhances primary production, leading to increased phyto- and zooplankton biomass. The meridional structure with two plankton maxima is closely linked to the cross-front overturning circulation which in turn is caused by the large scale topography, i.e. the northern slope of the Atlantic Indian Ridge.

Investigations of interannual variability in the circumpolar model version lead to the conclusion that the ecosystem's response to anomalies associated with the Antarctic Circumpolar Wave (ACW) varies regionally. In the Pacific sector, large anomalies in winter mixed layer depth cause an increased iron supply and enhanced primary production and plankton biomass in the following summer, whereas in the Atlantic sector variability in primary production is caused mainly by fluctuations of oceanic upwelling. Thus, the ACW induces regional oscillations of phytoplankton biomass in both sectors, but not a propagating signal. Furthermore, interannual variability in plankton biomass and primary production is strong in parts of the Seasonal Ice Zone (specifically near Maud Rise) and in the CCSZ around the Antarctic continent. High productivity in the Ross Sea can be attributed to persistent oceanic upwelling mainly during the winter season, an early sea-ice breakup in the Ross-Polynya and a shallow mixed layer in summer. Fluctuations induced by the ACW strongly influence the ecosystem on a regional and local scale, but the associated variability in vertical carbon fluxes is negligible compared to the long-term carbon sequestration of the Southern Ocean.

Keine noch so verführerische Wahrscheinlichkeit schütze vor Irrtum; selbst wenn alle Teile eines Problems sich einzuordnen scheinen wie die Stücke eines Zusammenlegspieles, müßte man daran denken, daß das Wahrscheinliche nicht notwendig das Wahre sei und die Wahrheit nicht immer wahrscheinlich.

Sigmund Freud, 1939

Inhaltsverzeichnis

Teil I

Einführung

”The life of the sea as a whole is the product of very many individual factors. But these factors are not self-sufficient and independent of one another, the individual relationship does not occur without coordinated interrelationships, thus it is not a matter of the simple sum of phenomena in the sea but of a product in which each single factor influences all the others, as a function of very many factors, which are all correlated with another, and which reciprocally supplement, restrict and interlock with another like the gear-wheels of a clock.” (Schütt, 1892)

1 Lebensraum Ozean

Auch mehr als 100 Jahre, nachdem Franz Schütt zusammen mit Victor Hensen und Karl Brandt die Grundlagen der Planktonforschung gelegt hat, sind viele der biologischen Prozesse im Ozean und ihre Verknüpfungen untereinander und mit abiotischen Faktoren nicht oder nur unzureichend verstanden. Zwar lassen sich viele Parallelen zu terrestrischen Ökosystemen ziehen, in denen die Wechselwirkungen und kontrollierenden Prozesse detailliert untersucht sind, doch haben die Andersartigkeit des Lebensraumes, die Möglichkeit zur Bewegung in drei Dimensionen und die reduzierte Wirkung der Schwerkraft zur Ausbildung von charakteristischen Unterschieden geführt.

Analog zu den Landpflanzen stellen die Phytoplankter, also die mikroskopisch kleinen, einzelligen, in der Wassersäule schwebenden autotrophen Organismen, die ,,Urproduzenten” der Nahrung im Ozean dar (Stiasny, 1913). Während jedoch terrestrische Primärproduzenten einen beträchtlichen Aufwand in den Aufbau eines soliden ,,Gerüstes” stecken müssen, mit dessen Hilfe sie entgegen der Schwerkraft in die Höhe, d.h. dem Licht entgegen wachsen können, werden die marinen Phytoplankter vom Wasser in der Schwebe gehalten. Da die Photosynthese, also der Aufbau organischer Substanz, stets dem gleichen Muster folgt, sind die Faktoren, die das Wachstum kontrollieren, sehr ähnlich; die Prozesse, über die die

Wechselwirkung vermittelt wird, können aber sehr verschieden sein:

- Die Verfügbarkeit von Licht ist Voraussetzung für das Ablaufen der Photosynthese. Wie im terrestrischen Ökosystem wird das Wachstum der photosynthetisierenden Phytoplankter daher wesentlich durch die solare Einstrahlung bestimmt. Neben dem Tages- und Jahresgang der Sonne in der jeweiligen geographischen Breite und dem Einfluß des Wetters oder eventuelle Bedeckung durch Eis oder Schnee ist hier auch eventuelle (Selbst-) Beschattung durch andere Primärproduzenten zu berücksichtigen. Typisches Beispiel auf dem Land ist die Beschattung durch Bäume oder andere hochwachsende Pflanzen in einem Wald; das Analogon in der freien Wassersäule des Ozeans, dem Pelagial, stellt die Extinktion durch Schwebstoffe oder anderes Plankton dar.

  Das Leben des Phytoplanktons als frei in der Wassersäule schwebender Organismus führt aber zu einer direkten Abhängigkeit von physikalischen Bedingungen: Im Gegensatz zu Landpflanzen ist Phytoplankton nicht an einen Standpunkt gebunden, sondern wird von den Meeresströmungen bewegt. Einen wesentlichen Einfluß auf den Lebenszyklus einer Phytoplanktongemeinschaft hat daher die Tiefe der vom Wind durchmischten Schicht (Deckschicht) an der Oberfläche des Ozeans. Sind die Vermischungstiefen zu groß, verbringen die Phytoplankter einen großen Teil der Zeit in lichtärmeren Schichten und haben nur unzureichend Licht für die Photosynthese. Als Abschätzung kann die Annahme dienen, daß die Deckschicht nicht tiefer als 40 bis 80 m sein darf (Sverdrup, 1953; Sakshaug and Holm-Hansen, 1984; Smetacek und Passow, 1990), um den Aufbau einer Phytoplanktonblüte (Phytoplanktonbiomasse >1 μg Chl a/l) zu erlauben.

- Analog zur Wirkung auf terrestrische Primärproduzenten beeinflußt die Umgebungstemperatur die Wachstumsrate der Phytoplankter. Empirisch ermittelte Wachstumsraten liegen zwischen 0.85 Verdopplungen pro Tag bei 0°C und 2.2 Verdopplungen pro Tag bei etwa 15°C (Eppley, 1972). Auch bei niedriger Temperatur kann sich also ein großer Bestand von Phytoplanktonbiomasse aufbauen - die benötigte Zeitspanne ist jedoch länger. Da einige Phytoplanktonarten an extreme Temperaturbereiche adaptiert sind, können selbst im Meereis (genauer: in den das Meereis durchziehenden Solekanälen und in den mit Wasser gefüllten Hohlräumen zwischen Eisplättchen) hohe Konzentrationen dieser Arten beobachtet werden.

- Nährstoffe können das Wachstum auf dem Land wie im Ozean begrenzen. Wegen der großen Konzentrationsunterschiede unterscheidet man Makronährstoffe (Nitrat, Phosphat, Silikat), deren typische Konzentrationen im Ozean einige μmol/l betragen, und Mikronährstoffe (Eisen, Cadmium,

Mangan, Zink), deren Konzentrationen üblicherweise in nmol/l angegeben werden. Der Bedarf des Phytoplanktons an Makro- und Mikronährstoffen entspricht diesen Größenordnungen.

Die Nährstoffversorgung der ozeanischen Deckschicht kann durch Diffusion, durch *Entrainment* als Folge einer Vertiefung der Deckschicht, sowie durch *upwelling* nährstoffreichen Wassers erfolgen - auch hier prägen physikalische Bedingungen die Stoffumsätze im Ökosystem.

Aus der Kinematik enzymgesteuerter Reaktionen läßt sich ableiten, daß die Aufnahme der Nährstoffe durch eine Michaelis-Menten-Funktion (Monod, 1950) beschrieben werden kann; Beobachtungen der Nährstoffzehrung stützen diesen Ansatz. Die Aufnahme verschiedener Nährstoffe erfolgt im allgemeinen in einem festen Verhältnis. Redfield et al. (1963) ermittelten empirisch das Verhältnis der molaren Konzentrationen der Elemente C:N:Si:P als 106:16:16:1, wobei dieses *Redfield Ratio* i. a. sowohl für die im Plankton gebundene wie die im Meerwasser gelöste organische und anorganische Substanz, jedoch nicht für anorganischen Kohlenstoff gilt. Allerdings gibt es sowohl räumliche als auch zeitliche Variationen in der Elementzusammensetzung, z.B. durch erhöhten Eintrag atmosphärischen Distickstoffoxids aufgrund anthropogener Stickstoffemissionen („saurer Regen"; Fanning, 1992; Pahlow und Riebesell, 1999). Darüberhinaus sind bei einigen Phytoplanktonarten abweichende Aufnahmeverhältnisse nachgewiesen worden. So zeichnen sich z.B. einige antarktische Diatomeen durch eine besonders dicke Silikatschale aus (Quéguiner et al., 1997; Schülke, 1998); das Si:N-Aufnahmeverhältnis sowie die Si:N-Elementzusammensetzung ist bei diesen Arten nicht 1, sondern kann 3 übersteigen (Nelson und Smith, 1986; Shiomoto und Ishii, 1995; Quéguiner et al., 1997; Hense, 1997). Durch eine Verschiebung des Aufnahmeverhältnisses in Verbindung mit dem Absinken organischen Materials kommt es zu Veränderungen der Elementzusammensetzung auch im tiefen Ozean (Pahlow und Riebesell, 1999) und in marinen Sedimenten (Romero et al., 2000). Solche Prozesse sind wichtige Bestandteile der Biogeochemie des Ozeans, die die Wechselwirkungen zwischen dem biologischen, geologischen und chemischen System der Erde - die Kreisläufe von Material und der Energie dieser Systeme - beschreibt.

Im Gegensatz zu diesen "bottom up"-Faktoren, die unmittelbar die Primärproduktion, also den Aufbau organischer Substanz kontrollieren, üben die "top-down" Faktoren wie Fraßdruck, Parasiten- und Virenbefall, einen Einfluß auf den Bestand der Pflanzen- bzw. Phytoplanktonbiomasse aus.

- Analog zu den Landpflanzen ist die natürliche Mortalität des Phytoplanktons gering (Peters und Thomas, 1996); es kann aber durch Fraßdruck stark

dezimiert werden. Während Protozooplankter (z.B. Ciliaten) hauptsächlich autotrophe Protisten fressen, stellen die Mesozooplankter, zu denen vor allem Copepoden gehören, die Freßfeinde der „größeren" Phytoplankter (Diatomeen) dar[1]. Schwarmorganismen wie Krill oder Salpen können über 100% der Primärproduktion vertilgen (Dubischar und Bathmann, 1997).

- Viren und Parasiten können zu einer Dezimierung des Phytoplanktonbestandes führen. Sie sind in allen Weltmeeren verbreitet und können eine Unterdrückung des Wachstums (Onji et al., 2000) und die Auflösung von Zellen (Brussard, 1997) verursachen; doch ist ihr Einfluß im allgemeinen regional begrenzt. In der Nordsee wurde ein erhöhter Befall von Diatomeen durch parasitoide Flagellaten im Sommer und Herbst beobachtet (Drebes et al., 1996; Kühn et al., 1996). Im Südpolarmeer wurde ein erhöhter Virenbefall an Algen in der Meereiszone gefunden, während im offenen Ozean der Virenbefall eher gering ist (Marchant et al., 2000).

Obwohl die globale Biomasse der Phytoplankter deutlich kleiner ist als die der Landpflanzen, ist der Umsatz von Kohlendioxid während der Photosynthese von gleicher Größenordnung. Neben dem Absinken kalter Wassermassen in den hohen Breiten und der damit verbundenen Verfrachtung von Kohlendioxid in tiefere Schichten (physikalische CO_2-Pumpe) bildet die Aufnahme von Kohlendioxid durch Phytoplankter und die Sedimentation von Zellen (biologische CO_2-Pumpe) eine wesentliche Senke im globalen Kohlenstoffkreislauf (Volk und Hoffert, 1985). Wie lange dieser biologisch fixierte Kohlenstoff der Atmosphäre entzogen bleibt, hängt davon ab, wie groß der Anteil der sogenannten Exportproduktion ist und wieviel von dieser Biomasse letztlich im Sediment abgelagert wird. Andererseits bilden das Ausgasen von Kohlendioxid in wärmeren Ozeanregionen und die Produktion von Kohlendioxid durch Atmung der Lebewesen bzw. durch Abbau organischer Substanz Quellen von atmosphärischem CO_2. Die Rolle der biologischen Komponente in den Kohlenstofflüssen im Ozean ist/war Gegenstand der Untersuchungen, die im Rahmen der Joint Global Ocean Flux Studies (JGOFS) in verschiedenen Ozeanregionen durchgeführt werden/wurden.

[1] Beobachtungen aus verschiedenen Ozeanregionen weisen darauf hin, daß Copepoden sich schlechter reproduzieren, wenn sie Diatomeen fressen; sie bevorzugen daher andere Phytoplanktonarten (Ban et al., 1997). Dennoch sind Copepoden die unmittelbaren Freßfeinde der Diatomeen.

2 Biologische Provinzen

Wie im terrestrischen gibt es auch im marinen Lebensraum Bereiche, deren Produktivität groß ist und die als ,,reiche Ökosysteme" bezeichnet werden, und andererseits Regionen, die als Wüsten angesehen werden können. Die tropischen Regenwälder gehören zu den reichen Ökosystemen, analog dazu bilden die Küstenauftriebsgebiete die produktivsten Regionen im Ozean. An den Westküsten der Kontinente in niederen Breiten wird das Wasser des oberflächennahen Ozeans unter dem Einfluß der Passatwinde und der Coriolis-Kraft von der Küste weg gedrückt; die entstehende Divergenz wird durch einen Auftrieb von nährstoffreichem Wasser aus dem tieferen Ozean ausgeglichen. In den ausgedehnten Küstenauftriebsgebieten vor den Westküsten Afrikas und Amerikas sowie in den kleineren, durch saisonal auftretende Monsunwinde erzeugten regionalen Küstenauftriebsgebieten vor z.B. Somalia und Saudi-Arabien, führt der Auftrieb von nährstoffreichem Wasser zusammen mit den flachen Deckschichten zu hoher Primärproduktion und Phytoplanktonbiomasse und begünstigt somit nicht nur die Vermehrung der Zooplankter, sondern auch der sich vom Phytoplankton ernährenden Fische, wie z.B. Anchovies (*Engraulis ringens*). Piscivore Fische (z. B. *Tuna*) und Vögel profitieren von dem reichhaltigen Angebot und sind daher in Auftriebsgebieten zahlreich vorhanden.

Der Auftrieb nährstoffreichen Wassers unterliegt sowohl saisonaler als auch zwischenjährlicher Variabilität. Jahreszeitliche Schwankungen in Auftriebsgebieten, wie sie im Indischen Ozean aufgrund des Monsuns auftreten, sorgen für Unterschiede in der Primärproduktion und in der Zusammensetzung des Planktons (z.B. van Couwelaar, 1997; Saravanane et al., 2000).

Ähnliche Auswirkungen haben die unregelmäßig auftretenden[2] Anomalien des gekoppelten atmosphärisch-ozeanischen Systems im Rahmen der El Niño-Southern Oscillation (ENSO). Die während dieser Zeit abgeschwächten Passatwinde bewirken ein reduziertes upwelling von Nährstoffen, was zu reduzierter Primärproduktion und Planktonbiomasse und zu abnehmendem Fisch- und Vogelbestand führt. Da die Wirtschaft in dieser Region stark von Fisch und Guano abhängt, sind erhebliche sozioökonomische Probleme die Folge.

Hingegen sind weite Teile des offenen Ozeans sogenannte ,,ozeanische Wüsten". Insbesondere die Subtropenwirbel zeichnen sich durch geringe Phytoplanktonbiomasse aus. Zwar sorgen flache Deckschichten hier ganzjährig für ein gutes Lichtangebot, aber dadurch, daß sich auch im Winter die Deckschicht nicht vertieft, findet auch kein Entrainment ,,neuer" Nährstoffe statt. Daher erfolgt die Zufuhr nährstoffreichen Wassers aus den tieferen Schichten hauptsächlich durch Diffusion und eddy-pumping (Oschlies und Garçon, 1998) und somit sehr langsam. Die Nährstoffe, die durch die Remineralisierung der Bakterien wieder freige-

[2] Der mittlere Abstand zwischen zwei El Niño-Ereignissen liegt bei 7 Jahren.

setzt werden, werden von den Phytoplanktern sofort wieder aufgenommen und in Biomasse umgesetzt. Dieses als „regeneratives System" bezeichnete Ökosystem ist das ganze Jahr über nährstofflimitiert. Die jahreszeitliche und zwischenjährliche Variabilität dieses Systems ist gering (Longhurst, 1995)

Regionale „Oasen" in der „Wüste" des offenen Ozeans, bzw. Regionen erhöhter Produktion finden sich an hydrographischen Fronten (LeFèvre, 1986; Lutjeharms et al., 1986; Read et al., 2000). Dies sind Orte mit hohen Gradienten von Temperatur, Salzgehalt und Nährstoffen, die sich durch erhöhte Vermischung und zum Teil durch erhöhte Wirbelaktivität auszeichnen. Sie können regional begrenzt sein, wie z.B. die Tidenfronten, oder auch beckenweite Ausmaße annehmen, wie z.B. die Frontensysteme des Südpolarmeeres.

Die räumliche und zeitliche Variabilität in diesen Gebieten ist sehr hoch. Bedingt durch barokline Instabilitäten und Mäanderbildung entstehen mesoskalige Auf- und Abtriebsgebiete, die eine hohe Korrelation mit der Verteilung der Nährstoffe (McGillicuddy et al., 1999), des Planktons (Machu et al., 1999), der Cephalopoden (Rodhouse et al., 1996) und der Vögel (Abrams und Lutjeharms, 1986) zeigen.

Eine Besonderheit stellen diejenigen Gebiete im Ozean dar, die sich durch hohe Nährstoffkonzentrationen auszeichnen, deren Phytoplanktonbiomasse aber dennoch gering ist - die sogenannten HNLC (high nutrient-low chlorophyll)-Gebiete. Ausgedehnte HNLC-Gebiete liegen im äquatorialen Pazifik, im Nordpazifik sowie im Südpolarmeer, das Gegenstand der hier vorgestellten Untersuchungen ist. Aufgrund von Labor- und Feldexperimenten wird vermutet, daß durch Mikronährstoffe, insbesondere Eisen, das Phytoplanktonwachstum in diesen Regionen kontrolliert wird. Nach der von Martin (1990) verbreiteten Eisenhypothese haben die während des letzten glazialen Maximums (vor etwa 18 000 Jahren) freigelegten Schelfbereiche zu einem erhöhtem Staub- bzw. Eiseneintrag geführt, was die Primärproduktion und somit den Entzug von Kohlendioxid aus der Atmosphäre stimuliert habe. In einem späterem Fernsehinterview drehte Martin diese Kausalkette um: "Give me half a tanker of iron and I'll give you the next ice age". Inzwischen wurden die Methoden zur Konzentrationsbestimmung von Mikronährstoffen, insbesondere von Eisen, weiter entwickelt und in verschiedenen Ozeanregionen sowohl Labor- als auch *in situ*-Eisendüngungsexperimente durchgeführt (Coale et al., 1996; Boyd et al., 2000; Smetacek et al., 2001). Obwohl diese Experimente gezeigt haben, daß Eisenzugabe zwar das Phytoplanktonwachstum stimuliert, daß die Auswirkungen auf die Exportproduktion und auf höhere trophische Ebenen jedoch ungewiß sind, gibt es aktuelle Überlegungen, Ozeanregionen großflächig mit Eisen zu düngen, um dem Anstieg der atmosphärischen Kohlendioxidkonzentration und damit der anthropogenen Verstärkung des Treibhauseffekts entgegenzuwirken (Jones und Young, 2000; Markels und Barber, 2000; Pearce, 2000).

3 Südpolarmeer

Im Gegensatz zum Nordpolarmeer, das ringsum von Landmassen umgeben ist, sind die Grenzen des Südpolarmeeres nur durch die Hydrographie und die physikalischen Bedingungen definiert. Seine südliche Berandung bildet der Antarktische Kontinent, der im Wechsel der Jahreszeiten von einer bis zu 200 Mill. km^2 großen Meereisdecke umgeben wird. Die nördliche Grenze wird durch den Antarktischen Zirkumpolarstrom (ACC, Antarctic Circumpolar Current) gebildet, der der Westwinddrift folgt und die Weltozeane verbindet. Dieses etwa 24 000 km lange Stromsystem mit einem zirkumpolaren Transport von rund 130 Sv wird durch mehrere Fronten in hydrographische Provinzen unterteilt. Südlich der Subtropenfront (STF) und der Subantarktischen Zone (SAZ) werden die Subantarktische Front (SAF), die Polarfrontzone (PFZ), die Antarktische Polarfront (APF), die Antarktische Zone (AZ), sowie die südliche ACC-Front (SACCF) (Orsi et al., 1995) unterschieden (Abb. 1).

In den Randmeeren des Südpolarmeeres, im Weddellmeer und (zu einem kleineren Teil) im Rossmeer, in denen die Zirkulation durch große zyklonale Wirbel bestimmt wird, werden wesentliche Komponenten des Antarktischen Bodenwassers gebildet, das den Boden des Weltozeans bis etwa 40°N bedeckt (Foster und Carmack, 1976; Emery und Meincke, 1986). Einerseits leistet dieser Vorgang einen wichtigen Beitrag zum Antrieb der globalen thermohalinen Zirkulation, andererseits wird dabei CO_2 in die tieferen Ozeanschichten verfrachtet (physikalische Pumpe, s.o.) und so dem Kohlenstoff-Kreislauf über mehrere hundert Jahre entzogen.

Entlang des Antarktischen Kontinents verläuft der Antarktische Küstenstrom, der den küstennahen Winden westwärts folgt. Im Übergangsgebiet zwischen West- und Ostwinden, entlang von 63°S (vgl. Beckmann et al., 1999), ist die Antarktische Divergenz lokalisiert. Im Gegensatz zur Antarktischen Konvergenz (die später in Antarktische Polarfront umbenannt wurde; Wyrtki, 1960), wo das Wasser von der Oberfläche *absinkt* und Antarktisches Zwischenwasser (AAIW) bildet, sorgt die zyklonale Rotation des Windfeldes hier für großskaligen *Auftrieb*.

Wie im zweiten Abschnitt dieser Einführung beschrieben, ist die Region zwischen der Antarktischen Polarfront und der Linie der maximalen Meereisausdehnung, die sogenannte Permanent Open Ocean Zone (POOZ; Abb. 1), ein HNLC-Gebiet mit einer Phytoplanktonkonzentration von weniger als 1μg/l (Tréguer und Jaques, 1992). Tiefe Deckschichten durch starke Winde (Mitchell et al., 1991), Fraßdruck durch Schwarmorganismen wie Salpen (*Salpa thompsonii*) oder Krill (*Euphausia superba*) (Smetacek et al., 1990; Dubischar und Bathmann, 1997) und die Limitierung durch Mikronährstoffe wie Eisen (Martin et al., 1990) werden als mögliche Ursachen geringer Produktivität bzw. geringer Phytoplanktonbiomasse vermutet.

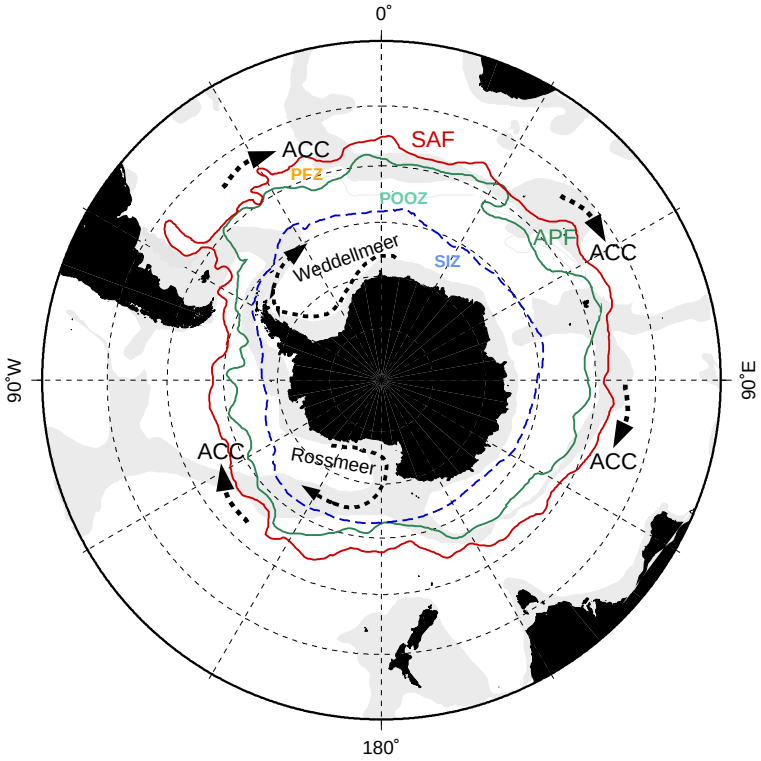

Abbildung 1: Schematische Karte des Südpolarmeeres mit der Lage der Subantarktischen Front (SAF) sowie der Antarktischen Polarfront (APF) nach Orsi et al. (1995). Gebiete mit einer Wassertiefe $<$ 3500 m sind grau schattiert. Die gestrichelte, blaue Linie deutet die winterliche Meereisausdehnung an. ACC = Antarktischer Zirkumpolarstrom; PFZ = Polarfrontzone; POOZ = Permanent Open Ocean Zone; SIZ = Seasonal Ice Zone.

Dagegen zeichnet sich die Antarktische Polarfront als ein Streifen erhöhter Phytoplanktonkonzentration (2 - 4 μg Chl a/l) ab, der sowohl in Messungen (Tréguer und Jaques, 1992; Bathmann et al., 1997) als auch auf Satellitenbildern (Stramski et al., 1999) identifiziert werden kann (Abb. 2). Hypothesen für die Ursachen dieser erhöhten Phytoplanktonbiomasse berufen sich auf besondere hydrographische Verhältnisse an der Front, insbesondere flachere Deckschichten (Strass et al., 2001) und erhöhte Vertikalgeschwindigkeiten (Naveira Garabato, 2001) und den damit verbundenen Eintrag von Makro-Nährstoffen (Lutjeharms et al., 1985), alternativ aber auch auf erhöhte Eisenkonzentrationen durch Abschmelzen von Eisbergen oder durch lokales *upwelling* (de Baar et al., 1995, Veth et al., 1997) oder das Fehlen von Schwarmorganismen (Dubischar und Bathmann, 1997). Mesoskalige Variabilität (Bildung von Mäandern und isolierten Wirbeln und die damit verbundene Vertikalbewegung) an der Front spiegelt sich in der Verteilung des

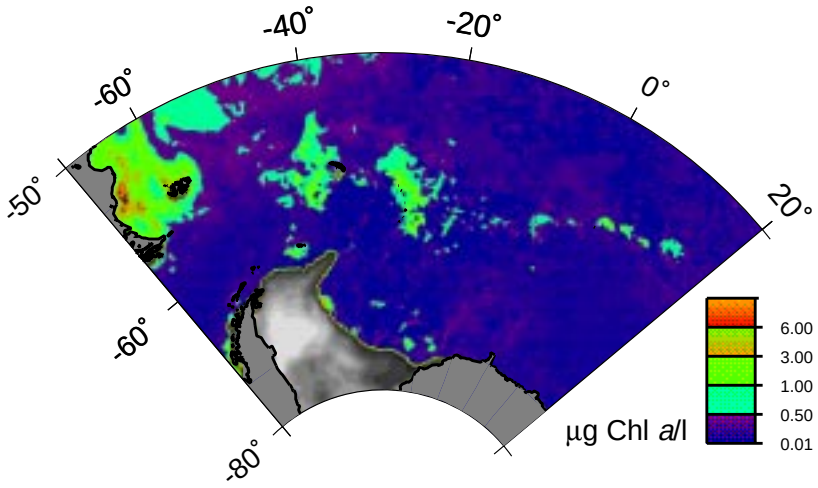

Abbildung 2: Vom *Sea-viewing Wide Field-of-view Sensor* (SeaWIFS) beobachtete Chlorophyllkonzentrationen im atlantischen Sektor des Südpolarmeeres im März 1998 (A. Belém, pers. Mitteilung).

Salzgehaltes und der Temperatur (Strass et al., 2001), sowie in der Verteilung der Nährstoffe (Hartmann et al., 1997), des Phyto- und Zooplanktons (Klaas et al., 1997; Dubischar, 2000) aber auch der Seevögel (van Franeker und van den Brink, 1997) wider. Die dominanten Phytoplanktonarten in dieser Region sind häufig stark silifizierte Diatomeen, wie *Fragilariopsis kerguelensis* und *Thalassiothrix sp.*, deren Si:N-Aufnahmeverhältnis und Si:N-Elementzusammensetzung nicht 1:1, sondern 4:1 (Quéguiner et al., 1997; Hense, 1997), teilweise 8:1 beträgt (de Baar; pers. Mitteilung). *Fragilariopsis kerguelensis* leistet den größten Teil an der Exportproduktion mit etwa 60-90% und ist daher auch in den Sedimenten die dominierende Art (Defelice und Wise, 1981; Pichon et al., 1987; Zielinski und Gersonde, 1997). Unmittelbar südlich der Antarktischen Polarfront befindet sich ein breites Band mit großen biogenen Silikatablagerungen, das als „Silikatgürtel" oder „Opalgürtel" bezeichnet wird. Offenbar spielen diese stark silifizierten Diatomeen also eine wichtige Rolle in der Biogeochemie des Südpolarmeeres.

Regionen erhöhter Phytoplanktonkonzentrationen finden sich auch an der antarktischen Halbinsel und in den eisfreien Teilen der Kontinentalschelfe in Ross- und Weddellmeer sowie in der Eisrandzone. In der kurzen eisfreien Zeit im Sommer entwickeln sich Phytoplanktonblüten mit Konzentrationen über 8 μg Chl a/l in der Coastal and Continental Shelf Zone (CCSZ) bzw. von etwa 4 μg Chl a/l in der Seasonal Ice Zone (SIZ; Tréguer und Jaques, 1992).

Eine für diese Region ungewöhnliche Phytoplanktonblüte wurde in dem auch im Sommer meist eisbedecktem Gebiet vor dem Ronne-Schelfeis im Jahre 1998

beobachtet. Starke nordwärtige Winde führten hier im Dezember 1997 / Januar 1998 zur Entstehung einer ausgedehnten Fläche offenen Wassers (Ronne-Polynya; Hunke und Ackley, 2001), in der sich eine Phytoplanktonblüte mit Konzentrationen bis zu 3 μg Chl a/l bildete (Moore und Abbott, 2000). Dieses Ereignis ist eng mit der Antarktischen Zirkumpolarwelle (ACW) korreliert, die als eine Folge von miteinander verbundenen Anomalien von Meereisausdehnung, Luftdruck, Meeresoberflächentemperatur und meridionalem Windschub entlang 56°S beschrieben wurde (White und Peterson, 1996) und wahrscheinlich durch die ENSO getriggert wird. Diese Anomalien bilden eine Welle mit der zirkumpolaren Wellenzahl 2, die in etwa 8 Jahren den Kontinent umrundet. Ergebnisse eines Kohlenstoffflußmodells (Le Quéré et al., 2000) weisen darauf hin, daß diese Welle Anomalien in der ozeanischen CO_2-Aufnahme erzeugt. Jedoch sind die biologischen Prozesse in diesem Modell stark vereinfacht parametrisiert; einen Einblick in die grundlegenden Wechselwirkungen zwischen den Komponenten kann dieses Modell nicht liefern.

Die vorliegende Arbeit entstand am Alfred-Wegener-Institut für Polar- und Meeresforschung (AWI), Bremerhaven, im Rahmen von interdisziplinären Studien, die sich mit den physikalischen und biologischen Prozessen im Südpolarmeer befassen. Ziel dieser Arbeit ist ein besseres Verständnis der biologischen und der gekoppelten physikalisch-biologischen Prozesse im Südpolarmeer, wobei der Schwerpunkt auf einer Untersuchung der für regionale und zwischenjährliche Variabilität wichtigen Mechanismen liegt. Um dies zu erreichen, wurde ein Spektrum von Modellen unterschiedlicher Komplexität entwickelt: Ein im Hinblick auf die spezielle Situation des pelagischen Ökosystems im Südpolarmeer neu entwickeltes Ökosystemmodell wurde zunächst in einer null-dimensionalen, über die Deckschicht integrierten Version betrieben. Die Forderung nach räumlich und zeitlich variablen physikalischen Randbedingungen und nach einer Berücksichtigung möglicher Effekte der horizontalen und vertikalen Advektion von Plankton und Nährstoffen mündete in die Entwicklung eines gekoppelten biologisch-physikalischen Modells, das einerseits in einer wirklichkeitsnah idealisierten, wirbelauflösenden Konfiguration, andererseits in einem zirkumpolaren Modellgebiet mit realistischem atmosphärischem Antrieb und einem interaktiven, dynamisch-thermodynamischen Meereismodell betrieben wurde.

Den Kern der Arbeit bildet die inhaltlich unveränderte Wiedergabe von drei Manuskripten, die zur Begutachtung bei internationalen Fachzeitschriften eingereicht wurden. Bereits im *Journal of Marine Systems* erschienen ist die erste Publikation, in der die Grundzüge des Biologischen Modells der Antarktischen Polarfront (BIMAP, vgl. auch Anhang A) vorgestellt und Experimente mit einem vorgegebenen Jahresgang der Deckschichttiefe präsentiert werden.[3] Die Resultate

[3] Ideen und Grundzüge der Entwicklung von BIMAP wurden auch in der UNESCO-Zeitschrift $\text{WIND}_{\text{O}}\text{W}$ (Anhang B) veröffentlicht.

geben Aufschluß über die realistische Wahl der Parameter und über die Sensitivität hinsichtlich verschiedener Si:N-Aufnahmeverhältnisse, zeigen aber auch die Grenzen solcher physikalisch stark vereinfachter Simulationen, in denen horizontale Gradienten und der Effekt der Advektion vernachlässigt werden.

Das zweite Manuskript bezieht sich auf numerische Simulationen, in denen die Wirkung mesoskaliger Variabilität an der Antarktischen Polarfront auf die Dynamik des pelagischen Ökosystems untersucht wird. Durch Hinzufügen eines prognostischen Eisen-Kompartiments wurde das Modell um die Berücksichtigung möglicher Wachstumslimitation durch Mikronährstoffe erweitert. Die Kopplung an ein drei-dimensionales, hochauflösendes Ozeanmodell auf der Basis des *s-coordinate Primitive Equation Model* (SPEM, Haidvogel et al. 1991) ermöglicht eine realitätsnahe Beschreibung des gekoppelten physikalisch-biologischen Systems im atlantischen Sektor des ACC. Das Modell wird mit Hilfe von Beobachtungen validiert und zur Untersuchung der physikalischen und biologischen Prozesse genutzt, die für die beobachtete regionale Planktonverteilung im ACC sorgen.

Im dritten Manuskript wird die mit der Antarktischen Zirkumpolarwelle (ACW) verbundene Variabilität des Ökosystems im ACC (in der POOZ) und im saisonal eisbedeckten Bereich (SIZ und CCSZ) untersucht. Hierzu wurde das biologische Modell an ein zirkumpolares Meereis-Ozean-Modell (Timmermann et al., 2001a) gekoppelt. Das voll gekoppelte Modell wird mit Daten aus der Reanalyse/Analyse des European Centre for Medium-Range Weather Forecasts (ECMWF) angetrieben und reproduziert die ACW in Übereinstimmung mit früheren Analysen. Neben einer Beschreibung der im simulierten Ökosystem gefundenen Variabilitätsmuster, die auch die Ronne-Polynya einschließt, enthält diese Publikation eine Untersuchung der Prozesse, die die Wechselwirkung zwischen atmosphärischen Anomalien und dem pelagischen Ökosystem vermitteln. Es stellt sich heraus, daß eine Betrachtung der Deckschichttiefe allein nicht genügt, um die komplexe Wechselwirkung zwischen der Hydrographie und dem Ökosystem zu beschreiben.

Die Arbeit schließt mit einer Zusammenfassung des Erreichten und mit einem Ausblick auf offene Fragen und mögliche nächste Schritte.

Now the question is: on what does the peculiar position of plankton organisms maxima and minima depend?.

Theodor Büse, 1915

Teil II

Plankton Dynamics in Frontal Systems of the Southern Ocean

Inga Hense, Ulrich V. Bathmann and Ralph Timmermann

Alfred-Wegener-Institut für Polar- und Meeresforschung, Bremerhaven, Germany

published in Journal of Marine Systems 27 (2000) 235-252

Abstract

A biological model of the Antarctic Polar Front (BIMAP) has been developed. The model comprises two biochemical cycles, silica and nitrogen, and five to seven compartments. Model runs are initialized using the WOCE-data set and forced by an annual cycle of solar radiation and mixed layer depth. Sensitivity experiments indicate that disregarding remineralization and dissolution of silica does not affect phyto- and zooplankton biomass significantly. Experiments with different half saturation constants of silicate uptake indicate that values between 4 and 8 μmol/l are reasonable for the plankton community at the Antarctic Polar Front. The role of iron limitation is investigated using different Si:N-uptake ratios and reduced growth rates. While reducing the maximum growth rate leads only to slightly lower phyto- and zooplankton biomasses, different Si:N-uptake ratios affect the development and maximum of plankton biomass significantly. Specifically, primary production and plankton biomass are strongly reduced by increasing the silica to nitrogen uptake ratio to values greater than 2. An Si:N-uptake ratio between 2 and 4 appears to be reasonable for the region of the Polar Front.

Keywords: plankton model, frontal system, silica and nitrogen, uptake ratio, iron limitation

1 Introduction

Although the Southern Ocean is rich in nutrients, phytoplankton biomass is generally low. Hence the Southern Ocean is one of the three large HNLC-areas (high nutrient low chlorophyll). In contrast to this, the Antarctic Polar Front is characterized by high phytoplankton biomass (Chl a concentrations from 2 up to 4.5 μg/l), highlighting this region as an exceptional zone with frequent plankton blooms in the ambient HNLC area (Smetacek et al., 1997). Although numerous expeditions have been carried out in this region (e.g. Hart, 1934; Dafner and Mordasova, 1994; Fronemann et al., 1995; Bathmann et al., 1997) the factors controlling phytoplankton blooms in this area remain uncertain. Besides possible limitation of light due to a deep mixed layer south of the frontal region, grazing and also possible limitation of micronutrients have been considered:

- Smetacek and Passow (1990) re-evaluated the investigations of Sverdrup (1953) and Sakshaug and Holm-Hansen (1984) and proposed that phytoplankton blooms will only develop in a mixed layer less than 40 m deep. In the region of the Polar Front favourable physical conditions may enhance phytoplankton growth: Strong upwelling in frontal regions is linked to a shallow mixed layer and a higher supply of nutrients in the euphotic zone (Veth et al., 1997).

- While grazing of zooplankton and of swarm organisms like salps could inhibit the build-up of phytoplankton blooms in vast areas of the Southern Ocean (Dubischar and Bathmann, 1997), swarm organisms are generally not present in the region of the Polar Front (Foxton, 1966).

- Iron concentration is generally low in the Southern Ocean and may limit the growth rate of phytoplankton (e.g. Gran, 1931; Martin and Fitzwater, 1988; de Baar, 1994). Higher iron concentration in the region of the Polar Front coincided with the development of a phytoplankton bloom in 1992 (De Baar et al., 1995).

Furthermore, in some regions of the Southern Ocean silicate concentration is low ($<$ 10 μmol/l). Measured half saturation constants of silica uptake range between 1.1 (Nelson and Tréguer, 1992) and 88.7 μmol/l (Sommer, 1986) which has implications on silica consumption and therefore on diatom growth. In the region of the Polar Front the bloom forming phytoplankter are large-celled or long-chained diatom species (e.g. $Fragilariopsis\ kerguelensis$, $Corethron\ criophilum$, $Thalassiothrix\ sp.$) whose growth rate might be limited by low silicate concentrations (Tréguer and Jaques, 1992; Nelson and Tréguer, 1992; Dafner and Mordasova, 1994; Quéguiner et al., 1997). Non-Si requiring phytoplankton

occurs only in low concentrations and diatoms clearly dominate the plankton community in the region of the Polar Front (e. g., Laubscher et al., 1993; Smetacek et al., 1997; Bracher et al., 1999). The smaller size class of the plankton community which consist of pico- and nanoplankton can be characterized by a low and stable biomass of maximum concentrations of 0.2 μg Chl a/l (Smetacek, 1999).

To study the processes stimulating and controlling phytoplankton blooms in the Southern Ocean a Biological Model for the Antarctic Polar Front (BIMAP) was developped. BIMAP is a hierarchy of models with different complexity. Zero-dimensional model runs are intended to accompany and prepare three-dimensional model runs, as they are computationally cheap and allow for a larger number of sensitivity studies.

Questions that need to be addressed include the following:

1. How is phytoplankton growth affected by silica enrichment in diatom frustules?
   Traditionally, the uptake ratio of silica to nitrogen was regarded as 1. Even in a couple of diatom species, Brzezinski (1985) recorded a Si:C-ratio of 0.13 and an Si:N-ratio of 1. However, recent studies recorded an Si:N-ratio of 4 or an Si:C-ratio of 0.6 in the Southern Ocean plankton community (Nelson and Smith, 1986; Shiomoto and Ishii, 1995; Hense et al., 1998). Consistent with that is an Si:N-uptake ratio or "disapearence ratio" of about 4 in that region (Minas and Minas, 1992; Dafner and Mordasova, 1994; Hense et al., 1998), explained by heavily silicified diatoms or a faster regeneration of nitrogen than of silica after a bloom decay.

2. Is phytoplankton growth limited by a deficiency of micronutrients like iron?
   Besides the already mentioned direct reduction of phytoplankton growth rates, Hutchins and Bruland (1998) as well as Takeda (1998) pointed out that iron deficiency may lead to a silica enrichment in diatoms. As this would affect the Si:N-uptake ratio, it might lead to a depletion of dissolved silicate and thus, subsequently, to further nutrient limitation of phytoplankton growth. Thus, iron limitation and variations in the Si:N-uptake ratio appear to be related issues.

3. How does hydrography affect the ecosystem at the Polar Front? Or, more specifically, what is the effect of different annual cycles of the mixed layer depth on the development of phytoplankton blooms?

In this paper we present a series of experiments with a vertically integrated model which are intended to be a first approach to answering these questions.

2 Model Description

2.1 Prognostic variables

BIMAP comprises two biochemical cycles. Following Fasham et al. (1990), nitrogen is distributed between the phyto- and zooplankton pools and the nutrients nitrate and ammonium. As the model is supposed to reflect the plankton community in the Antarctic Polar Front, we complemented this by a silica cycle. The two cycles are coupled by a constant Si:N-uptake ratio for phytoplankton growth.

Thus, our standard model comprises the five compartments phytoplankton (P), zooplankton (Z), nitrate (N_i), ammonium (N_a) and silicate (S_i). Sensitivity experiments investigating the effect of remineralization of detritus and dissolution of silica are performed including the two additional compartments Det_N and Det_{Si} which comprise the nitrogen and silica part of detritus, respectively. Biomass in these compartments is computed in μmol N/l and μmol Si/l, respectively. We assume a C:Chl a-ratio of 50. Conversion from carbon to nitrogen units is done using the Redfield ratio.

We decided to disregard the dissolved organic nitrogen (DON) as there still is some uncertainty about the role of DON. Only the labile substances are known and these are remineralized rapidly - thus we directly lead the DON exuded by phytoplankton into the ammonium pool.

2.1.1 Phytoplankton

Following Fasham et al. (1990), temporal changes of the phytoplankton concentration are due to primary production, grazing by zooplankton, natural mortality and effects of mixing:

$$\frac{dP}{dt} = (1-\gamma)\cdot\sigma\cdot P - g_Z - \mu_P\cdot P + D_P \tag{1}$$

The growth rate σ considers the maximum (light dependent) growth rate ω and a limitation by nutrients η. We will further call it the actual growth rate: $\sigma = \omega\cdot\eta$. The biomass which is exuded as DON during the cell division is $\gamma\cdot\sigma$. Following Williams (1990) who suggested that 1/20 of the phytoplankton primary production will be exuded we choose γ = 0.05. While g_Z decribes the losses by grazing through zooplankton, represented by herbivorous copepods, μ_P represents the mortality of phytoplankton which we assume to be 0.05 as natural mortality is quite low for Antarctic species (Peters and Thomas, 1996). The effect of entrainment, detrainment and diffusion over the pycnocline is denoted as D_P.

Following the law of minimum (Liebig, 1840), the actual growth rate for

diatoms considers possible limitation either by nitrate or by silicate:

$$\eta = min\left(\frac{N_i}{k_{N_i}+N_i}, \frac{S_i}{k_{S_i}+S_i}\right). \tag{2}$$

A Michaelis-Menten-type relation is assumed for all nutrients using the half saturation constants k_{S_i} and k_{N_i}. For nitrate we chose a $k_{N_i} = 0.3$ μmol/l (Sommer, 1986). For silicate, measured half saturation constants differ between natural Antarctic assemblage and cultures. For Antarctic diatoms in culture, Sommer (1986) recorded half saturation constants up to 89 μmol/l. In experiments during cruises in the Indian sector of the Southern Ocean, Jaques (1983) recorded a half saturation constant of 12 μmol/l for Antarctic diatoms. In a naturally occuring Antarctic diatom assemblage, Nelson and Tréguer (1992) recorded half saturation constants from 1.1 to 4.6 μmol/l. We decided to choose $k_{S_i} = 4.6$ μmol/l. The effect of different values for k_{S_i}, however, is investigated in a series of sensitivity experiments.

Following Evans and Parslow (1985) and Fasham et al. (1990) the light dependent growth rate ω is described by

$$\omega = \frac{1}{h} \cdot \int_{\Delta t} \int_{0}^{h} \frac{V_P \cdot \alpha \cdot I(z,t)}{\sqrt{V_P^2 + \alpha^2 \cdot I^2(z,t)}} \cdot e^{-(k_w + k_c \cdot P)\cdot z} dz\, dt \tag{3}$$

where h denotes the mixed layer depth and I is the intensity of the photosynthetic active radiation (PAR) in a depth z below the surface. For the conversion from solar radiation to PAR we use a factor of 43 % according to Jerlov (1976) and Jitts et al. (1976) and assume a surface albedo of 0.8. As the Southern Ocean belongs to oceanic type I (Jerlov, 1976; Bracher and Tilzer, 2001), we chose $k_w = 0.04$ m^{-1} (Lorenzen, 1972) as the attenuation coefficient of sea water. The self-shading parameter $k_c = 0.07$ m^2 mmol N^{-1} and the initial slope $\alpha = 0.027$ (W m^{-2})$^{-1}$ d^{-1} of the PI-curve were taken from cruise measurements during the SO-JGOFS cruise ANT XIII/2 (Bracher et al., 1999). For the maximum growth rate V_p we took the maximum growth rate from Eppley (1972), which is 1.2 doublings per day at maximum temperatures of about 6°C at 50°S.

2.1.2 Zooplankton

Temporal changes of the zooplankton biomass are due to grazing, mortality, excretion and effects of entrainment and diffusion:

$$\frac{dZ}{dt} = \beta \cdot g_Z - \mu_Z \cdot Z^2 - \varepsilon \cdot Z + D_Z \tag{4}$$

As we are mostly interested in the factors controlling the building up of phytoplankton blooms, we only consider the herbivorous part of zooplankton. The assimilation efficiency is denoted as β; so $\beta \cdot g_Z$ gives the growth rate of zooplankton

biomass while $(1-\beta)\cdot g_Z$ is the part of ingested food which is excreted as faecal pellets. The grazing rate g_Z is derived from experiments with the abundant herbivorous copepod species *Calanoides acutus* (Schnack, 1985) and reads

$$g_Z = 0.063 \cdot (79.5 \cdot P)^{1.3} \cdot \frac{10^{-3}}{0.14 \cdot 86400} \cdot Z. \tag{5}$$

The number 79.5 and the fraction $10^{-3}/(0.14 \cdot 86400)$ result from the conversion from carbon [μg/l] to nitrogen units [μmol/l], assuming the average carbon content of an adult individuum of *Calanoides acutus* to be 0.14 mg (Schnack, 1985). Following Fasham (1995) and Steele and Henderson (1992), the mortality of zooplankton through higher predators is parameterized as a quadratic function. The natural mortality rate is quite low for adult copepods (< 0.01 d^{-1} according to Huntley et al., 1994 and Aksnes, 1996), therefore the greatest part of mortality is the loss to higher predators. Choosing μ_Z = 2 l (μmol N)$^{-1}$ d^{-1} leads to a mortality of 10 to 18 % per day for typically occuring zooplankton concentrations. The excretion rate of 20.2 ng N (mg dry wt)$^{-1}$ h^{-1} (Huntley and Nordhausen, 1995) has been converted to ε = 0.0078 d^{-1}. Again, D_Z denotes the mixing across the pycnocline and effects of changes in mixed layer depth.

2.1.3 Nutrients

Temporal changes of the concentrations of nutrients are due to uptake of phytoplankton, exudation, excretion and entrainment and diffusion. Although we do not allow ammonium supply to limit phytoplankton growth, the uptake ratio between ammonium and nitrate is determined using their concentrations N_a and N_i and half saturation constants k_{N_a} and k_{N_i}:

$$\frac{dN_i}{dt} = -\sigma \cdot \frac{\frac{N_i}{k_{N_i}+N_i}}{\frac{N_i}{k_{N_i}+N_i} + \frac{N_a}{k_{N_a}+N_a}} \cdot P + D_{N_i} \tag{6}$$

$$\frac{dN_a}{dt} = -\sigma \cdot \frac{\frac{N_a}{k_{N_a}+N_a}}{\frac{N_i}{k_{N_i}+N_i} + \frac{N_a}{k_{N_a}+N_a}} \cdot P + \gamma \cdot \sigma \cdot P + \varepsilon \cdot Z + D_{N_a} \tag{7}$$

$$\frac{DS_i}{Dt} = -\sigma \cdot r \cdot P + D_{S_i} \tag{8}$$

Following observations in the Southern Ocean of Nelson and Smith (1986), Shiomoto and Ishii (1995) and Hense et al. (1998), we chose an Si:N-uptake ratio $r = 4$ for the reference simulation.

2.1.4 Detritus

In a couple of sensitivity experiments we investigate the influence of remineralization and silica dissolution on the development of plankton dynamics. For these

experiments we add a detritus pool decomposed into a nitrogen part Det_N and a silica part Det_{S_i}. Temporal changes in both compartments are due to mortality of phyto- and zooplankton, production of faecal pellets, remineralization and the effects of entrainment, diffusion and sinking:

$$\frac{d\,Det_N}{dt} = \mu_P \cdot P + \mu_Z \cdot Z + (1-\beta) \cdot g_Z - \tau_{N_a} \cdot Det_N + D_{Det_N} \quad (9)$$

$$\frac{d\,Det_{S_i}}{dt} = (\mu_P \cdot P + \mu_Z \cdot Z + g_Z) \cdot r - \tau_{S_i} \cdot Det_{Si} + D_{Det_{Si}} \quad (10)$$

Using the term $(1-\beta) \cdot g_Z$ we assume that faecal pellet production is proportional to zooplankton grazing. As silica is not stored in zooplankton biomass, the whole ingested silica part of phytoplankton is led to the silica part of the detritus pool. The detritus losses through remineralization or dissolution are denoted as $\tau_{N_a} \cdot Det_N$ and $\tau_{S_i} \cdot Det_{S_i}$, respectively, and form additional sources of silicate and ammonium. Time constants of mineralization to ammonium and silica dissolution were derived from observations of Biddanda (1988) and measurements of Tréguer et al. (1989). Their values are $\tau_{N_a} = 0.07\ \mathrm{d}^{-1}$ and $\tau_{S_i} = 0.018\ \mathrm{d}^{-1}$.

2.1.5 Entrainment and Diffusion

Cross-pycnocline mixing and entrainment are computed using the Fickian diffusion approach and assuming a linear profile between the mixed layer base ($z = -h$) and an arbitrary reference depth ($z = -h_b$). The resulting fluxes for any tracer concentration T within the mixed layer are

$$D_T = \frac{1}{h}\left(a_v \frac{T_b - T}{h_b - h} + w_{ent}(T_{ent} - T)\right), \quad (11)$$

where the subscript b denotes the respective concentration at $z = -h_b$ and variables without subscript denote properties of the mixed layer. We chose $a_v = 10^{-3}\ \mathrm{m}^2\ \mathrm{s}^{-1}$ as the vertical diffusion cofficient; w_{ent} represents the entrainment velocity. In contrast to Fasham et al. (1990), no discontinuity in tracer concentrations at the nutricline is assumed. Closer to observed nutrient profiles in the region of the Antarctic Polar Front (Löscher et al., 1997), we assume a linear profile between $z = -h$ and $z = -h_b$. From that we estimate the tracer concentration involved in the entrainment flux to be

$$T_{ent} = T + \frac{T_b - T}{h_b - h}\,\delta h \quad (12)$$

where δh represents the thickness of an entrainment zone assumed to be 8 m (Lemke et al., 1990).

Except for zooplankton, concentrations within the mixed layer are modified only in case of entrainment, but not for mixed layer retreat. Zooplankton, however,

is able to actively stay in the mixed layer, so that its concentration increases in case the mixed layer gets shallower. For this reason, as in Fasham et al. (1990), the entrainment velocity used in equations (11) and (12) is restriced to positive values for all compartments except for zooplankton.

For detritus, an additional term accounting for sinking with a velocity V

$$D_V = -V \cdot \frac{Det}{h} \tag{13}$$

is applied to both Det_N and Det_{Si}.

2.2 Initialization and Forcing

Model runs are initialized with winter concentrations in all compartments. For phytoplankton we chose of 0.2 μg Chl a/l, for zooplankton 0.1 μg C/l. Following the WOCE-data set, initial nutrient concentrations are 26 μmol/l for nitrate, 0.2 μmol/l for ammonium and 14 μmol/l for silicate.

Nutrient data from the WOCE-data set are also used at the lower boundary which was chosen to be at $h_b = 300$ m. Phyto- and zooplankton and detritus concentrations at $z = -h_b$ are assumed to be zero. For zooplankton this might not be totally correct, but we only consider herbivorous zooplankton and these concentrate in the mixed layer (in the upper 100 m depth according to Fransz and Gonzalez, 1997).

The model is forced by annual cycles of the mixed layer depth and solar radiation. Mixed layer depth is derived from a regional application of the *s*-Coordinate Primitive Equation Model SPEM (Haidvogel et al., 1991; modified by Song and Haidvogel, 1994, and Beckmann et al., 1999). For the solar radiation we consider the daily and annual cycles, latitude and mean cloud cover, using the standard astronomical formulae of Zillmann (1981) and Laevastu (1960). The cloud cover was chosen to be 80%, in agreement with the reanalysis data of the ECMWF. A daily time step is applied. Parameter values for the reference experiment are given in Table 1.

1. phytoplankton		
Initial slope of the PI-curve	α	$0.027 \frac{\mathrm{m}^2}{\mathrm{W \cdot d}}$
maximum growth rate	V_P	1.2 d^{-1}
mortality rate	μ_P	0.05 d^{-1}
Half saturation constant for silicate	k_{S_i}	4.6 μmol/l
Half saturation constant for nitrate	k_{N_i}	0.3 μmol/l
Half saturation constant for ammonium	k_{N_a}	0.3 μmol/l
exudation fraction	γ	0.05 d^{-1}
2. zooplankton		
assimilation efficiency	β	0.67 d^{-1}
excretion rate	ε	0.0078 d^{-1}
mortality rate	μ_Z	2.0 $\frac{l}{\mu \mathrm{mol \cdot d}}$
3. nutrients		
Si:N ratio *in the standard model runs*	r	4 mol/mol
4. detritus *(for sensitivity model runs)*		
silica dissolution rate	τ_{S_i}	0.018 d^{-1}
remineralization rate	τ_{N_a}	0.07 d^{-1}
sinking rate	V	1, 5, 10 m d^{-1}

Table 1: BIMAP Parameters, their symbols and values in the reference experiment.

3 Results

3.1 The reference simulation

The reference simulation features a pronounced seasonal cycle of plankton and nutrients (Fig.1) with concentrations in good agreement with observations.

In October, when the solar radiation increases and the mixed layer retreats, phytoplankton growth begins (Fig.1a). Phytoplankton biomass reaches its maximum in January with concentrations of up to 3 μg Chl a /l when the mixed layer is shallowest ($\leq$ 20m). Typical summer concentrations of phytoplankton measured in that region are in the range from 2 to 4.5 μg Chl a /l (Lutjeharms, 1985; Dafner and Mordasova, 1994; Bathmann et al., 1997). Zooplankton starts to develop in November shortly after the onset of phytoplankton growth and reaches its maximum between November and February with maximum concentrations of 7 μg C /l (Fig. 1b). Observed maximum zooplankton biomass in summer is in the range from 8 to 16 mg ash free dry weight (AFDW) m^{-3} (Fransz and Gonzalez, 1997). Assuming that 1 mg AFDW m^{-3} comprises 0.46 mg C m^{-3} (Paffenhoefer and Harris, 1976), these observed zooplankton concentrations convert into 3.7 - 7.4 μg C /l. Simulated summer zooplankton concentrations are therefore in good agreement with measurements.

While nitrate concentration remains high, silicate is depleted from November onwards (Fig. 1c), leading to a nutrient limitation which is visible in the increasing difference between light limited and actual growth rate (Fig. 1d). Simulated silicate and nitrate concentrations are in the range of observations with concentrations $<$ 1 μmol /l in summer (Quéguiner et al., 1997) for silicate and about 22 μmol /l for nitrate (Löscher et al., 1997; Hartmann et al., 1997). The absence of a strong decrease in nitrate concentration in summer is a prominent feature of the ecosystem near the Antarctic Polar Front and has been repeatedly observed (Löscher et al., 1997; Hartmann et al., 1997; Dafner and Mordasova, 1994) and is also a distinctive feature of model studies in the Southern Ocean (e.g., Pondaven et al., 1999; Lancelot et al., 2000).

Maximum daily primary production is 0.6 g C m^{-2} or about 30 mmol silicate m^{-2} in November (Fig. 1e) and agrees well with observations ranging from 0.3 to 1.2 g C m^{-2} (Dafner and Mordasova, 1994; Quéguiner et al., 1997; Bracher et al., 1999).

From February onwards, an increasing mixed layer depth (Fig. 1f) leads to entrainment of further nutrients and therefore allows for further growth of phytoplankton. However, the decline of the solar radiation and further deepening of the mixed layer lead to a decrease of phytoplankton biomass. In April, phytoplankton concentration has gone down below 1 μg Chl a /l and zooplankton has decreased to concentrations lower than 1 μg C /l.

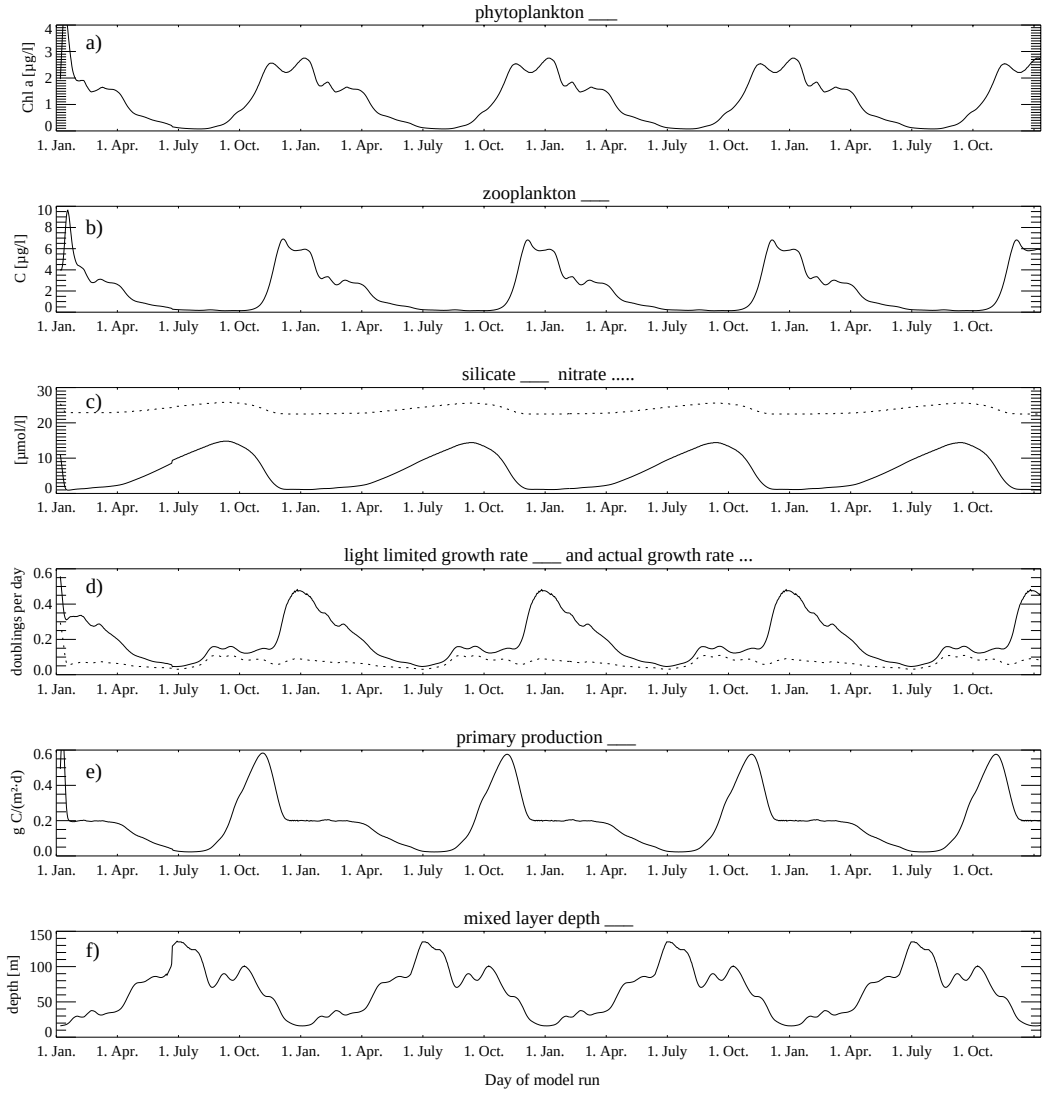

Figure 1: Simulated concentrations of (a) phytoplankton, (b) zooplankton, (c) silicate and nitrate, (d) light limited growth rate and actual growth rate, (e) vertically integrated daily primary production and (f) mixed layer depth in the reference experiment.

During the winter, nutrients are replenished due to further entrainment and cross-pycnocline mixing. Maximum concentrations of 15 μmol/l for silicate and 26 μmol/l for nitrate occur just before the phytoplankton starts to develop. Winter concentrations of silicate and nitrate compare well with measurements during Polarstern cruise ANT X/4 (Lemke et al., 1992).

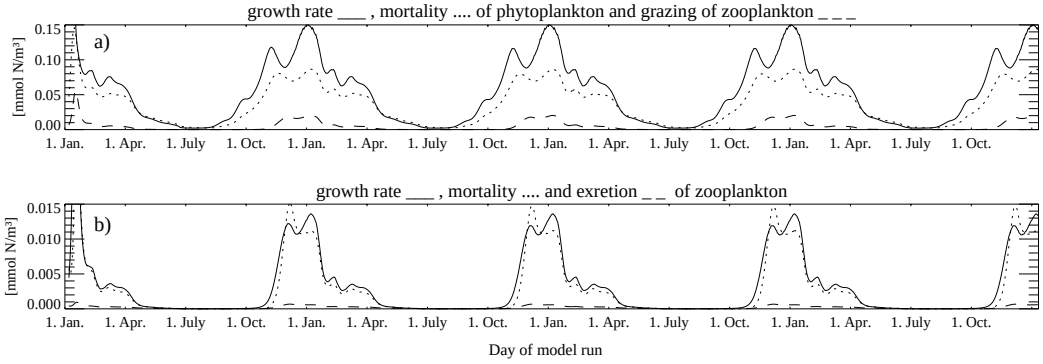

Figure 2: Nitrogen fluxes for the compartments a) phyto- and b) zooplankton. Displayed are (a) phytoplankton growth (solid) and mortality (dotted), and zooplankton grazing (dashed), and (b) zooplankton growth (solid), mortality (dotted) and excretion(dashed). Note the different scales.

Time series of the nitrogen fluxes between the different compartments (Fig. 2a, b) indicate that phytoplankton growth is predominantly balanced by phytoplankton mortality (despite the long time scale involved) while zooplankton grazing appears to play a minor role. Similar to that, zooplankton growth is balanced by mortality (including feeding pressure by higher predators) while excretion is negligible.

Simulated ammonium concentrations (not shown) are maximum 0.1 μmol/l and therefore significantly lower than observed ammonium concentrations (0.2 to 0.4 μmol/l in the mixed layer; Tréguer and Jaques, 1992).

Thus our reference experiment gives thorouhgly reasonable results, although ammonium concentration is underestimated.

3.2 Experiments with remineralization and dissolution of silica

To investigate the effect of remineralization and dissolution of silica, a series of sensitivity experiments with different sinking velocities has been performed. All experiments (Fig. 3) show only minor differences from the reference simulation.

The effect of remineralization and dissolution of silica is most obvious in the experiment with a low sinking rate of 1 m/d: Compared to simulations with higher sinking velocity, a longer residence time in the mixed layer leads to higher concentrations of biogenic silica (which comprises the silica part of living phyto-

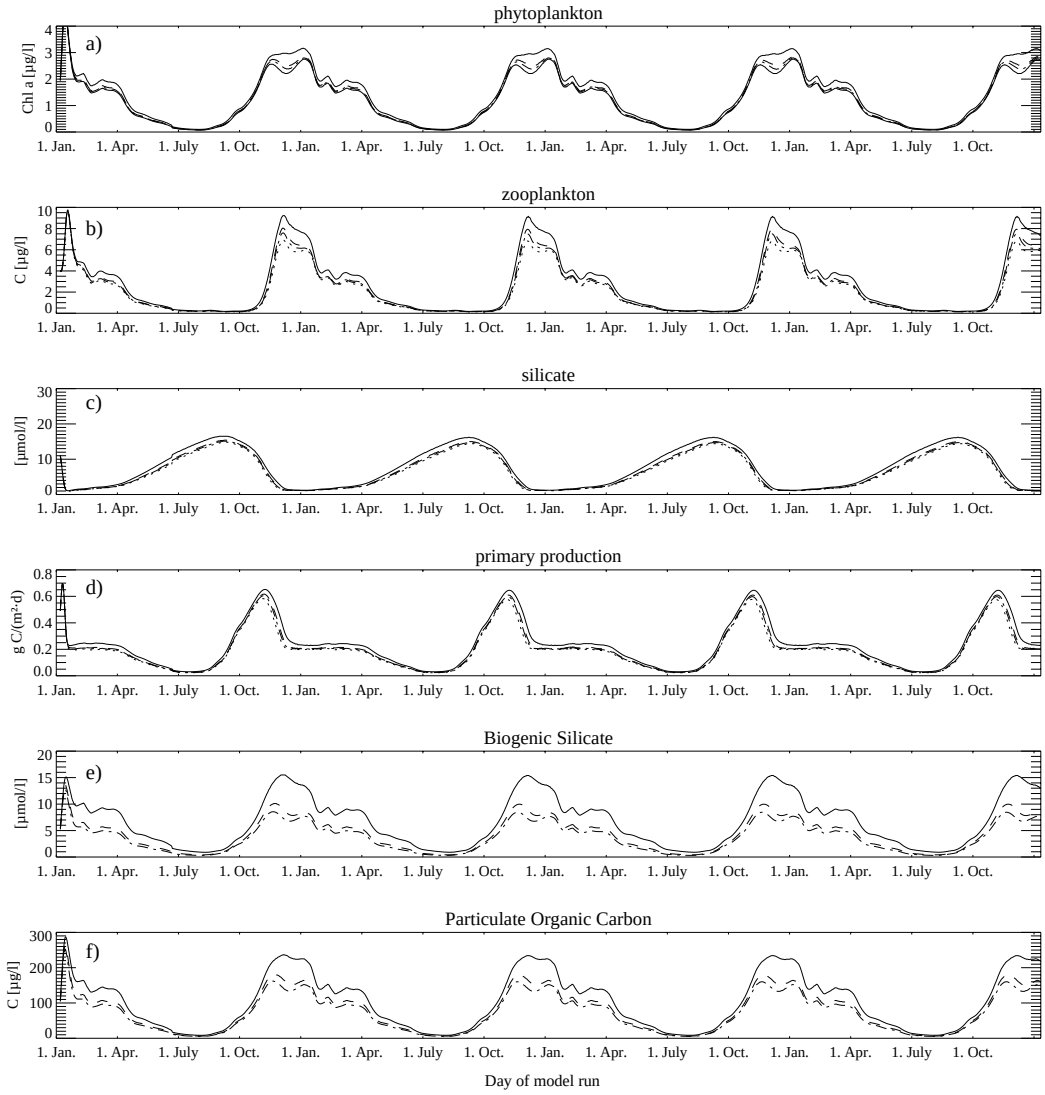

Figure 3: Simulated concentrations of (a) phytoplankton, (b) zooplankton, (c) silicate and (d) vertically integrated primary production in the reference simulation (dotted) and experiments with remineralization and dissolution of silica using different sinking velocities of 1m per day (solid), 5m per day (dashed) and 10m per day (dashed-dotted).

plankton cells and detritus) and thus to a more pronounced contribution of silica dissolution. Due to the higher silicate concentrations in summer, primary production is increased and higher phyto- and zooplankton biomasses are produced (Fig. 3a-d).

The maximum simulated BSi concentrations of 15 μmol /l for a sinking rate of 1 m/d and 10 and 7 μmol /l for sinking rates of 5 and 10 m/d (Fig. 3e), respectively, agree well with results from a more complex plankton model (Lancelot et al., 2000) and with BSi concentrations observed between 2.76 and 11.7 μmol/l (Quéguiner et al., 1997).

Simulated maximum POC concentrations are in the range of 150 - 250 μg/l (Fig. 3f) which also agrees with observations (Bathmann et al, 1997). Ammonium concentrations (not shown) in these experiments are more realistic than in the reference simulation with concentrations between 0.4 and 0.5 μmol/l for sinking rates of 5 and 10 m/d, respectively, but overestimated with concentrations up to 1.3 μmol/l in the experiment with $V = 1$ m/d.

We conclude that disregarding dissolution and remineralization leads to an underestimation of ammonium concentration but has no significant effect on the development and the amount of plankton biomasses.

3.3 Experiments with different half saturation constants of silicate

Laboratory experiments with different diatom species gave silicate half saturation constants of 4.2 μmol/l for *Thalassiothrix antarctica*, 34.5 μmol/l for *Corethron criophilum* and 88.7 μmol/l for *Fragilariopsis kerguelensis* (Sommer, 1986; Sommer, 1991). For a natural diatom community, Nelson and Tréguer (1992) recorded half saturation constants of 1.1 to 4.6 μmol/l.

For the reference simulation we chose $k_{S_i} = 4.6$ μmol/l. In order to investigate the sensitivity to different half saturation constants we performed a series of experiments with $k_{S_i} = 1.1, 8.0$ and 34.5 μmol/l, respectively.

It turns out that the experiment with $k_{S_i} = 8$ μmol/l reveals an annual cycle of plankton growth and decay which is quite similar to the reference simulation (Fig. 4a,b). However, concentrations of dissolved silicate are slightly higher both in summer and in winter (Fig. 4c).

In contrast to that, reducing the silicate half saturation constant to 1.1 μmol/l (Fig. 4, solid line) leads to slightly lower concentrations of phyto- and zooplankton in November compared to the reference simulation (Fig. 4, dotted line). Primary production starts earlier but also ends up earlier due to a strong silicate depletion (Fig. 4d). While maximum silicate concentrations are only 10 μmol/l, silicate is totally depleted with concentrations near 0 μmol/l for almost five months.

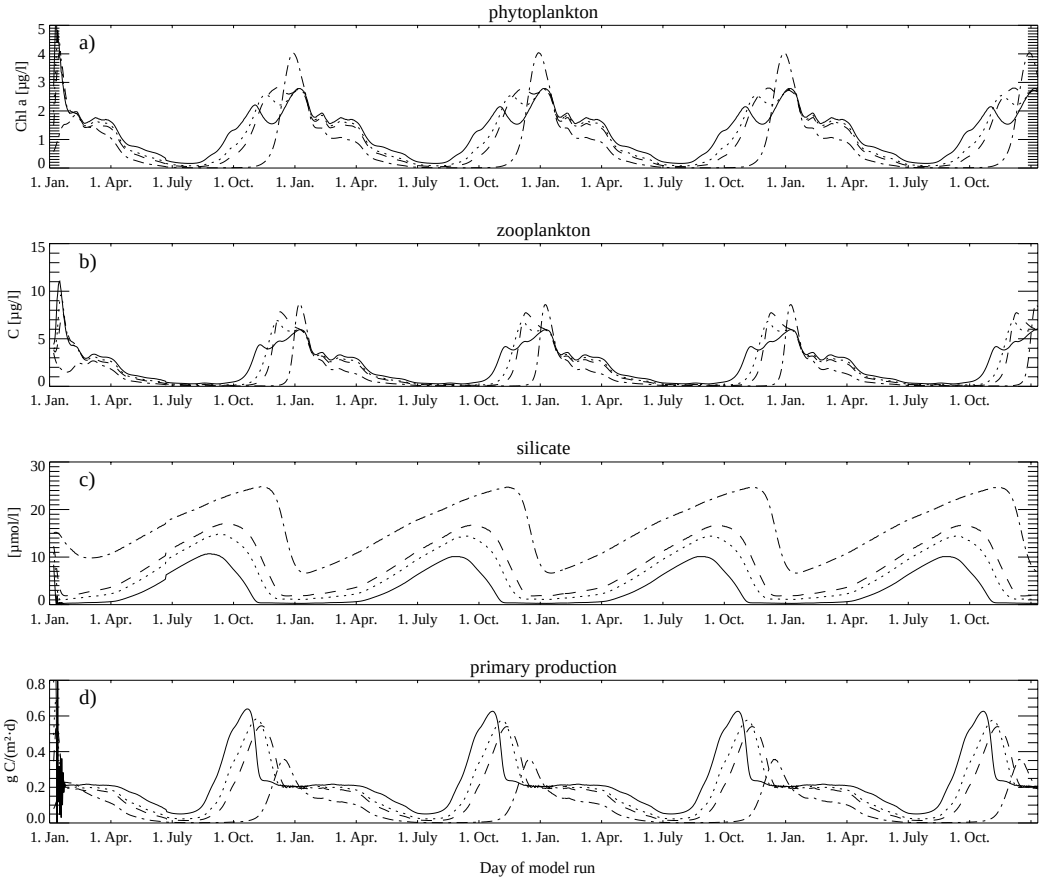

Figure 4: Simulated concentrations of (a) phytoplankton, (b) zooplankton, (c) silicate and (d) vertically integrated primary production in the reference simulation (dotted) and experiments with half saturation constants k_{S_i} of 1.1 (solid), 8 (dashed) and 34.5 (dashed-dotted).

In the experiment with a half saturation constant of 34.5 μmol/l (Fig. 4, broken line), the onset of phytoplankton growth is delayed by roughly two months. Due to the reduced growth rates, no silica depletion occurs (silicate remains high with minimum concentrations of 6 μmol/l); hence the maximum phyto- and zooplankton concentrations are even higher than in the reference simulation. However, the bloom is much shorter so that integrated daily primary production is quite low with maximum values of 0.3 g C m^{-2}.

From the annual cycles of nutrient concentrations which show an unrealistic depletion for a long period in case of $k_{S_i} = 1.1$ μmol/l or (equally unrealistic) no depletion at all in case of $k_{S_i} = 34.5$ μmol/l we conclude that these half saturation constants are not typical for a natural diatom community at the Antarctic Polar Front.

3.4 The role of iron

As already mentioned, field and laboratory experiments have indicated that iron addition enhances phytoplankton growth or vice versa iron deficiency could slow down primary production (e.g., Martin and Fitzwater, 1988). In addition to that, Hutchins and Bruland (1998) as well as Takeda (1998) recorded higher Si:N-uptake ratios in case of iron deficiency. As measurements of half saturation constants or equally suited criteria of the iron's impact on phytoplankton growth are not available for the Southern Ocean, the effect of iron limitation is tested by a couple of model experiments with reduced growth rates and different Si:N-uptake ratios.

3.4.1 Reduced growth rates

As iron-enrichment experiments indicate that the phytoplankton growth rate is reduced by maximum 30% due to iron deficiency (e.g. Takeda, 1998), model runs with either the maximum growth rate or the actual growth rate reduced by 30% were carried out (Fig. 5).

A reduced maximum growth rate ($V_P = 0.8$ instead of 1.2) has no significant effect on phyto- and zooplankton biomass (Fig. 5 a, b). However, phytoplankton growth starts a little later and silicate is not as strongly depleted as in the reference simulation (Fig. 5 c).

Reducing the actual growth rate by 30% leads to a higher phyto- and zooplankton biomass in January. The onset of the phytoplankton bloom is delayed by roughly two weeks and therefore the maximum of primary production occurs later than in the reference simulation. Maximum primary production, however, is not significantly affected (Fig. 5d).

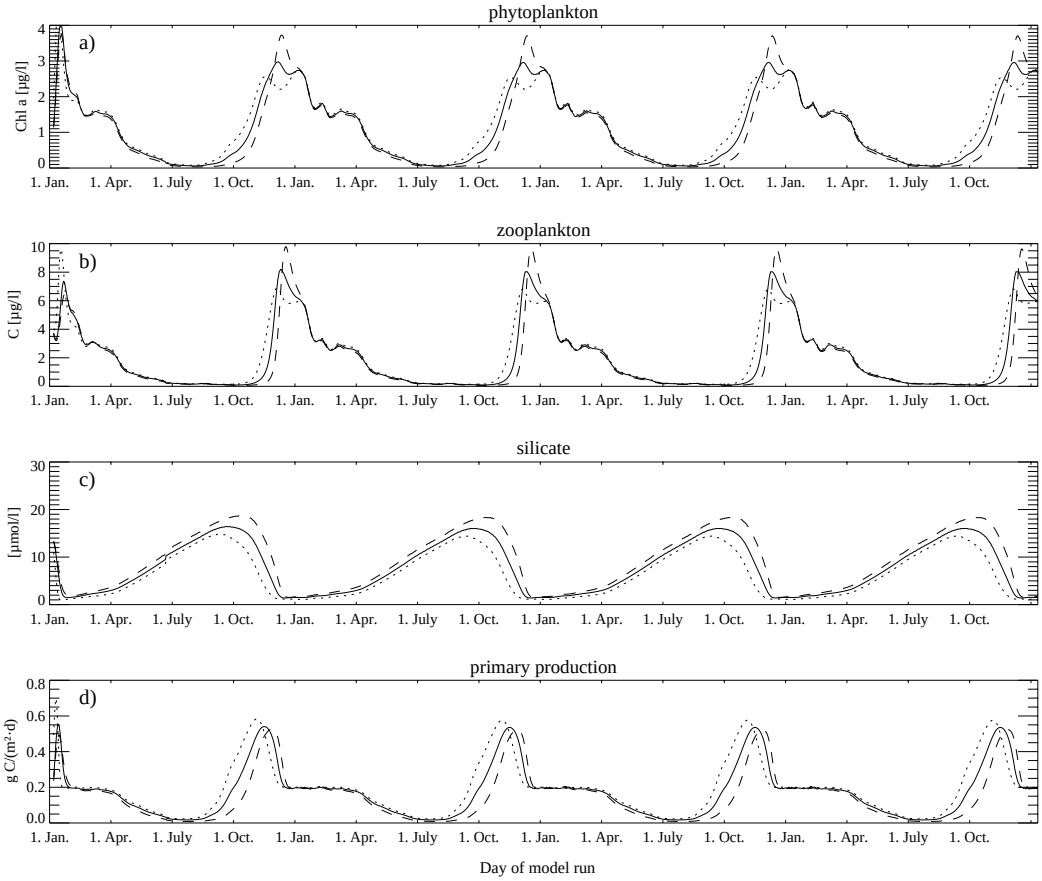

Figure 5: Simulated concentrations of (a) phytoplankton, (b) zooplankton, (c) silicate and (d) vertically integrated primary production in the reference simulation (dotted) and experiments with reduced maximum growth rate (solid) and reduced actual growth rate (dashed).

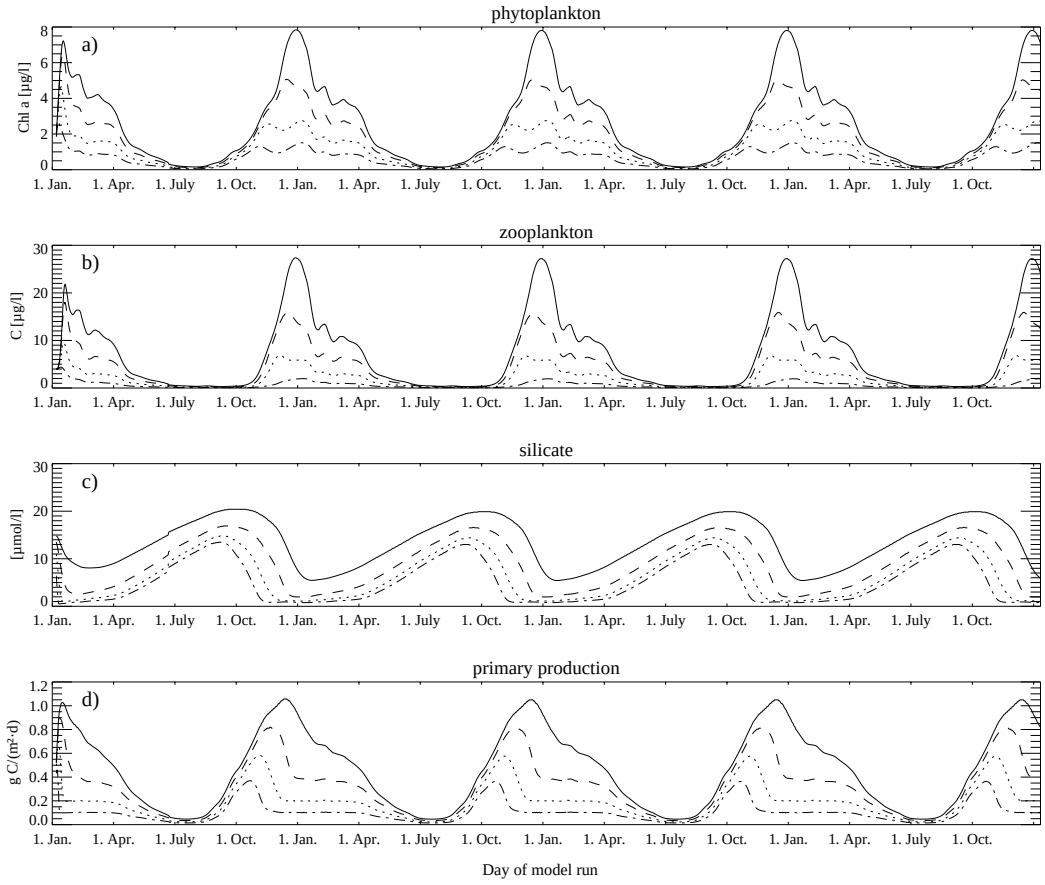

Figure 6: Simulated concentrations of (a) phytoplankton, (b) zooplankton, (c) silicate and (d) vertically integrated primary production in the reference simulation (dotted) and experiments with an Si:N ratio of 1 (solid), Si:N of 2 (dashed) and Si:N of 8 (dashed-dotted).

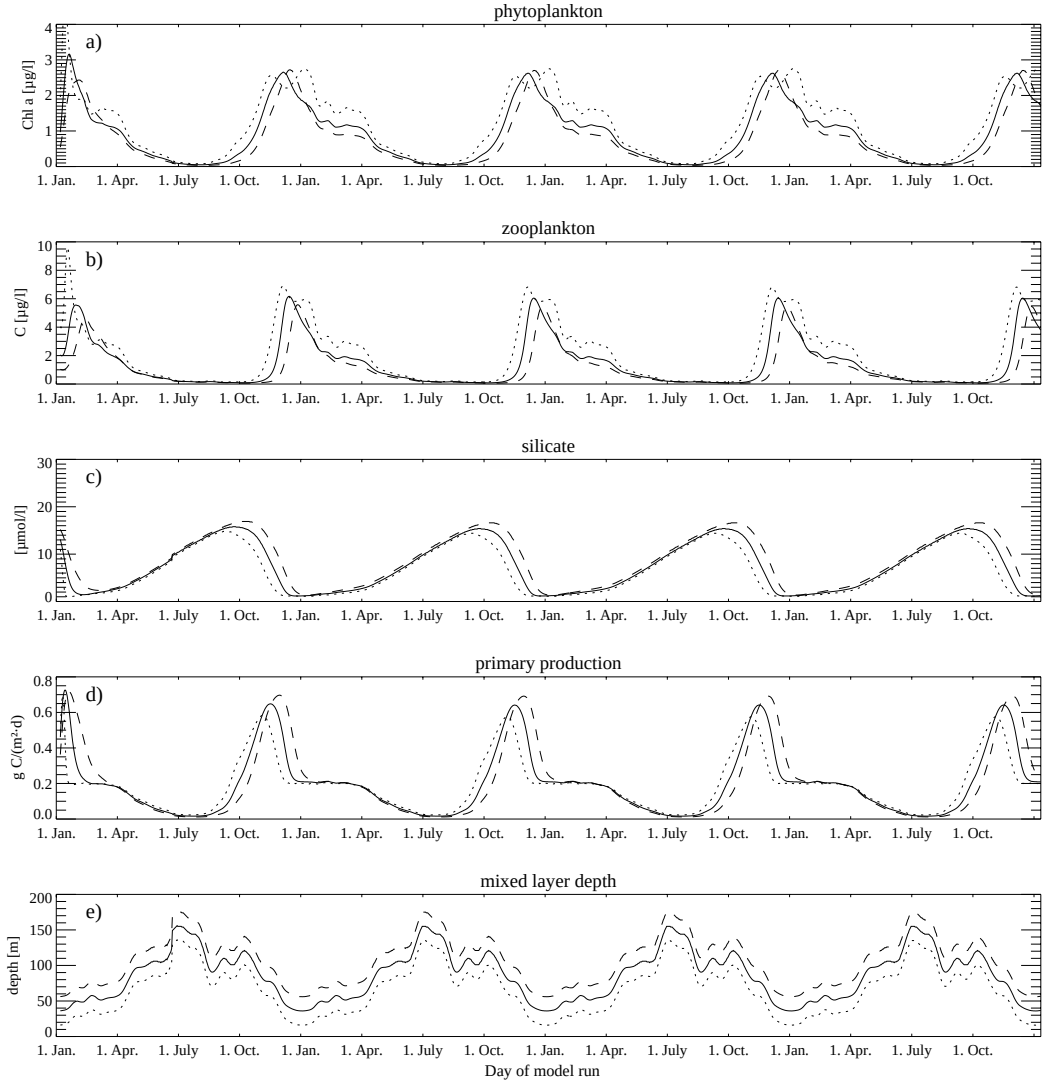

Figure 7: Simulated concentrations of (a) phytoplankton, (b) zooplankton, (c) silicate, (d) vertically integrated primary production and (e) the mixed layer depth in the reference simulation (dotted) and experiments with changing the offset of the mixed layer depth of 20 m (solid) and 40 m (dashed).

3.4.2 Different Si:N-uptake ratios

Different Si:N-uptake ratios lead to pronounced changes in plankton biomass (Fig. 6). Assuming a silicate to nitrate uptake ratio $r = 1$ (solid line) instead of 4 (dotted), the simulation features a stronger seasonal cycle of both phyto- and zooplankton and nutrients (Fig. 6a-c). Maximum phytoplankton and zooplankton concentrations in this experiment are 8 μg Chl a /l and 30 μg C /l, respectively. While the high simulated integrated primary production of about 1.2 g C m^{-2} d^{-1} (Fig. 6d) agrees with observations of Quéguiner et al. (1997), phyto- or zooplankton concentrations that high have never been recorded in the region of the Antarctic Polar Front.

Looking at the other extreme, an Si:N-uptake ratio of 8 leads to a maximum phytoplankton concentration of only 1.5 μg Chl a /l and a maximum zooplankton concentration of 2 μg C /l. Silicate depletion starts early in spring thus slowing down phytoplankton growth for the rest of the summer season. As a consequence, daily integrated primary production is strongly reduced with maximum values of 0.3 g C m^{-2} d^{-1}. Apparently, with increasing Si:N-uptake ratio, limitation of silicate becomes more and more important and as a consequence thereof, primary production and phyto- and zooplankton biomass decrease.

3.5 The influence of mixed layer dynamics

To study the impact of mixed layer dynamics on the development of a phytoplankton bloom, two experiments were performed with the mixed layer depth constantly increased by 20 and 40 m, respectively (Fig. 7). In both experiments, phyto- and zooplankton show slightly lower biomasses in January. Apart from that, the effect is rather small.

4 Discussion

We have demonstrated that the zero-dimensional version of BIMAP gives a reasonable simulation of the annual cycle of plankton growth and decay in the Antarctic Polar Front. Maximum phyto- and zooplankton concentrations as well as the annual cycle of nutrient depletion and replenishment are realistically reproduced. Vertically integrated daily primary production agrees well with calculations based on measurements. Thus, the assumption of an Si:N-uptake ratio of 4 appears to be justified. Although zero-dimensional, the model appears to capture essential aspects of hydrography through the annual cycle of mixed layer depth and the effects of diffusion and entrainment.

Model experiments including two compartments for the nitrogen- and the silica-fraction of detritus indicate that dissolution of silica only plays a minor role

for nutrient supply in the mixed layer. While Nelson et al. (1995) estimated that globally 50 $\%$ of the produced biogenic silica dissolves in the upper 100 m depth, they also pointed out that there are significant regional differences. According to Nelson and Gordon (1982), the Antarctic Circumpolar Current belongs to the region with the lowest silica dissolution rates in surface water which is consistent with the recorded high opal sedimentation in this region (DeMaster, 1981). There is some discussion going on about factors accelerating silica dissolution (e.g. Nelson et al., 1995; Bidle and Azam, 1999). However, considering effects like eddy pumping and the strong vertical movements associated with a meandering front, it is reasonable to conclude that in frontal regions remineralization might only play a minor role in nutrient supply.

Experiments with different values for the half saturation constant k_{S_i} for silica uptake feature a surprisingly low sensitivity for a moderate range of values. While the experiments with $k_{S_i} = 1.1, 4.6$ and 8 μmol/l all reproduce silicate depletion in summer (probably exaggerated in case of $k_{S_i} = 1.1$ μmol/l), summer silicate concentrations are overestimated in the experiment with $k_{S_i} = 34.5$ μmol/l. Pondaven et al. (1998) simulated silicate limitation at the KERFIX station assuming a half saturation constants of 8 μmol/l and pointed out that simulations with lower half saturation constants underestimate the summer silicate concentrations. However, in the region of the Antarctic Polar Front silicate depletion with minimum values of 2 μmol/l and lower was frequently reported (Dafner and Mordasova, 1994; Quéguiner et al., 1997, Hartmann et al., 1997) which leads us to conclude that half saturation constants for silica uptake in the range from 4 to 8 μmol/l are suitable for a realistic simulation of the plankton community in the region of the Antarctic Polar Front.

Possible effects of iron limitation were investigated in a series of experiments with different Si:N-uptake ratios or reduced maximum or actual growth rates. It turns out that primary production as well as phyto- and zooplankton biomass are affected more by variations of the Si:N-uptake ratio than by limiting the growth rate itself. Specifically, reducing the *maximum* growth rate V_P by 30 % only delays the onset of the phytoplankton bloom by roughly half a month while - due to the effect of nutrient limitation - plankton concentrations and primary production are not significantly affected.

Reducing the *actual* growth rate by 30 % also reveals no significant effect on the maximum primary production; however, the annually integrated primary production (Table 2) is reduced by 20 % compared to the reference simulation. Nevertheless, similar to the experiment with $k_{S_i} = 34.5$ μmol/l, maximum phytoplankton concentration in January is increased. Thus, if an observer takes a snapshot of an ecosystem like that, phytoplankton biomass may be even higher than in a situation without iron limitation.

In contrast to that, the system's response to different Si:N-uptake ratios is

Experiment	Vertically integrated primary production [g C m^{-2} yr^{-1}]
Reference	69
Remin.: Sinking 1 m/d	83
Remin.: Sinking 5 m/d	74
Remin.: Sinking 10 m/d	72
$k_{S_i} = 1$ mmol m^{-3}	80
$k_{S_i} = 8$ mmol m^{-3}	61
$k_{S_i} = 35.5$ mmol m^{-3}	29
Maximum growth rate ω reduced	61
Actual growth rate σ reduced	53
Si:N-uptake ratio r = 1	166
Si:N-uptake ratio r = 2	113
Si:N-uptake ratio r = 8	38
offset of h of 20 m	69
offset of h of 40 m	70

Table 2: Vertically integrated primary production in the reference simulation and the experiments with remineralization and varied sinking rates, varied half saturation constants k_{S_i}, varied growth rates, varied Si:N-uptake ratios r and modified annual cycles of mixed layer depth.

much more pronounced. Annually integrated primary production in experiments with Si:N-uptake ratios r = 8, 4, 2, and 1 ranges from 38 to 166 g C m^{-2} yr^{-1}. Comparing this range to the modest response to a reduced maximum growth rate (Table 2) underlines the ecosystem's high sensitivity to different Si:N-uptake ratios. In the experiment with r=1, which - according to Hutchins and Bruland (1998) and Takeda (1998) - can be identified as a scenario without iron limitation, the maximum simulated biomass is 8 μg/l. This is comparable to experiments of Lancelot et al. (2000) in which a low Fe:C-ratio was assumed. However, as plankton concentrations that high do not meet observations, we conclude that $r = 1$ does not provide a realistic approach for the plankton community at the Antarctic Polar Front.

Results from experiments with an Si:N-uptake ratio of $r = 2$ are closer to observations. Maximum phytoplankton concentrations of about 5 μg/l compare well with an observed maximum phytoplankton concentration of 4.5 μg/l which was found in a watermass near the Polar Front, distinguished from the surroundings by higher concentrations of dissolved iron (de Baar et al., 1995; Bathmann et al., 1997).

Compared to the reference simulation, both experiments can be characterized by higher phyto- and zooplankton biomass, apparently overestimating typical plankton stocks near the Antarctic Polar Front.

In contrast to that, results from experiments with $r = 8$ are quite similar to the simulation with a half saturation constant of 1.1 mmol m^{-3}. Silica depletion starts in spring and persists for an unrealistically long period. However, maximum concentrations of phytoplankton of about 2 μg/l are still in the range of observed values (Tréguer and Jaques, 1992).

From this study we conclude that an Si:N-uptake ratio between 2 and 4 is reasonable for the region of the Polar Front. Furthermore, we suggest that if varying iron supply causes variations of the Si:N-uptake ratio, this will have a much greater impact on primary production and the maximum phytoplankton stock than the modification of the maximum growth rate itself.

The experiments with different annual cycles of mixed layer depth show surprisingly low sensitivity of the annual primary production. Even in case the mixed layer does not get shallower than 60 m plankton concentrations are only little reduced. Apparently, the reduced light supply in the experiments with a deeper summer mixed layer is compensated for by a better nutrient supply. However, the zero-dimensional version of BIMAP provides only a crude approximation of hydrography near the Antarctic Polar Front. Mesoscale variability, reflected by up- and downwelling, eddy pumping and meandering (e.g. Veth et al., 1997) cannot be described. Moreover, no information about horizontal variability is provided. Dafner and Mordasova (1994) pointed out that the horizontal gradient of silicate can reach 7.22 μmol l^{-1} km^{-1} in the Antarctic Polar Front. Nutrient limited pat-

ches of phytoplankton might therefore be surrounded by plankton communities of totally different characteristics.

Conclusions

The zero-dimensional version of BIMAP is able to reproduce characteristic features of the annual cycles of phyto- and zooplankton growth and decay. Experiments with different half saturation constants for silicate uptake indicate that values in the range from 4 to 8 μmol/l allow for a realistic description of the plankton community near the Antarctic Polar Front. Experiments with different scenarios of iron limitation indicate that plankton blooms in the Southern Ocean are affected rather through an increased Si:N-uptake ratio than by a reduced maximum growth rate. Although Si:N-uptake ratios of 2 and 8 do not lead to totally unrealistic results, an Si:N-ratio between 2 and 4 appears to be typical of phytoplankton in this region.

Modifications of the annual cycle of mixed layer depth reveal a surprisingly low response of the simulated ecosystem, so coupling BIMAP to a threedimensional mesoscale ocean model to fully cover effects of hydrography appears to be a natural step to an improved description of the ecosystem at the Antarctic Polar Front.

Acknowledgements

The authors wish to thank the reviewers for their helpful comments. Alfred Wegener Institute publication 1788.

References

Aksnes D.L. (1996) Natural mortality, fecundity and development time in marine planktonic copepods - implications of behaviour. Mar. Ecol. Prog. Ser., 131, 315-316.

de Baar H.J.W. (1994) von Liebig's Law of the minimum and plankton ecology (1899-1991). Progress in Oceanography, 33, 347-386.

de Baar H.J.W., J.T.M. de Jong, D.C.E. Bakker, B.M. Loescher, C.Veth, U. Bathmann, V. Smetacek (1995) Importance of iron for plankton blooms and carbon dioxide drawdown in the Southern Ocean. Nature, 373, 412-415.

Bathmann U.V., R. Scharek, C. Klaas, C.D. Dubischar, V. Smetacek (1997a) Spring development of phytoplankton biomass and composition in major water masses of the Atlantic Sector of the Southern Ocean. Deep-Sea Res. II, 44/1-2, 51-68.

Beckmann, A., H. H. Hellmer, R. Timmermann (1999) A numerical model of the Weddell Sea: large scale circulation and water mass distribution. Journal of Geophysical Research, 104/C10, 23375-23391.

Biddanda B. A. (1988) Microbial aggregation and degradation of phytoplankton-derived detritus in seawater. II. Microbial metabolism. Mar. Ecol. Prog. Ser., 42, 89-95.

Bidle K. D., F. Azam (1999) Accelerated dissolution of diatom silica by marine bacterial assemblages. Nature, 397, 508-512.

Bracher A.U., M.M. Tilzer (2001) Underwater light field and phytoplankton absorbance in different surface water masses of the Atlantic sector of the Southern Ocean. Polar Biology, 24/9, 687-696.

Bracher A. U., B. M. A. Kroon, M.I. Lucas (1999) Primary production, physiological state and composition of phytoplankton in the Atlantic sector of the Southern Ocean. Marine Ecology Progress Series, 190, 1-16.

Brzezinski M. A. (1985) The Si:C:N ratio of marine diatoms. Interspecific variability and the effect of some environmental variables. J. Phycol., 21, 347-357.

Dafner E. V., N. V. Mordasova (1994) Influence of biotic factors on the hydrochemical structure of surface water in the Polar Frontal Zone of the Atlantic Antarctic. Marine Chemistry, 45, 137-148.

DeMaster D. J., T. M. Nelson, S. L. Harden, C. A. Nittrouer (1991) The cycling and accumulation of biogenic silica and organic carbon in Antarctic deep-sea and continental margin environments. Marine Chemistry, 35, 489-502.

Dubischar C.D., U. V. Bathmann (1997) Grazing impact of copepods and salps on phytoplankton in the Atlantic sector of the Southern Ocean. Deep-Sea Research, 44/1-2, 415-434.

Eppley R.W. (1972) Temperature and phytoplankton growth in the sea. Fish. Bull., 70, 1063-1085.

Evans G.T., J. S. Parslow (1985) A model of annual plankton cycles. Biol. Oceanogr., 3, 327-347.

Fasham M. J. R., H. W. Ducklow, S. M. McKelvie (1990) A nitrogen-based model of plankton dynamics in the oceanic mixed layer. Journal of Marine Research, 48, 591-639.

Fasham M. J. R. (1995) Variations in the seasonal cycle of biological production in subarctic oceans: A model sensitivity analysis. Deep-Sea Res. I, 42/7, 1111-1149.

Foxton P. (1966) The distribution and life history of $Salpa\ thompsoni$ (Foxton) with observations on a related species $Salpa\ gerlachei$ (Foxton). Discovery reports, 34, 1-116.

Fransz H. G., S. R. Gonzalez (1997) Latitudanal metazoan plankton zones in the Antarctic Circumpolar Current along 6°W during austral spring 1992. Deep Sea Research, 44/1-2, 395-414.

Fronemann P. W., R. Perissinotto, C.D. McQuaid, R.K. Laubscher (1995) Summer distribution of netphytoplankton in the Atlantic sector of the Southern Ocean. Polar Biology, 15, 77-84.

Gran H. H. (1931) On the conditions for the production of plankton in the sea. Rapports et Procès-verbaux des Réunions, Conseil International pour l'exploration de la Mer, 75, 37-46.

Haidvogel D.B., J. L. Wilkin, R. E. Young (1991) A semi-spectral primitive equation ocean circulation model using vertical sigma and orthogonal curvilinear horizontal coordinates. J. Comput. Phys., 94, 151-185.

Hart T. J. (1934) On the phytoplankton of the South-West Atlantic and the Bellingshausen Sea, 1929-1931. Discovery Reports, 8, 1-268.

Hartmann C, B. Hollmann, G. Kattner, K.-U. Richter, A. Terbrüggen (1997) Nutrients, Dissolved and Particulate Matter. In: Reports on Polar Research: The expedition Antarktis XIII/1-2 of the research vessel "Polarstern" in 1995/96, Bathmann U. V., M. Lucas, V. Smetacek, with contributions of the participants (eds.), 44-52.

Hense I., U. Bathmann, C. Hartmann, V. Strass, V. Smetacek (1998) Spiny phytoplankton-slowing down the carbon pump in the Southern Ocean? published as a supplement to EOS, Transactions, American Geophysical Union, 79/1, OS31C-10.

Huntley M. E., M. Zhou, M. D. G. Lopez (1994) $Calanoides\ acutus$ in Gerlache Strait, Antarctica II. Solving an inverse problem in population dynamics. Deep-Sea Research I, 41, 209-227.

Huntley M. E., W. Nordhausen (1995) Ammonium cycling by Antarctic zooplankton in winter. Marine Biology, 121, 457-467.

Hutchins A. D., K. W. Bruland (1998) Iron-limited diatom growth and Si:N uptake ratios in a coastal upwelling regime. Nature, 393, 561-564.

Jaques G. (1983) Some ecophysiological Aspects of the Antarctic Phytoplankton. Polar Biology, 2, 27-33.

Jerlov N.G. (1976) Marine Optics. Elsevier.

Jitts H. R., A. Morel, Y. Saijo (1976) The relation of oceanic primary production to available photosynthetic irradiance. Aust. J. Mar. Fresh. Res., 27, 441-454.

Laevastu T. (1960) Factors affecting the temperature of the surface layer of the sea. Comment. Phys. Math., 25/1.

Lancelot C., E. Hannon, S. Becquevort, C. Veth, H.J.W. de Baar (2000) Modeling phytoplankton blooms and carbon export production in the Southern Ocean: dominant controls by light and iron in the Atlantic sector in Austral spring 1992. Deep-Sea Res., 47/9, 1621-1662.

Laubscher R. K., R. Perissinotto, C. D. McQuaid (1993) Phytoplankton production and biomass at frontal zones in the Atlantic sector of the Southern Ocean. Polar Biol., 13, 471-481.

Lemke P., W.B. Owens, W.D. Hibler, III (1990) A coupled sea ice - mixed layer - pycnocline model for the Weddell Sea. Journal of Geophysical Research, 95/C6, 9513-9525.

Lemke P., with contributions of the participants (1992) The expedition Antarktis X/4 of the research vessel ”Polarstern” in 1992. Reports on Polar Research, 140, 1-90.

Liebig von J. (1840) Organic chemistry and its application to agriculture and physiology. Taylor and Walton, London.

Lorenzen C. J. (1972) Extiction of light in the ocean by phytoplankton. J. Cons., 34, 262-267.

Löscher B.M., H. J. W. de Baar, J. T. M. de Jong, C. Veth, F. Dehairs (1997) The distribution of Fe in the Antarctic Circumpolar Current. Deep-Sea Res. II, 44/1-2, 143-187.

Lutjeharms J. R. E., N. M. Walter, B. R. Allanson (1985) Oceanic frontal systems and biological enhancement. In: Antarctic nutrient cycles and food webs, W.R. Siegfried, P.R. Condy, R. M. Laws (eds.). Springer Verlag, 11-21.

Martin J. H., S. E. Fitzwater (1988) Iron deficiency limits phytoplankton growth in the northeast Pacific subarctic. Nature, 331, 341-343.

Minas H. J., M. Minas (1992) Net community production in "High Nutrient-Low Chlorophyll" waters of the tropical and Antarctic Oceans: grazing versus iron hypothesis. Oceanologica Acta, 15, 145-162.

Nelson D. M., L.I. Gordon (1982) Production and pelagic dissolution of biogenic silica in the Southern Ocean. Geochim. Cosmochim. Acta, 46, 491-501.

Nelson D. M., W.O. Smith Jr. (1986) Phytoplankton bloom dynamics of the western Ross Sea ice edge, II, Mesoscale cycling of nitrogen and silicon. Deep-Sea Res., 33/1, 1389-1412.

Nelson D. M., P. Tréguer (1992) Role of silicon as a limiting nutrient to Antarctic diatoms: evidence from kinetic studies in the Ross Sea ice-edge zone. Mar. Ecol. Prog. Ser., 80, 255-264.

Nelson D. M., P. Tréguer, M.A. Brzezinski, A. Leynaert, B. Quéguiner (1995) Production and dissolution of biogenic silica in the ocean: Revised global estimates, comparison with regional data and relationship to biogenic sedimentation. Global Biogeochem. Cycle, 9/3, 359-372.

Paffenhoefer G. A., R. P. Harris (1976) Feeding, growth and reproduction of the marine planktonic copepod Pseudocalanus elongatus. Journal of the Marine Biological Association of the United Kingdom 56, 327-344.

Peters E., D. N.Thomas (1996) Prolonged darkness and diatom mortality I: Marine Antarctic species. J. of Exp. Mar. Biol. Ecol., 207, 25-41.

Pondaven P., C. Fravalo, D. Ruiz-Pino, P. Tréguer, B. Quéguiner, C. Jeandel (1998) Modelling the silica pump in the Permanently Open Ocean Zone of the Southern Ocean. J. Mar. Systems, 17, 587-619.

Pondaven P., D. Ruiz-Pino, J. N. Druon, C. Fravalo, P. Tréguer (1999) Factors controlling silicon and nitrogen biogeochemical cycles in high nutrient, low chlorophyll systems (the Southern Ocean and the North Pacific): Comparison with a mesotrophic system (the North Atlantic). Deep-Sea-Res. I, 46, 1923-1968.

Quéguiner B., P. Tréguer, I. Peeken, R. Scharek (1997) Biogeochemical Dynamics and the Silicon Cycle in the Atlantic Sector of the Southern Ocean During Austral Spring 1992. Deep-Sea Research, 44/2, 69-90.

Sakshaug E., O. Holm-Hansen (1984) Factors governing pelagic production in polar oceans. In: Marine phytoplankton and productivity. Lecture notes on coastel and estuarine studies, 8, O. Holm-Hansen, L. Bolis, R. Gilles (eds.). Springer Verlag, 1-18.

Schnack S. B. (1985) Feeding by $Euphausia\ superba$ and copepod species in response to varying concentrations of phytoplankton. In: Antarctic nutrient cycles and food webs, W.R. Siegfried, P.R. Condy, R.M. Laws (eds.). Springer Verlag, 311-323.

Shiomoto A., H. Ishii (1995) Distribution of biogenic silica and particulate organic matter in coastal and oceanic surface waters off the South Shetland Islands in summer. Polar Biol., 15, 105-113.

Smetacek V., U. Passow (1990) Spring bloom initiation and Sverdrup' s critical-depth model. Limnol. Oceanogr., 35/1, 228-234.

Smetacek V., H. J. W. de Baar, U. V. Bathmann, K. Lochte, M. M. Rutgers van der Loeff (1997) Ecology and biogeochemistry of the Antarctic Circumpolar Current during austral spring: a summary of Southern Ocean JGOFS cruise ANT X/6 of R.V. Polarstern. Deep-Sea Res. II, 44/1-2, 1-21.

Smetacek V. (1999) Diatoms and the Ocean Carbon Cycle. Protist, 150, 25-32.

Sommer U. (1986) Nitrate- and silicate-competition among antarctic phytoplankton. Marine Biology, 91, 345-351.

Sommer U. (1991) Comparative nutrient status and competitive interactions of two Antarctic diatoms ($Corethron\ criophilum$ and $Thalassiothrix\ antarctica$). J. Plankton Res., 13, 61-75.

Song, Y., D. B. Haidvogel (1994) A semi-implicit ocean circulation model using a generalized topography-following coordinate. J. Comput. Phys., 115, 228-244.

Steele J. H., E. W. Henderson (1992) The role of predation in plankton models. J. Plankton Res., 14, 157-172.

Sverdrup H. U. (1953) On conditions for the vernal blooming of phytoplankton. J. Cons. Cons. Int. Explo. Mer., 18, 287-295.

Takeda S. (1998) Influence of iron variability on nutrient consumption ratio of diatoms in oceanic waters. Nature, 393, 774-777.

Tréguer J., A. Kamatami, S. Gueneley, B. Quéguiner (1989) Kinetics of dissolution of Antarctic diatoms frustules and the biogeochemical cycle of silicon in the Southern Ocean. Polar Biol., 9, 397-403.

Tréguer J., G. Jacques, (1992) Dynamics of nutrients and phytoplankton, and fluxes of carbon, nitrogen and silicon in the Antarctic Ocean. Polar Biology, 12, 149-162.

Veth C., I. Peeken, R. Scharek (1997) Physical anatomy of fronts and surface waters in the ACC near the 6°W meridian during austral spring 1992.. Deep-Sea Research, 44/1-2, 23-50.

Williams P. J. (1990) The importance of losses during microbial growth: commentary on the physiology, measurement and ecology of the release of dissolved organic material. Marine Microbial Food Webs, 4, 175-206.

WOCE Hydrographic Program Office, *http://whpo.ucsd.edu/index.html*, 1997.

Zillmann J. W. (1981) A study of some aspects of the radiation and heat budgets of the southern hemisphere oceans. In: Meteorological study, 26, Bureau of Meteorology, Dept. of the Interior, Canberra, Australia, 526pp.

With the knowledge we now have of the distribution of nitrates and phosphates, we should expect that the diatoms would develop simultaneously over the whole area, and that the Atlantic waters outside the coastal Bank should have a production as rich or richer than the waters of the coastal current. As this is not the case, we are ... forced to suppose that there is one or more factors limiting or stimulating growth of the phytoplankton besides those which we have until yet taken into account.

Gran, 1930

Teil III

Regional ecosystem dynamics in the ACC: Simulations with a three-dimensional ocean-plankton model

Inga Hense, Ralph Timmermann, Aike Beckmann and Ulrich V. Bathmann

Alfred-Wegener-Institut für Polar- und Meeresforschung, Bremerhaven, Germany

submitted September 27, 2001 to Progress in Oceanography

Abstract

Within the high nutrient — low chlorophyll regime of the Antarctic Circumpolar Current (ACC), high phytoplankton concentrations are frequently observed in the vicinity of the Antarctic Polar Front (APF). As is typical for frontal systems, hydrography in this region is characterized by meanders and eddies as well as up- and downwelling cells which redistribute nutrients and influence the depth of the euphotic zone.

To study the processes leading to the observed phytoplankton distribution, a coupled ocean plankton model for ecosystem studies in the ACC has been developed. The ocean component is an eddy-resolving version of the s-Coordinate Primitive Equation Model (SPEM). The model has a horizontal resolution of 1/12° and a vertical resolution increased near the surface. The biological model (BIMAP) comprises two biogeochemical cycles - silica and nitrogen - and a prognostic iron compartment to include possible effects of micronutrient limitation.

Model results indicate that part of the ecosystem's regional variability can be attributed to the effect of vertical and horizontal advection. However, frontal dynamics alone cannot explain the observed enhanced concentrations of phytoplankton biomass near the APF and the minima in the northern and southern ACC. Simulations which neglect possible effects of iron limitation cannot reproduce the observed large scale phytoplankton distribution. Only when iron limitation is taken into account, the model simulates plankton concentrations in close agreement with observations during the SO-JGOFS cruises. While in the northern ACC phytoplankton growth is limited by silicate, primary production is limited by iron limitation south of the APF. Near the APF, mesoscale iron upwelling enhances primary production, leading to increased phyto- and zooplankton biomass. The

meridional structure with two plankton maxima is closely linked to the cross-front overturning circulation. This double-cell circulation with two upwelling branches is caused by the northward sloping large scale bottom topography.

Keywords: Antarctic Polar Front, ocean-plankton model, phytoplankton distribution, iron limitation

1 Introduction

After the *Discovery* cruises of 1929-1931 in the southwest Atlantic and the Bellinghausen Sea, Hart (1934) pointed out the discrepancy between the high stock of nutrients and low abundance of phytoplankton, and suggested that trace elements like iron could be responsible for the low phytoplankton stock. Since 1934 the reasons for the so called "Antarctic Paradox" are a matter of debate and several hypotheses about the "mystery" HNLC (high nutrient low chlorophyll) area in the Southern Ocean have been set up. Otherwise, satellite images (Sullivan, 1993; Stramski et al., 1999) and observations during field studies (e.g. Bathmann et al., 1997) distinguish the region of the Antarctic Polar Front as an area with higher phytoplankton stocks compared to the surrounding HNLC water, leading to the question about the dominant factors controlling the development of phytoplankton blooms.

First of all, the special hydrographic conditions at the Antarctic Polar Front are discussed to be responsible for the observed enhancement of primary production. The Antarctic Polar Front (APF) is located in the centre of the Antarctic Circumpolar Current (ACC), which is the earth's only closed zonal oceanic current system (Burkov, 1993). The APF was first termed by Wyrtki (1960) who renamed the former expression of the Antarctic Convergence. Since then, several definitions of the Antarctic Polar Front have been specified (see review of Belkin & Gordon, 1996); the most common defines the APF as the northernmost extent of the subsurface 2°C isotherme (Botnikov, 1963). The position of the front is influenced by local bathymetry (e.g. Trathan et al., 1997) and may vary due to fluctuations of the surface wind stress (e.g. Smith & Fandry, 1978).

At the APF, relatively warm water from the north meets colder water from the south which is subducted due to the large scale convergence and contributes to the formation of the Antarctic Intermediate Water. This process, however, occurs on much longer time scales than those important for plankton dynamics. As strong meridional gradients of temperature and salinity are found down to the bottom, the APF has a strong expression throughout the water column (Gouretski & Danilov, 1994). The strong horizontal density gradient leads to baroclinic instability which in some regions is stimulated by local bottom topography (Chelton et al., 1990;

Veth et al., 1997). As a consequence, meander currents establish and isolated eddies are formed. Warm or cold core eddies (or rings) on either side of the front are frequently observed (Ikeda et al., 1989; Gouretski & Danilov, 1994). Eddies are often assumed to promote phytoplankton growth as they contribute to cross frontal and vertical nutrient exchange (e.g. Pingree et al., 1979; Flierl & Davis, 1993). However, enhanced phytoplankton biomass in the vicinity of the Antarctic Polar Front is also observed outside of eddies.

Other authors suggest that the mixed layer depth is influenced by mesoscale frontal dynamics. Strass et al. (2001) hypothesize that cross-frontal circulation leads to a shallow mixed layer not only in the upwelling areas but also directly above the front. Light limitation due to a deep mixed layer is discussed to be a dominant factor in controlling phytoplankton blooms in the Southern Ocean (e.g. Sakshaug & Holm-Hansen, 1984; Smith & Nelson, 1985; Mitchell et al., 1991), where the wind stress is extraordinarily strong compared to other regions of the world ocean (Wearn & Baker, 1981; Gille et al., 2001) and deep vertical mixing is observed; a shallow mixed layer near the front would thus promote phytoplankton growth.

Another effect of frontal dynamics on phytoplankton growth in the Antarctic Polar Front is the vertical nutrient transport arising from up- and downwelling events in eddies or due to the meandering current. Mesoscale vertical velocities in frontal regions are in the range between 1 m/d and more than 100 m/d (Eriksen et al., 1991; Pollard & Regier, 1992; Strass, 1994) and therefore affect hydrography on time scales corresponding to those of phytoplankton growth. Consequently, nutrient upwelling at hydrographic fronts has been described to promote primary production (Allanson & Parker, 1983; Moon et al., 1998; Fronemann et al., 1999). Model experiments for the sub-tropics and mid-latitudes suggest that eddy pumping can contribute up to one third of nutrient fluxes into surface layers (Oschlies & Garcon, 1998) and can increase primary production by roughly 10 %, locally even up to 100 % (Spall & Richards, 2000).

Apart from macronutrients, primary production may be limited by the availability of micronutrients like copper, nickel, iron or zink (Morel et al., 1991). Martin (1990) proposes that iron limitation is the dominant factor controlling phytoplankton biomass in the HNLC areas. Indeed, laboratory and field studies (not only in the Southern Ocean) have shown that phytoplankton growth is increased in iron enriched water (e.g. Zettler et al., 1996; Scharek et al., 1997), while iron deficiency limits phytoplankton growth (e.g. Hutchins et al., 1999). A mesoscale iron fertilization experiment in the Indian sector of the Southern Ocean (SOIREE - Southern Ocean Iron Release Experiment) produced a significant increase of phytoplankton biomass (Boyd et al., 2000).

In large parts of the surface ocean, aeolian mineral dust is regarded as the main source for iron (e.g. Zhuang et al., 1992). Low aeolian (iron-rich) dust input due

to the absence of continents upwind have been discussed to explain the HNLC area of the Southern Ocean (Martin et al., 1990; Kumar et al., 1995).

The observation of enhanced iron concentrations (Löscher et al., 1997) near melting icebergs in the vicinity of the APF led to the hypothesis that an enhanced iron supply may cause the observed increase of phytoplankton biomass in that region (de Baar et al., 1995; Bathmann et al., 1997). However, as the effect of melting icebergs is purely local and intermittent (Löscher et al., 1997), it cannot cause the regularly observed enhanced biologic activity near the APF. Thus, iron upwelling due to mesoscale frontal dynamics appears to be the only plausible source of regionally enhanced iron concentrations.

Iron upwelling has been reported to promote phytoplankton blooms in various oceanic regions (e.g., Gordon et al., 1998). Even a small transport of iron into the euphotic zone may have a significant effect on carbon export (Coale et al., 1996). Recent studies indicate that 70-80 % of the global carbon export production result from upwelling of dissolved iron (Archer & Johnson, 2000).

To investigate which physical or biogeochemical factors may be responsible for higher chlorophyll concentrations in the frontal area, a modified version of the Biological Model for the Antarctic Polar Front (BIMAP; Hense et al., 2000) is coupled to a high resolution application of the ocean circulation model SPEM (Haidvogel et al., 1991). Although we use a state-of-the-art primitive equation ocean model in an eddy resolving configuration, our main focus here is not the investigation of frontal dynamics. Instead, we use the model to provide adequate transport, mixing rates and boundary conditions for the ecosystem model.

The paper starts with a review of recent observations which we use for assessment and validation of model results. Chapter 3 gives a description of the coupled model. Results from experiments with different nutrient limitation scenarios are presented in chapter 4. Simulated chlorophyll concentrations of the different experiments are compared to observations. The effect of iron upwelling on primary production and plankton biomass is quantified. The paper closes with a discussion and conclusions.

2 Observations

Observed summer surface chlorophyll concentrations in the region of the Antarctic Polar Front (APF) reveal a mesoscale meandering structure and a band of high phytoplankton biomass with concentrations up to 1.6 μg Chl a/l between 50°S and 51°S (Fig. 1).

A comparison with hydrographic observations (Hense, 1997; Strass et al., 2001) indicates that this band was aligned with the location of the APF, with the maximum concentrations directly south of the northernmost occurence of the

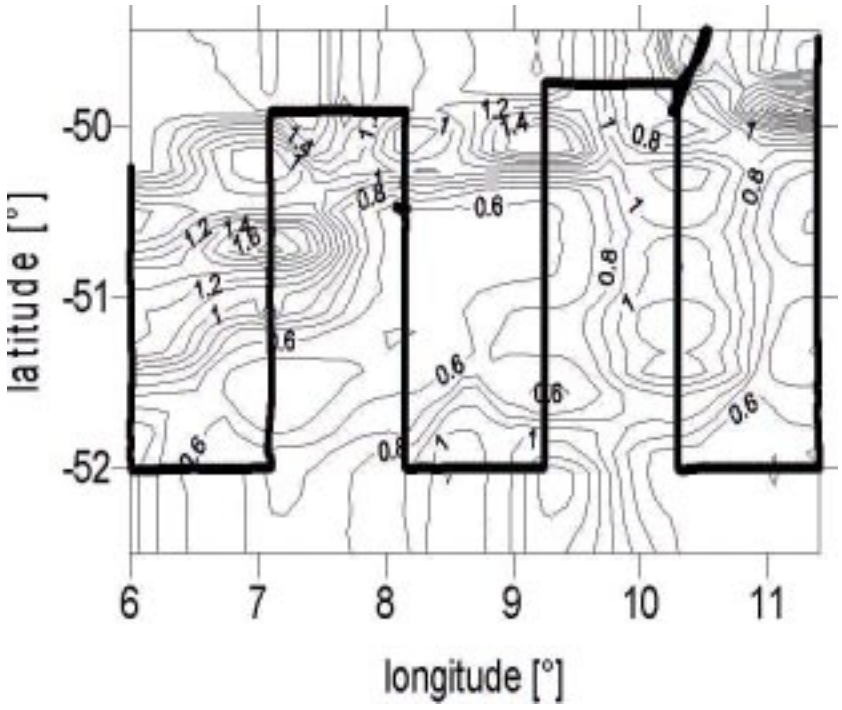

Figure 1: Horizontal distribution of chlorophyll concentration [μg/l] at the surface in December/January 1995/96, after Hense (1997). Data were collected during Polarstern cruise ANT XIII/2 (Bathmann et al., 1997b)

2°C-isotherme in 200 m depth, above the belt of large horizontal temperature gradients.

Similar correlations between hydrography and phytoplankton distribution can be found in meridional transects from different Southern Ocean-JGOFS cruises (Bathmann et al. 1997a, 1997b; Hense 1997) which show an enhanced phytoplankton biomass with typical surface concentrations between 1.5 and 2.5 μg Chl a/l near the APF while low chlorophyll concentrations with values below 1 μg Chl a/l occur further north and south (Fig. 2).

Differences between these two datasets may be due to different locations of the Polar Front, seasonal variations or interannual variability. They illustrate the natural variability of the system - both datasets represent merely snapshots of a highly diverse dynamic system.

Like the concentrations of phytoplankton, the distributions of nutrients are correlated with mesoscale hydrography (Hartmann et al., 1997) with silicate concentrations featuring strong meridional gradients. Typically, silicate at the APF is nearly depleted in summer with values < 1 μmol/l in areas with high phytoplankton concentration, while nitrate concentrations at the APF remain high with

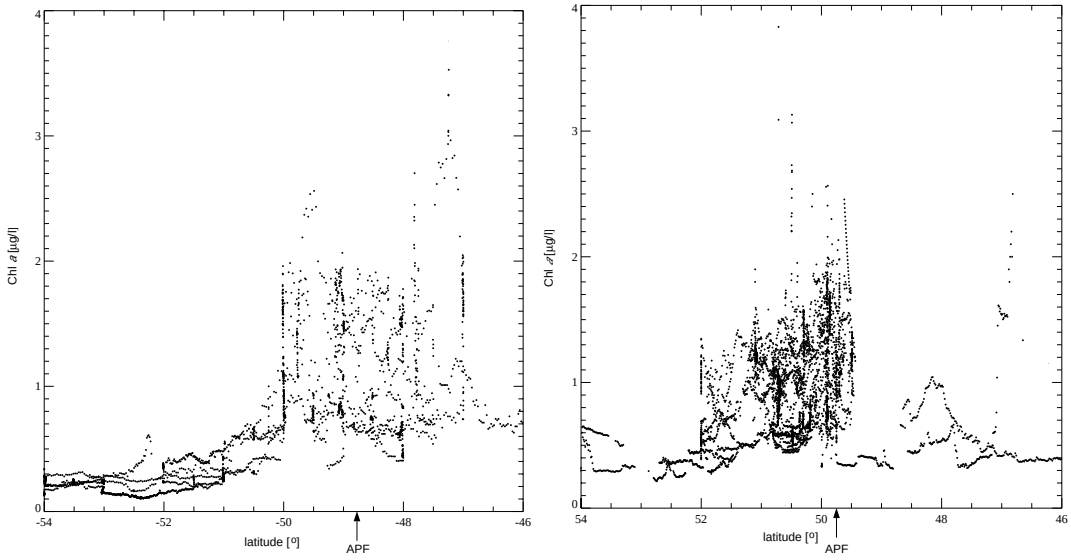

Figure 2: Meridional transects of surface chlorophyll concentration [μg/l] observed a) in October/November 1992 [after Bathmann et al., 1997a] and b) in December/January 1995/96 [after Hense, 1997].

values exceeding 20 μmol/l . In the southern ACC, typical concentrations are 20-30 μmol/l for both nitrate and silicate (Hartmann et al, 1997; Loescher et al., 1997; Veth et al., 1997); silicate concentration further increases to the south.

3 Model Configuration

3.1 Model Concept

Following the pioneering NPZD (nitrogen - phytoplankton - zooplankton - detritus) model of Fasham et al. (1990) several marine plankton models with different complexity have been developed. The most complex marine biological model is certainly ERSEM (Baretta et al., 1995; Ebenhoeh, 1996), with a large number of state variables including also benthic processes. Due to limited computing resources, this model is restricted to regional applications like in the North Sea or the Mediterranian Sea.

For the Southern Ocean, one-dimensional plankton models like SWAMCO (Lancelot et al., 2000) or the KERFIX simulation of Pondaven et al. (1998) have been used to investigate ecosystem dynamics in the context of research cruises or station time series. The physical environment in these models has been reduced to

a variability of the mixed layer depth.

On the other hand, coupled ocean-ecosystem models with simple parameterizations of biogeochemical fluxes have been developed for global (Six & Maier-Reimer, 1996) and regional applications (Oschlies & Garçon, 1999). Typically, horizontal resolution of these models is 1/3 to 3° and thus far too coarse to resolve mesoscale dynamics.

Our concept follows a third approach: We here present an ecosystem model of intermediate complexity which comprises two biogeochemical cycles and considers possible iron limitations. Wherever possible we use observations to derive parameters for the different fluxes of nutrients and organic matter. While the model is complex enough to cover many aspects of the nonlinear ecosystem dynamics, it is efficient with respect to computing resources which allows coupling to a three-dimensional, eddy-resolving ocean model, and integration for several annual cycles.

3.2 The ecosystem model

The Biological Model for the Antarctic Polar Front (BIMAP) comprises the biogeochemical cycles of silica and nitrogen. Following Fasham et al. (1990), nitrogen is distributed between the compartments phytoplankton (P), zooplankton (Z), the nitrogen-consisting detritus (D_N), and the nutrients nitrate (N_n) and ammonium (N_a). As the model is supposed to reflect the plankton community in the Antarctic Polar Front which largely consists of diatoms, a silica cycle is coupled to this by using a fixed Si:N-uptake ratio for phytoplankton growth; silicate concentration and the silica part of detritus are denoted as Si and D_{Si}, respectively. The model has been adopted from the zerodimensional simulations of Hense et al. (2000), and, for model experiments considering iron limitation, has been complemented by a compartment for dissolved iron (Fe).

Here, we would like to give the complete set of equations. Parameter values and references are combined in Table 1. For further information of how the individual values were derived from the different measurements the reader is refered to Hense et al. (2000).

3.2.1 Prognostic Equations

Evolution of any biological tracer (T_b) in the three-dimensional model is determined by the nonlinear advection-diffusion equation

$$\frac{\partial T_b}{\partial t} + \vec{u} \cdot \nabla T_b = \left(\frac{\partial T_b}{\partial t} \right)_b + \mathcal{D}^{T_b} \tag{14}$$

which on the left hand side features the local time derivative and the effect of advection. The right hand side includes changes due to biological processes which

1. Phytoplankton	
Initial slope of the PI-curve (Bracher et al., 1999)	$\alpha = 0.027 \frac{\mathrm{m}^2}{\mathrm{W \cdot d}}$
Self-shading parameter (Bracher et al., 1999)	$k_c = 0.07 \frac{m^2}{\mathrm{mmol}}$
Maximum growth rate (Eppley, 1972)	V_P = 1.2 d^{-1}
Mortality rate (Hense et al., 2000)	μ_P = 0.05 d^{-1}
Half sat. const. for silicate (Nelson & Tréguer, 1992)	k_{S_i} = 4.6 μmol/l
Half sat. const. for nitrate (Sommer, 1986)	k_{N_N} = 0.3 μmol/l
Half sat. const. for ammonium	k_{N_a} = 0.3 μmol/l
Half sat. const. for iron (Landry et al., 1997)	k_{Fe} = 0.12 nmol/l
Exudation coefficient (Williams, 1990)	$\gamma = 0.05$ d^{-1}
2. Zooplankton	
Assimilation efficiency (Schnack, 1985)	$\beta = 0.67$ d^{-1}
Excretion rate (Huntley & Nordhausen, 1995)	ε = 0.0078 d^{-1}
Mortality rate (Hense et al., 2000)	$\mu_Z = 2.0 \frac{l}{\mu \mathrm{mol \cdot d}}$
3. Nutrients	
Si:N uptake ratio (Hense et al.,2000)	$r_{Si} = 3 \ \frac{mol}{mol}$
Fe:N uptake ratio (Sarthou et al., 1997)	$r_{Fe} = 2.65 \cdot 10^{-5} \ \frac{mol}{mol}$
4. Detritus	
Silica dissolution rate (Tréguer et al., 1989)	τ_{S_i} = 0.018 d^{-1}
Remineralization rate (Biddanda, 1988)	τ_{N_a} = 0.07 d^{-1}

Table 1: Parameter values for reference experiment.

are described below. Advection of biological tracers is computed from the simulated ocean currents $\vec{u}$; the divergence $\mathcal{D}^{T_b}$ of turbulent fluxes is parameterized using the ocean model diffusivities ν^T with

$$\mathcal{D}^{T_b} = \nabla(\nu^T \nabla T_b). \tag{15}$$

3.2.2 Parameterization of biochemical fluxes

Phytoplankton

Local changes in phytoplankton concentration (P) are due to primary production $(1-\gamma)\cdot\sigma\cdot P$, grazing by zooplankton g_Z and natural mortality $\mu_P \cdot P$:

$$\left(\frac{\partial P}{\partial t}\right)_b = (1-\gamma)\cdot\sigma\cdot P - g_Z - \mu_P \cdot P \tag{16}$$

where γ is the exudation coefficient. The growth rate σ consists of the maximum (light dependent) growth rate ω and a possible nutrient limitation η:

$$\sigma = \omega \cdot \eta \quad \text{with} \quad 0 < \eta < 1. \tag{17}$$

Using the law of minimum (Liebig, 1840), the nutrient limited growth rate for diatoms considers possible limitation by nitrate, silicate or iron:

$$\eta = \min\left(\frac{N_n}{k_{N_n}+N_n}, \frac{Si}{k_{Si}+Si}, \frac{Fe}{k_{Fe}+Fe}\right). \tag{18}$$

A Michaelis-Menten type relation is assumed for all nutrients using the half saturation constants k_{N_n}, k_{Si} and k_{Fe}.

Following Evans and Parslow (1985) and Fasham et al. (1990) the light dependent growth rate ω is described by

$$\omega = \frac{1}{|z_2 - z_1|}\cdot\int_{z_1}^{z_2}\frac{V_P\cdot\alpha\cdot I(z,t)}{\sqrt{V_P^2+\alpha^2\cdot I^2(z,t)}}\cdot e^{-(k_w+k_c\cdot P)\cdot z}dz \tag{19}$$

where z_1 and z_2 give the depth interval over which primary production is integrated and $I(z,t)$ is the intensity of the photosynthetic active radiation (PAR) in a depth z below the surface. For the conversion from solar radiation to PAR we use a factor of 43 % according to Jerlov (1976) and Jitts et al. (1976). As the Southern Ocean belongs to oceanic type I (Jerlov, 1976; Bracher et al., 2001), we chose $k_w = 0.04$ m^{-1} (Lorenzen, 1972) as the attenuation coefficient of sea water. Further parameters are the initial slope α of the PI-curve, the self-shading parameter k_c and the maximum growth rate V_p.

The exudation of dissolved organic nitrogen (DON) during the cell division is parameterized as $\gamma\cdot\sigma\cdot P$ and is directly led into the ammonium pool.

Zooplankton

The zooplankton (Z) equation considers grazing and the mortality (μ_Z) and excretion (ε) rates using

$$\left(\frac{\partial Z}{\partial t}\right)_b = \beta \cdot g_Z - \mu_Z \cdot Z^2 - \varepsilon \cdot Z \tag{20}$$

where $\beta \cdot g_Z$ gives the growth of zooplankton biomass due to grazing while $(1-\beta) \cdot g_Z$ is the part of ingested food which is excreted as faecal pellets. The grazing rate g_Z has been calculated from experiments with the abundant herbivorous copepod species *Calanoides acutus* (Schnack, 1985) and reads

$$g_Z = \frac{0.063 \cdot 10^{-3}}{0.14 \cdot 86400\mathrm{s}} \cdot \left(79.5 \frac{\mathrm{m}^3}{\mathrm{mmol}} \cdot P\right)^{1.3} \cdot Z \tag{21}$$

(Hense et al., 2000). While the excretion is assumed to be proportional to Z, mortality is parameterized as a quadratic function of zooplankton concentration.

Nutrients

Local changes of the nutrient concentrations (N_n, N_a, Si, Fe) are due to uptake by phytoplankton $\sigma \cdot P$, exudation $\gamma \cdot \sigma \cdot P$, excretion $\varepsilon \cdot Z$ and remineralization τD. Although we do not allow ammonium supply to limit phytoplankton growth, the uptake ratio between ammonium and nitrate is determined using their concentrations N_a and N_n and half saturation constants k_{N_a} and k_{N_n}:

$$\left(\frac{\partial N_n}{\partial t}\right)_b = -\sigma \cdot \frac{\frac{N_n}{k_{N_n}+N_n}}{\frac{N_n}{k_{N_n}+N_n} + \frac{N_a}{k_{N_a}+N_a}} \cdot P \tag{22}$$

$$\left(\frac{\partial N_a}{\partial t}\right)_b = -\sigma \cdot \frac{\frac{N_a}{k_{N_a}+N_a}}{\frac{N_n}{k_{N_n}+N_n} + \frac{N_a}{k_{N_a}+N_a}} \cdot P + \gamma \cdot \sigma \cdot P + \varepsilon \cdot Z + \tau_{N_a} D_N \tag{23}$$

$$\left(\frac{\partial Si}{\partial t}\right)_b = -r_{Si} \cdot \sigma \cdot P + \tau_{Si} D_{Si} \tag{24}$$

$$\left(\frac{\partial Fe}{\partial t}\right)_b = -r_{Fe} \cdot \sigma \cdot P \tag{25}$$

Following the studies of Hense et al. (2000) who have shown that molar Si/N uptake ratios between 2 and 4 give resonable results in a zerodimensional ecosystem model, we conduct the reference experiment with a molar Si/N uptake ratio r_{Si}=3 but carry out two additional experiments with r_{Si}=2 and r_{Si}=4.

Remineralization of nutrients is denoted as $\tau_{N_a} D_N$ for ammomium and $\tau_{Si} D_{Si}$ for silicate. As quantitative knowledge about the time scales involved is

not available, we neglect iron remineralization. Thus, biology only acts as a sink for iron, while the only source is advection and diffusion from the deep ocean.

Iron/carbon uptake ratios have been derived from measurements in the Indian Sector of the Southern Ocean by Sarthou et al. (1997). Using the Redfield ratio between carbon and nitrogen we converted their estimates to $r_{Fe} = 2.65 \cdot 10^{-5}$ [Mol/Mol]. For iron limitation, we use a half-saturation constant k_{Fe} = 0.12 nmol/l which was derived from grow-out experiments with diatoms in the central equatorial Pacific (Landry et al., 1997). Compared to the model experiments of Lancelot et al. (2000) who chose k_{Fe} = 1.2 nmol/l using measurements from a Southern Ocean JGOFS cruise in 1992 (Scharek et al., 1997), our value seems to be rather small and from the wrong region. However, it appears that the quality of iron analyses back in 1992 is not sufficient to be used for quantitative deduction of growth rates (Scharek, pers. comm.). So, given the much larger database and the self-consistence of the Landry et al. (1997) estimation, we decided to use their data for the standard iron simulation. We will, however, adress this subject in a series of sensitivity experiments.

Detritus

Although remineralization appeared to have a rather low effect on the development of phytoplankton blooms in a zerodimensional model (Hense et al., 2000), detritus is considered to close the biogeochemical cycles in the 3-dimensional version. The detritus pool is decomposed into a nitrogen part D_N and a silica part D_{Si}. The evolution of these compartments follows the equations

$$\left(\frac{\partial D_N}{\partial t}\right)_b = \mu_P \cdot P + \mu_Z \cdot Z + (1-\beta) \cdot g_Z - r_{l_N}\, \tau_{N_a}\, D_N \qquad (26)$$

$$\left(\frac{\partial D_{Si}}{\partial t}\right)_b = (\mu_P \cdot P + \mu_Z \cdot Z + g_Z) \cdot r_{Si} \quad - r_{l_{Si}}\, \tau_{Si}\, D_{Si} \qquad (27)$$

and includes mortality of phyto- and zooplankton, production of faecal pellets and remineralization with the time scales τ_{N_a} and τ_{Si} (Hense et al., 2000).

As only roughly 50 % of the produced biogenic silica and 80 % of particulate organic nitrogen are remineralized in the upper water column while the rest of it sinks down to the deeper ocean (Nelson et al., 1995; Pondaven et al., 1999), detritus loss and remineralization fluxes are linked by a factor 2 for silica and a factor 1.25 for nitrogen based detritus. We use these numbers for the loss-to-remineralization ratios $r_{l_{Si}}$ and r_{l_N}, respectively. The drawback in this formulation is that we ignore the remineralization and dissolution in deeper layers. However, as the ocean in the investigated area is roughly 4000 m deep and model experiments are not run for more than 3 years, we do not expect significant differences in nutrient upwelling to be caused by this simplification.

3.3 The Ocean Model

The ocean model SPEM (Haidvogel et al., 1991; Beckmann et al., 1999) is based on the primitive equations in hydrostatic approximation and uses a terrain-following vertical coordinate. Horizontal and vertical advection are computed using an explicit 2nd order finite differences scheme (Haidvogel & Beckmann, 1999). Vertical turbulent transport of both oceanographic and biological tracers in our configuration is parameterized using the Pacanowski and Philander (1986) mixing scheme. As in Beckmann et al. (1999), lateral diffusivity is a function of the local Reynolds number. Lateral viscosity is assumed to be a quadratic function of the horizontal grid spacing $\Delta_{\vec{x}}$ and is prescribed as 200 m^2/s.

3.4 Model Domain and Grid

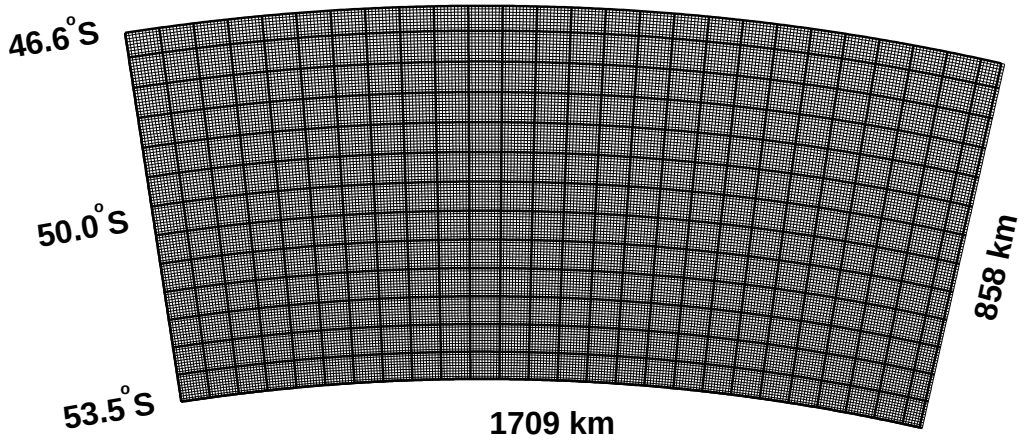

Figure 3: Horizontal model grid

The model domain comprises a periodic channel on a β-plane with closed boundaries in the north and south forming a region of 1709 by 858 km^2 of size centered at 50°S (Fig. 3), which in the Atlantic sector of the Southern Ocean is the approximate location of the Antarctic Polar Front. The model grid is isotropic and has a horizontal resolution of $1/12^\circ$ in the zonal and $1/12^\circ \cdot \cos\phi$ in the meridional direction, which leads to a grid spacing of roughly 6 km. Thus, the model runs in an eddy-resolving configuration which allows for the development of dynamic instabilities. The vertical grid is terrain-following with resolution increasing near the surface. For optimal representation of near-surface dynamics, nine of the 24 layers are situated in the uppermost 80 m.

Bottom topography is idealized with no variability in the zonal direction and represents the large-scale bathymetry of the Atlantic sector of the Southern Ocean

as derived from the dataset of Smith and Sandwell (1997). From a maximum water depth of 4000 m in the north, the seafloor rises to a minimum depth of 2500 m in the south (Fig. 4), representing the Atlantic Indian Ridge.

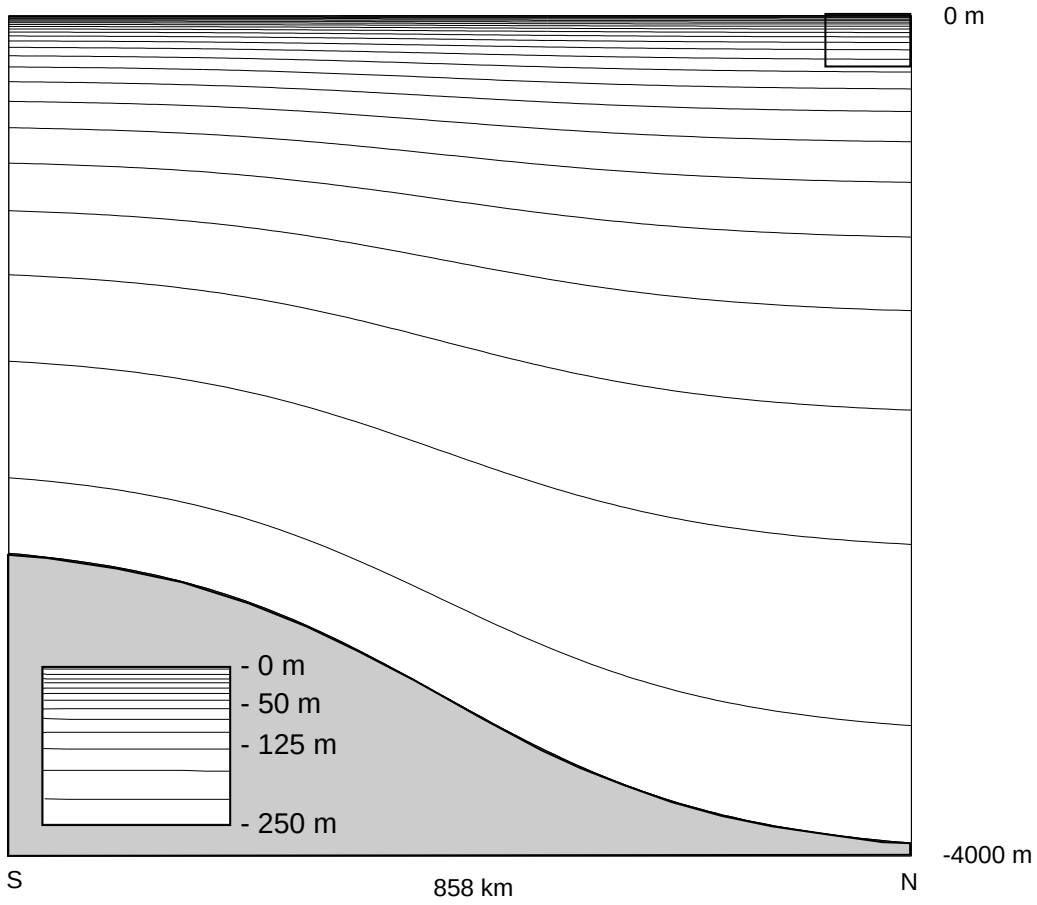

Figure 4: Vertical discretization of the water column

3.5 Initialization, Boundary Conditions and Timestepping

The ocean model as well as the nutrients silicate and nitrate are initialized using data from the WOCE dataset which were zonally averaged over the area of the model domain. The nutrient distribution is characterized by strong meridional gradients: Minimum surface concentrations of nitrate and silicate are 23 μmol/l and 4 μmol/l, respectively, and are found in the north. To the south, surface nutrient concentrations increase to 27.7 μmol/l and 35.7 μmol/l for nitrate and silicate, respectively.

Due to the lack of gridded data, iron concentration is initialized using the vertical profile

$$Fe^{t=0}(z) = 3 \cdot 10^{-3}\ \mathrm{mmol\,m^{-3}} + 1.425 \cdot 10^{-6}\ \mathrm{mmol\,m^{-4}}\ |z| \qquad (28)$$

which fits to iron concentrations at the surface and at the bottom derived from measurements in the APF region (Löscher et al., 1997). As no horizontal gradients are prescribed initially, any horizontal inhomogeneity in the iron distribution developing during the integration can be attributed to the combined effects of frontal and ecosystem dynamics.

At the northern and southern boundary of the model domain, a restoring to the initial salinity, temperature, and nitrate, silicate and iron concentrations is applied below 1600 m depth. In addition, a restoring zone for salinity and temperature along the periodic boundary ensures the persistence of the front even for an integration over several years. An eastward transport of 130 Sv through the model domain is prescribed.

Surface boundary conditions are derived from a diagnostic surface energy balance which is based on the treatment of open water in the thermodynamic sea ice model of Parkinson and Washington (1979) as implemented in the coupled sea ice-ocean model of Timmermann et al. (2001). For the solar radiation the daily and annual cycles as well as the latitude and mean cloud cover, using the standard astronomical formulae of Zillmann (1972) and Laevastu (1960), are considered. Total cloud cover was chosen to be 70% for the whole model domain, in agreement with the reanalysis of the ECMWF.

To avoid artificial up- and downwelling at the closed northern and southern boundaries due to Ekman transport, atmospheric surface stress is neglected. The wind-induced vertical shear required by the Pacanowski and Philander (1986) mixing scheme is prescribed as an empirical vertical profile (horizontally uniform) that was derived from model experiments which included surface stress by ECMWF wind forcing.

Forcing data were derived from the European Center for Medium-Range Weather Forecasts (ECMWF) reanalysis, including 6-hourly data of 10 m wind, and 2 m air and dew point temperatures. The model is integrated for 33 months. A 3 minutes time step is applied.

For the first 270 days, the biological variables are restored to their initial values while the ocean is free to develop dynamic instabilities. From there, we start the experiments with winter concentrations and a fully developed meandering current. Results presented below are from the period between October of the second year and September of the third year of integration.

4 Model Results

4.1 Hydrography and Frontal Dynamics

After 60 days of integration, the typical structure of a meandering front has evolved. From that point onwards, the level of mesoscale variability is retained over the full simulation. Vertically integrated transport (Fig. 5, top left) and surface velocities (Fig. 5, top right) after 350 days of integration feature a pronounced frontal jet with typical surface velocities of 0.5 m/s, a weak recirculation south of the jet and a realistic meandering structure: Agreeing with observations of Lutjeharms & Valentine (1984), the width of the frontal jet ranges between 120 and 140 km. Due to the high eastward velocities within the frontal zone, the meanders propagate eastward, against the direction of freely propagating Rossby waves (retrograde propagation). Their typical wavelength of 160-180 km is close to the 175 km wavelength observed by Cowles et al. (2000).

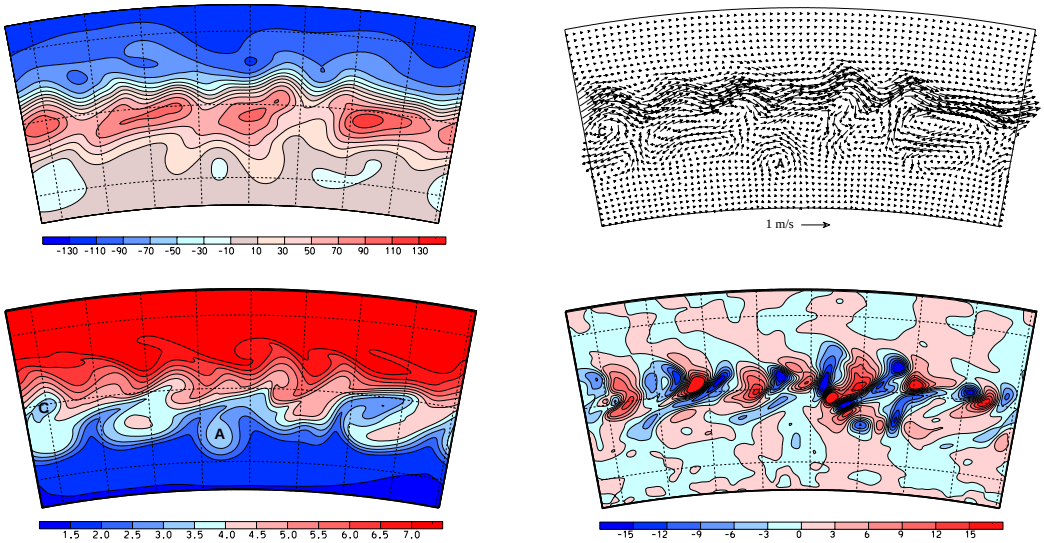

Figure 5: Snapshots of vertically integrated transport [Sv] (top left), surface horizontal velocity [m/s] (top right), surface temperature [°C] (bottom left) and vertical velocity [m/d] in 200 m depth (bottom right) after 350 days of integration. An anticyclonic eddy is marked as A, a cyclonic eddy as C.

Due to strong baroclinic instability, eddies are shed from the meander current. For the southern hemisphere, cyclones are formed south of the frontal jet, whereas anticyclones are shed north of it. However, as the frontal jet in our simulation is situated north of the maximum topographic slope, eddy generation is more efficient

on the southern (steeper) side where eddies leave the frontal jet and propagate prograde (i.e., in the direction of freely propagating waves; here: to the west) at about 20 cm/s.

Cyclonic and anticyclonic eddies (marked by “C” and “A” in Fig. 5) can be distinguished in the surface temperature (Fig. 5, bottom left) as cold and warm core anomalies, respectively. These eddies have a diameter of roughly 80 km which corresponds to the spatial decorrelation scale of 85 km derived from Geosat altimeter data for the ACC (Gille & Kelly, 1996). Observed diameters of eddies or rings in the ACC generally cover a wide range from 60 to 250 km (Bryden, 1983; Nowlin & Klinck, 1986; Gouretski & Danilov, 1994).

The meandering current and eddy formation lead to mesoscale up- and downwelling (Fig. 5, bottom right). Applying the principle of potential vorticity conservation, we can see that the gain of relative vorticity, i.e., the transition from anticyclonic to cyclonic flow is associated with local downwelling, while flow in transition from cyclonic to anticyclonic relative vorticity coincides with mesoscale upwelling regions (Onken, 1992). Thus, downwelling occurs on the upstream side (for an eastward current i.e. the western side) of each cyclonic meander ridge, while upwelling takes place downstream (here: east) of it. The model reproduces these structures in agreement with observations of Strass et al. (2001). Typical vertical velocities in these up- and downwelling cells range from 5 to 20 m/d and thus are considerably larger than the vertical velocities inside isolated eddies which do not exceed 3 m/d.

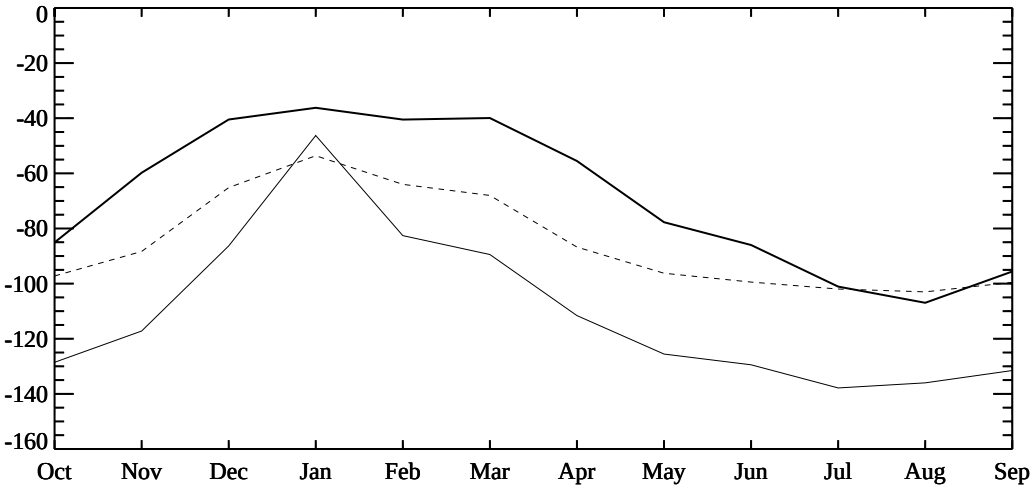

Figure 6: Zonal mean of the seasonal cycle of the mixed layer depth [m] in the vicinity of the front (bold), in the northern ACC (solid) and southern ACC (dashed).

As proposed from observations (e.g., Strass et al., 2001), mesoscale upwelling

near the meandering front affects the mixing depth near the surface: While the zonal mean mixed layer depth in the northern and southern ACC ranges from 60 to 155 m in the annual cycle, zonal mean mixed layer depth near the APF is only 35 m in summer and 120 m in winter (Fig 6). Local mixed layer depth near the APF can be as shallow as 20 m.

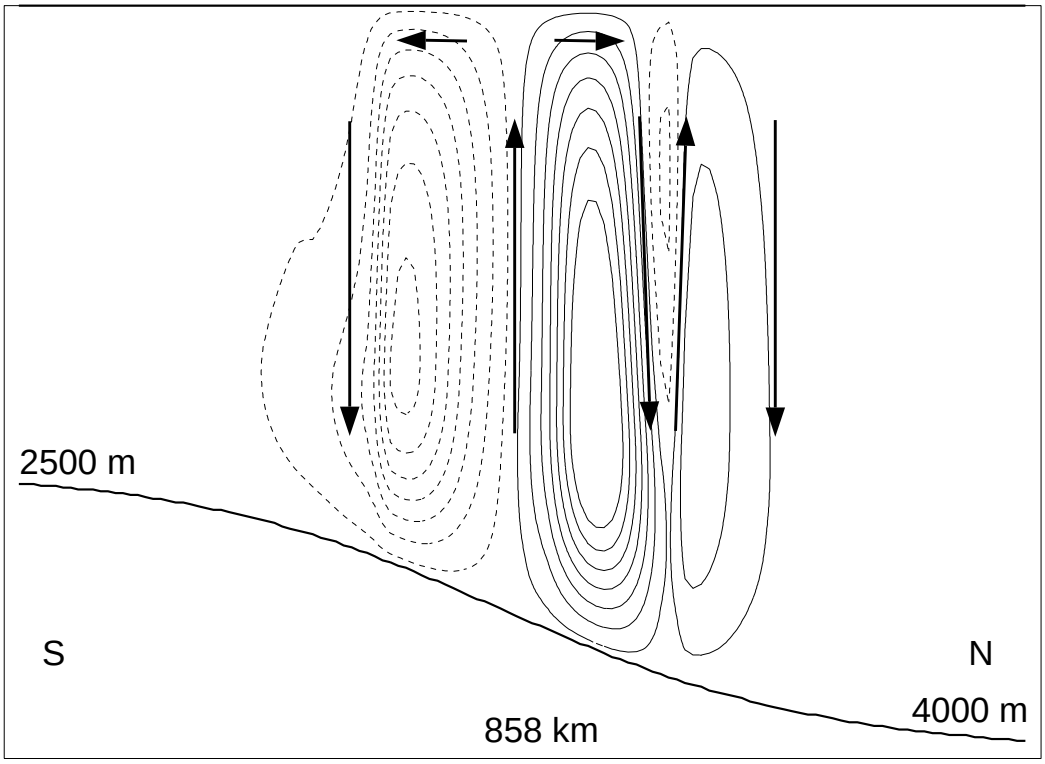

Figure 7: Yearly mean of the meridional overturning circulation. Contours range from -3.25 to 3.25 Sv; contour intervall is 0.5 Sv. Dashed lines indicate negative values. The same structure is visible in monthly means.

Mean cross front overturning circulation (Fig. 7) features two pronounced overturning cells producing an intense upwellig region which is situated roughly in the center of the model domain. Two weaker overturning cells further north, i.e. near the base of the prescribed ridge, produce a secondary upwelling region. Downwelling outside the frontal area but also in the convergence between the two upwelling cells closes the mass balance. At this point, we are not able to validate this structure. However, we will demonstrate that it produces a phytoplankton distribution in close resemblance to observations.

4.2 Ecosystem dynamics (1): No Iron Limitation

Following the studies of Hense et al. (2000), the first experiment was carried out with the compartments phytoplankton, zooplankton, nitrate, ammonium, silicate and the two detritus pools. Iron limitation in this experiment was omitted.

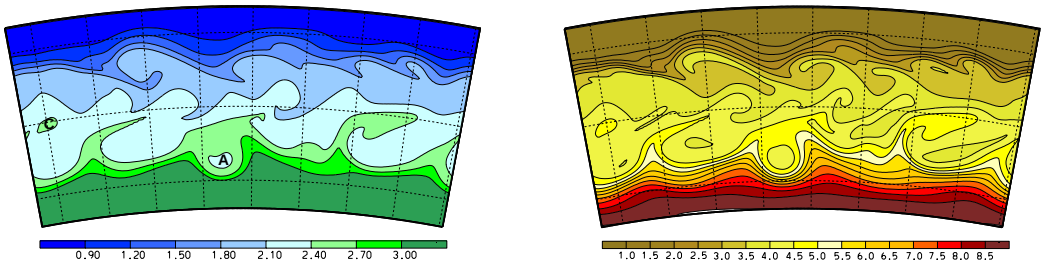

Figure 8: Snapshots of simulated summer surface concentration of phytoplankton [μg Chl a/l] (left) and zooplankton [μg C/l] (right) at day 350 in an experiment neglecting iron limitation.

A snapshot of simulated phytoplankton biomass in summer shows high chlorophyll concentrations in the frontal system and south of it (Fig. 8 a), reaching values of up to 3 μg Chl a/l near the southern boundary. The mesoscale phytoplankton distribution reflects the meanders and eddies discussed in the previous section. A cyclonic eddy (C) at the western boundary can be distinguished by slightly higher chlorophyll concentrations - corresponding to an increased silicate concentration in this cell - whereas in the anticyclonic eddy (A) further south chlorophyll concentrations are reduced. Nevertheless, locally enhanced phytoplankton biomass in the region of the front cannot be found; instead a strong north-south gradient of phytoplankton biomass is established and present throughout the year.

Following the distribution of phytoplankton biomass, zooplankton concentrations are increased in the southern part (Fig. 8 b), reaching values up to 9 μg C/l, while in the northern part zooplankton concentration does not exceed 2 μg C/l. Again the cyclonic eddy can be distinguished by slightly enhanced zooplankton concentrations whereas in the anticyclonic cell zooplankton concentrations are reduced.

In the zonal mean, the meridional gradient of silicate which limits phytoplankton growth in the north, is well pronounced (Fig. 9). Phyto- and zooplankton biomass as well as the total biogenic silica increase in the southern part of the model domain. Effects of mesoscale dynamics at the APF are not visible.

Similar to the studies of Hense et al. (2000), model experiments with different values for the Si:N uptake ratio r_{Si} feature variations of the maximum phyto- and zooplankton biomass with increasing concentrations for lower values of r_{Si},

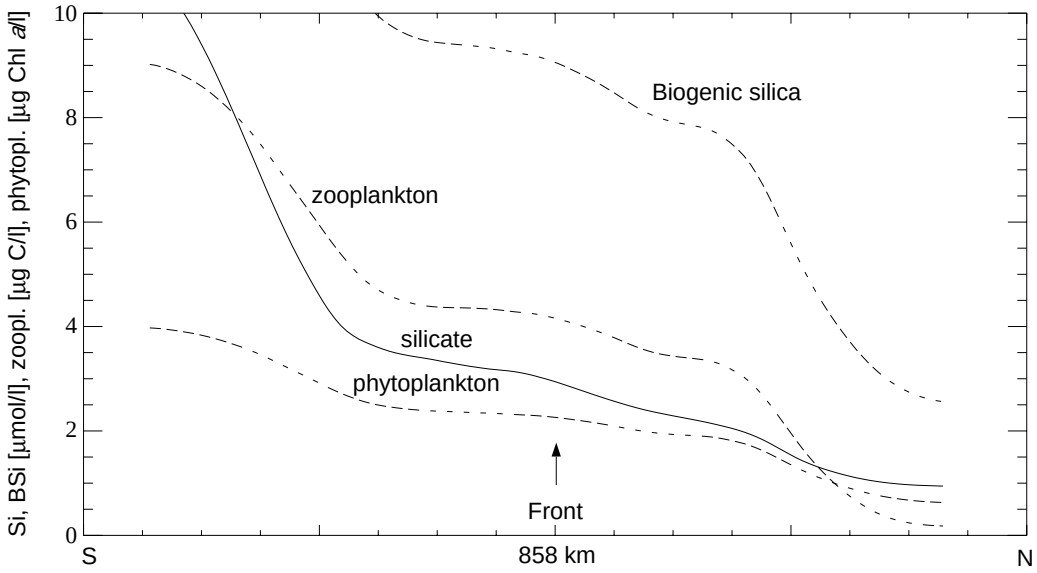

Figure 9: Zonal means of surface concentrations of dissolved silicate [μmol/l], biogenic silica [μmol/l], phyto- [μg Chl a/l] and zooplankton [μg C/l] at day 350.

but no change in the general horizontal distribution with high concentrations of phytoplankton in the southern, silicate-rich water mass and low concentrations of phytoplankton in the northern, silicate-poor water mass.

We conclude that the "traditional" model configuration which disregards possible iron limitation is not able to reproduce general features of the large scale plankton distribution in the Atlantic sector of the Southern Ocean, namely the occurence of the HNLC area in the southern ACC. As the model gives a reasonable representation of the local frontal dynamics, this does imply that frontal dynamics alone cannot be responsible for the observed phytoplankton maximum in the vicinity of the Antarctic Polar Front.

As a consequence, iron was implemented into the model to test wether limitation of the micronutrient is able to reflect the observed horizontal structure.

4.3 Ecosystem dynamics (2): Iron limitation

4.3.1 Reference Experiment

Introducing an additional iron compartment leads to pronounced changes in the simulated ecosystem. Similar to the experiment described in the previous section, phytoplankton growth starts in September/October (Fig. 10), following the increasing solar radiation.

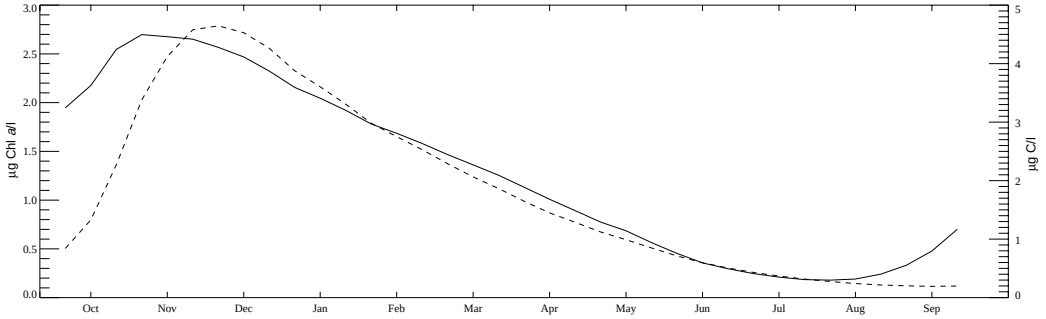

Figure 10: Seasonal cycle of surface phytoplankton (solid) and zooplankton (dashed) concentrations in the vicinity of the simulated front.

Distributions of iron and silicate at this time in spring show strong meridional gradients with an iron maximum in the north and a silicate maximum in the south (Fig. 11) while nitrate is more homogeneously distributed with concentrations between 20 and 21 μmol/l .

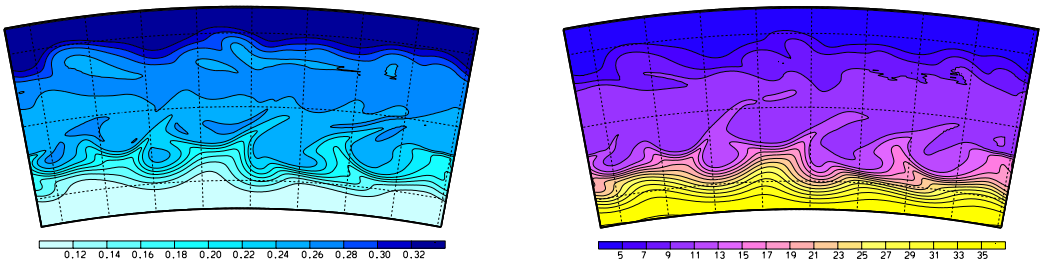

Figure 11: Snapshots of simulated spring surface concentration of a) dissolved iron [nmol/l] and b) dissolved silicate [μmol /l] at day 280 in the standard iron experiment.

A pronounced time lag between phytoplankton and zooplankton growth is visible in the time series in Fig. 10. Maximum concentrations of phytoplankton are reached in November/December; the zooplankton maximum occurs roughly 20 days later. Unlike the results in the ”no iron“-experiment, maximum concentrations of phyto- and zooplankton now occur in the vicinity of the Polar Front (Fig. 12, top panels) which agrees with observations.

Grazing pressure on phytoplankton is rather small and never exceeds primary production. Maximum simulated grazing rates are 3 % of the primary production and agree well with results from laboratory experiments of Dubischar and Bathmann (1997) who yielded grazing rates of 0.3-3.7% of primary production.

Again the large scale distribution is modulated by mesoscale structures which

are visible in all biological tracers.

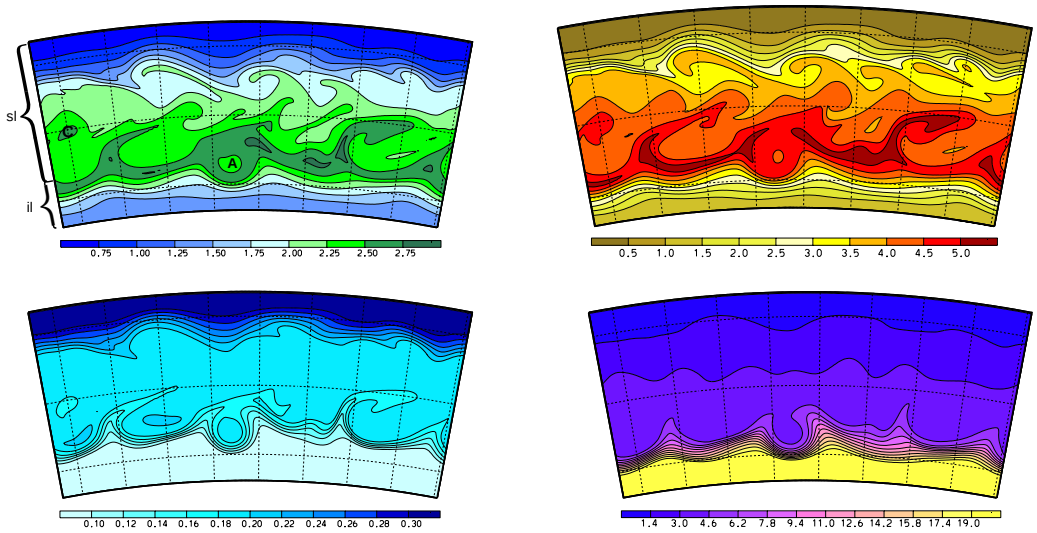

Figure 12: Snapshots of simulated summer surface concentration of phytoplankton [μg Chl a/l] (top left), zooplankton [μg C/l] (top right), dissolved iron [nmol/l] (bottom left) and dissolved silicate [μmol /l] (bottom right) at day 350 in the standard iron experiment. An anticyclonic eddy is marked as A, a cyclonic eddy as C. The symbols “sl” and “il” indicate the zones of silicate and iron limitation, respectively.

The cyclonic eddy at the western boundary can be distinguished by a higher phyto- and zooplankton biomass. This eddy was generated from a meander directly south of the front which carried higher plankton concentrations and is now an isolated maximum. In the southern anticyclonic eddy, on the other hand, plankton biomass is significantly lower and iron concentration higher than in the surrounding water mass. This eddy originates from a meander north of the front where silicate limits phytoplankton growth. Again, the properties of that water mass are retained in the eddy.

In the meandering current, low phytoplankton concentrations coincide with upwelling spots whereas maximum phytoplankton concentrations occur in downwelling areas. We argue that ”newly” upwelled water, rich in nutrients but poor in phytoplankton, is advected horizontally near the surface and phytoplankton grows until water is downwelled on the western side of a cyclonic meander ridge. This process leads to a typical mesoscale phytoplankton distribution and was also postulated from observations in the Atlantic region of the Antarctic Polar Front (Strass et al., 2001). In the downwelling areas, enhanced phytoplankton concentrations with values about 2.6 μg Chl a/l and a depth-integrated phytoplankton

stock of 275 mg m^{-2} agree with observed chlorophyll concentrations between 2 and 4 μg Chl a/l and a depth-integrated biomass of 177-277 mg m^{-2} (Tréguer & Jacques, 1992; Bathmann et al., 1997) in the region of the Polar Front.

Similar to the mesoscale distribution of phytoplankton in the meander current, also zooplankton concentration is increased in the downwelling regions with concentrations reaching 5 μg C/l . Compared to observations, which are in the range between 4 and 7 (Franz & Gonzalez, 1997; converted from dry mass, see Hense et al., 2000) model results appear thoroughly reasonable.

The same is true for the horizontal distribution of biogenic silica which follows the maxima and minima of plankton concentrations. Maximum simulated values of up to 10 μmol/l occur in the vicinity of the front and are in agreement with observed BSi concentrations of up to 11.7 μmol/l (Quéguiner et al., 1997).

Due to the uptake by phytoplankton, silicate and iron concentrations decrease during the summer (Fig. 12, bottom panels). Silicate increasingly limits phytoplankton growth in the north. Observed horizontal silicate gradients in the region of the Polar Front can be in the order of 7.22 μmol l^{-1} km^{-1} (Dafner & Mordasova, 1994) whereas nitrate is more homogenously distributed and shows only little seasonality (Löscher et al., 1997; Dafner & Mordasova, 1994). Model results are consistent with these observations: While surface silicate concentrations vary from < 1 μmol/l to 15 μmol/l in the annual cycle, nitrate concentrations are always larger than 20 μmol/l .

Due to the silicate limitation of phytoplankton growth, iron concentration remains high in the northern part of the model domain. In the southern ACC, however, where silicate supply is sufficient, phytoplankton growth is increasingly limited by iron depletion. Typical simulated surface iron concentrations in this region are as low as 0.1 nmol/l and therefore at the lower edge of observed iron concentrations.

Until the end of January, silicate is nearly depleted in areas with high iron concentration but does not drop below 20 μmol/l in the southern ACC.

From February onwards, phytoplankton growth decreases due to the decreasing solar radiation and increasing mixed layer depth (Fig. 10). However, even in winter a slightly enhanced phytoplankton biomass is found in the frontal region with concentrations of up to 0.3 μg Chl a/l - compared to 0.1 μg Chl a/l further north and south.

4.3.2 Sensitivity studies I

Motivated by observations of heavily silicified diatom species in the Southern Ocean (Shiomoto & Ishii, 1995; Quéguiner et al., 1997; Hense et al., 1998) and the results of zerodimensional model experiments with different Si/N uptake ratios (Hense et al., 2000), two additional experiments with r_{Si}=2 and r_{Si}=4 were

performed.

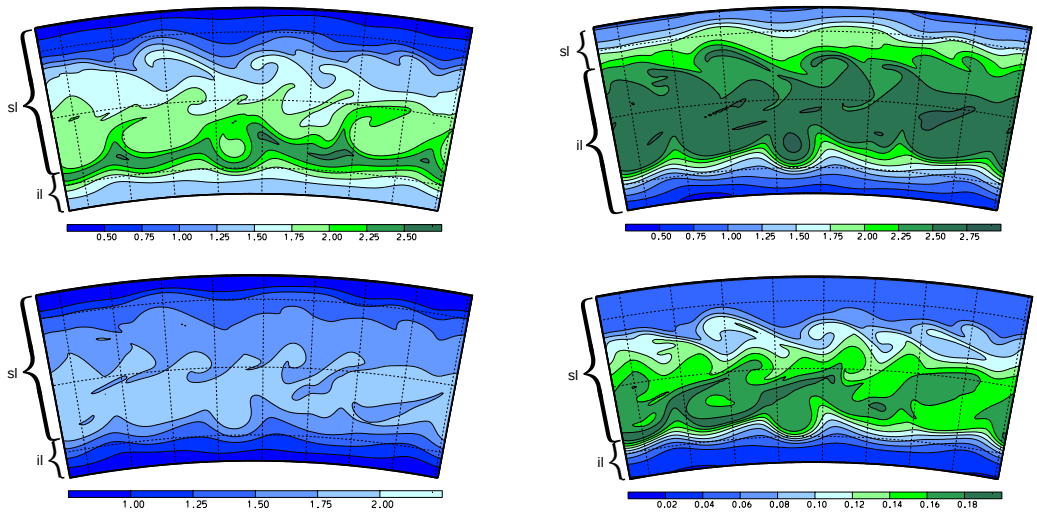

Figure 13: Snapshots of simulated summer surface concentration (day 350) of phytoplankton [μg Chl a/l] in the experiment of r=4 (top left), r=2 (top right), $k_{Fe} = 0.6$ nmol/l (bottom left) and $k_{Fe} = 1.2$ nmol/l (bottom right). The symbols "sl" and "il" indicate the zones of silicate and iron limitation, respectively.

Like the reference experiment, both simulations feature a phytoplankton distribution with a maximum in the vicinity of the APF (Fig. 13, top panels). The experiments differ, however, in location and width of the band with high phytoplankton concentrations.

In the experiment with $r_{Si} = 4$, the band of high phytoplankton concentrations is located further south and is narrower than in the standard iron experiment ($r_{Si} = 3$). Typical maximum phytoplankton concentrations are between 2 and 2.25 μg Chl a/l , while the reference experiment features a band of phytoplankton concentrations between 2.5 and 2.75 μg Chl a/l .

To the north, phytoplankton concentration decreases stronger compared to the reference run due to strong silicate limitation. Silicate limitation occurs in most of the model domain. Only in the southern area phytoplankton growth is limited by iron.

In the experiment with $r_{Si} = 2$ (Fig. 13, top right), on the other hand, the band of high phytoplankton concentrations is significantly wider than in the experiments with higher Si/N uptake ratios and centered directly at the simulated front. Typical maximum phytoplankton concentrations are between 2.5 μg Chl a/l and 2.75 μg Chl a/l and coincide with the results of the standard iron experiment. Iron

limitation dominates primary production in the greatest part of the model domain. Due to the lower incorporation of silica per nitrogen unit, less silicate is taken up and phytoplankton grows until iron limitation occurs.

The anticyclonic eddy in the south is now characterized by higher phytoplankton compared to the surrounding water mass and therefore differs from all the other experiments where this eddy always features reduced phytoplankton concentrations. The difference is that in this simulation primary production within the eddy is not limited by silicate depletion, due to higher silicate concentrations in the meander from which the eddy originates.

As seawater and culture experiments indicate that the Si/N uptake ratio is influenced by iron concentration (Takeda, 1998; Hutchins and Bruland, 1998), an iron dependent diagnostic Si/N uptake ratio has been introduced. Using data from experiments with an Antarctic diatom (Takeda, 1998) we deduced the linear relationship

$$r_{Si} = -1.3 \cdot 10^3 \frac{\mathrm{m}^3}{\mathrm{mmol}} \cdot Fe + 2.51 \tag{29}$$

for a series of sensititvity studies. However, it turned out that the range of the diagnostically derived Si/N uptake ratio is rather small with values between 2.2 in the north and 2.4 in the southern ACC. Consequently, model results from these experiments show only minor differences from the simulation with $r_{Si} = 2$.

4.3.3 Sensitivity studies II

To test the sensitivity on different half saturation constants for iron, we performed two experiments with iron half saturation constants k_{Fe} = 0.6 nmol/l and k_{Fe} = 1.2 nmol/l (Lancelot et al. 2000), respectively.

Both experiments feature a regionally increased plankton biomass near the APF (Fig. 13, bottom panels). Silicate limitation occurs in most of the model domain. However, the location of the boundary between silicate and iron limitation does not differ much from the standard iron experiment.

Striking are the differences in the concentration of phytoplankton. In both experiments phytoplankton concentrations are overall lower compared to the standard iron experiment. Whereas phytoplankton concentrations are maximum 1.8 μg Chl a/l in the simulation with k_{Fe}=0.6 nmol/l, phytoplankton concentration does not exceed 0.18 μg Chl a/l in the experiment with k_{Fe} = 1.2 nmol/l. Apparently, experiments with a half saturation constant of k_{Fe} = 1.2 nmol/l strongly underestimate primary production. We conclude that an iron half saturation constant of k_{Fe} = 1.2 nmol/l does not give an adequate representation of a natural diatom community.

4.3.4 Meridional structure of phytoplankton distribution

To perform a quantitative validation of the different experiments, simulated phytoplankton distributions are compared to observed chlorophyll concentrations on meridional transects from 1992 (Bathmann et al., 1997a) and 1995 (Hense, 1997; Bathmann et al., 1997b). To account for the interannual or regional variability in the location of the Antarctic Polar Front, all transects are displayed relative to the location of the APF (Fig. 14).

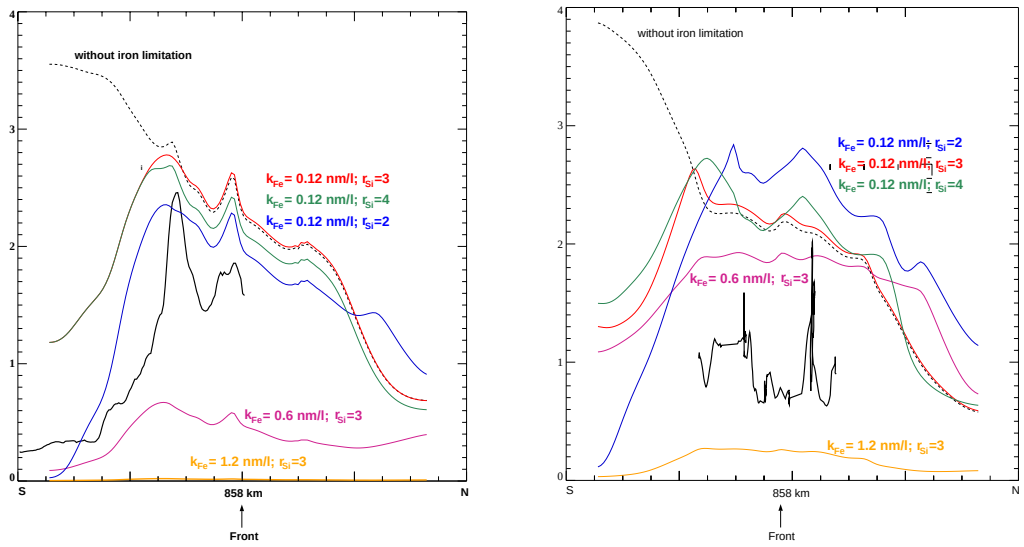

Figure 14: Meridional transects of observed and simulated chlorophyll concentrations [μg Chl a/l] from different experiments. Observations (bold line) are from a) November 1992 and b) December 1995. Model results are snapshots from the same time in the year. Displayed are the "no iron"-experiment (dashed line), and the iron experiments with different values for k_{Fe} and r (solid). Observed and simulated chlorophyll concentrations are centered about the location of the Antarctic Polar Front.

Comparing the experiments with observations of 1992 and 1995, it is striking that the horizontal pattern with enhanced chlorophyll concentration in the frontal region is only reflected in the experiments including iron limitation (Fig. 14). The "no iron" experiment can be distinguished by a pronounced increase in chlorophyll concentrations south of the front - which is not covered by observations. For the 1992 data, it is obvious that results from the simulation with a fixed ratio of $r_{Si} = 2$ agree well with observed chlorophyll concentration. Simulated chlorophyll concentration in the experiments with k_{Fe} = 1.2 nmol/l and k_{Fe} = 0.6 nmol/l are significantly lower than the observed values.

For the 1995 data, agreement with simulated chlorophyll concentrations is not as good. Compared to 1992, observed chlorophyll concentrations are significantly smaller and best agreement is achieved in the experiment with k_{Fe} = 0.6 nmol/l. For both datasets, however, the experiment with k_{Fe} = 1.2 nmol/l underestimates the observed chlorophyll concentrations significantly.

The differences in the observed chlorophyll concentrations between both years and the best fit of simulated chlorophyll concentration raise the question of causality. First of all, differences could be explained by dominance of different diatom species. Whereas in 1992 the diatom species *Corethron criophilum* and *Fragilariopsis kerguelensis* were dominant (Bathmann et al., 1997a), in 1995/96 the diatom species *Thalassiothrix sp.*, *Chaetoceros sp.* and *Pseudonitzschia sp.* dominated the phytoplankton community (Klaas et al., 1997; Schuelke, 1998). Moreover, whereas in 1992 relatively high iron concentrations were observed prior to the development of the phytoplankton bloom, iron concentration in 1995/96 was generally low (de Jong et al., 1997). Upwelling in this situation was observed to be relatively weak (Strass et al., 2001); so the differences might well be due to variability of regional or large scale hydrography - which cannot be covered by an idealized model with fixed lateral boundary conditions.

At a closer look at the meridional plankton distribution it is striking that model results and observations of both years show *two* pronounced phytoplankton maxima. Especially for 1992, the position of the two simulated maxima relative to the front is well reproduced by the model.

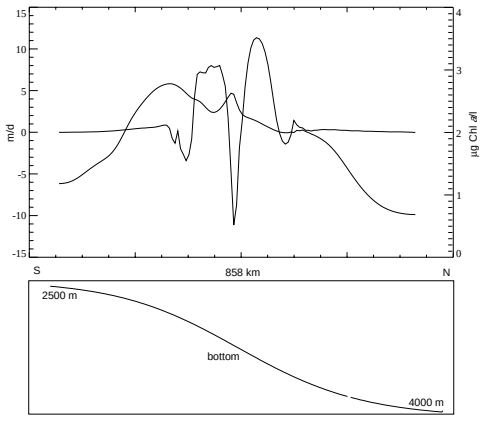

Figure 15: Meridional transect of the zonal mean vertical velocity (solid line) and simulated phytoplankton concentration (bold line) in November.

This double cell structure is also visible in the zonally integrated vertical velocity which in 200 m depth reveals two strong upwelling spots separated by a

pronounced downwelling cell (Fig. 15). Bottom topography plays a crucial role in the formation of these patterns: Experiments with a flat bottom (not shown) reveal much larger fluctuations in the meridional overturning circulation; the location of overturning cells needs to be stabilized by a large-scale sloping topography to produce two distinct phytoplankton maxima. As the model topography represents the northern slope of the Atlantic Indian Ridge it is reasonable to assume that a similar vertical velocity structure may be responsible for the observed double-peak plankton distribution. As in the mesoscale distribution, the *downwelling* area coincides with the phytoplankton maximum while the two upwelling spots bare themselves as low chlorophyll and high nutrient areas. Similar to the processes at the meander ridges, nutrient rich (i.e., iron rich), chlorophyll poor water is upwelled. Water and properties are spread horizontally near the surface and phytoplankton grows until the water and the phytoplankton community encounter a downwelling region and are shifted downwards, out of the euphotic zone (Fig. 16), where phytoplankton growth has to stop. Thus minimum (maximum) phytoplankton concentrations are found in upwelling (downwelling) areas. Outside the frontal system, newly upwelled water is mixed with water which is poor in either silicate or iron; thus phytoplankton blooms cannot develop.

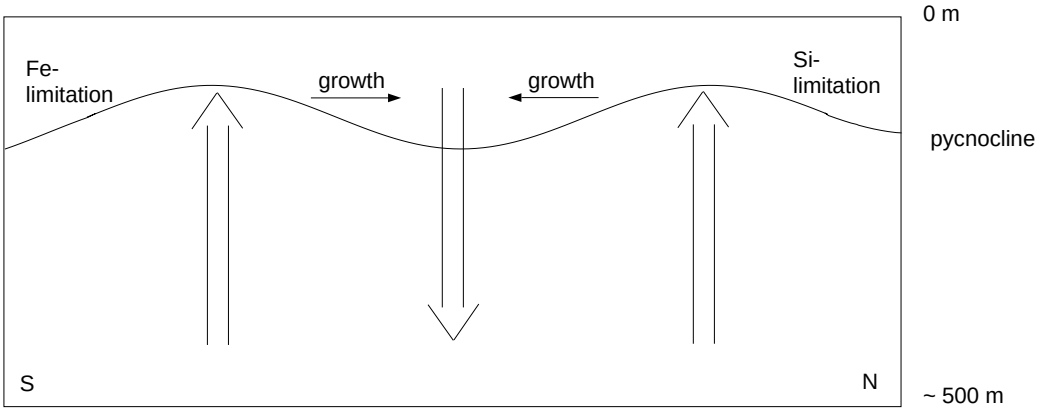

Figure 16: Schematic representation of up- and downwelling effect on phytoplankton growth.

4.3.5 The effect of iron upwelling on primary production and plankton biomass

To quantify the effect of iron upwelling on plankton biomass and primary production, we performed two experiments (with $r_{Si} = 2$ and $r_{Si} = 3$) in which

any vertical advection of iron was eliminated. In these “no iron upwelling” experiments, phytoplankton concentration in summer is still slightly enhanced in the vicinity of the front due to the convergent flow field in the downwelling areas, but maximum values are reduced by roughly 20% compared to the reference experiment (Fig. 17, left); maximum phytoplankton concentration in the frontal area is in the order of only 2.0 μg Chl a/l . Maximum zooplankton concentrations are reduced by 35 % and do not exceed 3.4 μg C/l (Fig. 17, right). A smaller mesoscale variability reflects the reduced impact of up- and downwelling.

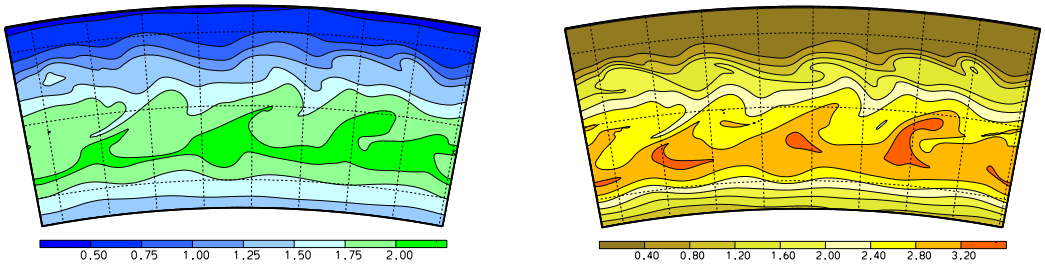

Figure 17: Phytoplankton (left) and zooplankton (right) concentrations at day 350 in the ”no iron upwelling” experiment. Units are μg Chl a/l for phytoplankton and μg C/l for zooplankton.

While the reference experiment features typical vertically integrated phytoplankton biomass maxima between 160 and 200 mg m^{-2} in summer, phytoplankton biomass near the APF is reduced by roughly 20 % in the “no iron upwelling” experiment. Again, the effect on zooplankton biomass is even stronger: Compared to the vertically integrated zooplankton biomass in the reference experiment which reaches 360-450 mg C m^{-2} in summer, zooplankton biomass in the ”no iron upwelling” experiments is reduced by 33 %.

In the reference experiment (and the similar experiment with $r_{Si} = 2$), annually integrated primary production reaches values between 80 and 120 g C m^{-2} yr^{-1} in the vicinity of the Polar Front and is significantly lower (between 20 and 50 g C m^{-2} yr^{-1}) in the southern and northern part of the model domain. These results are in agreement with estimates derived from sediment traps (80 g C m^{-2} yr^{-1}; Wefer and Fischer, 1991) or satellite images (75-165 g C m^{-2} yr^{-1}; Antoine et al., 1996; Longhurst et al., 1995). In the “no iron upwelling” experiment, primary production is reduced by 32% in the vicinity of the front whereas the differences north and south of the front are negliable.

We conducted a further experiment, in which we prevented the vertical advection of silicate instead of iron. Compared to the reference simulation, differences in this “no silicate upwelling” experiment are not significant, which indicates that

silicate even in the frontal region is supplied by horizontal rather than by vertical advection.

5 Discussion and Conclusions

A newly developed coupled ocean-ecosytem model in an eddy-resolving configuration for the region of the Antarctic Polar Front (APF) has been introduced. The model is based on biochemical fluxes of nitrogen and silicate and considers possible iron limitation. It is integrated for more than 2 years and is the first model which succesfully simulates both eddy-resolved hydrography and the annual cycle of plankton growth and decay in the Antarctic Circumpolar Current (ACC) and the ambient Southern Ocean.

We have demonstrated that regional hydrodynamics strongly affects the distribution of biological tracers. Eddies and the dynamics of the meander current lead to mesoscale variability of plankton biomass and nutrients as familiar from observations in the region of the ACC (eg. Smetacek et al., 1997; Strass et al., 2001). Formation of isolated eddies enables the encapsulation of nutrients and plankton from different regimes and their conservation within an ambient water mass. Biological processes in an isolated eddy thus can still reflect the properties of their source region. So, to get an idea of the “history” of an ecosystem sampled during a field experiment in a region of large mesoscale variability, it appears necessary to consider hydrography as well as nutrient and plankton distribution also on a larger scale than that of the actual sampling area.

However, frontal dynamics alone cannot explain the observed enhancement of phytoplankton biomass along the APF. Although our simulation covers the cross front circulation with a reduced surface mixed layer depth in the vicinity of the Antarctic Polar Front and deep mixed layers in the ambient ACC, experiments with nutrient limitation by either nitrogen or silicate cannot reproduce the characteristic plankton distribution with a chlorophyll maximum near the APF and a high nutrient-low chlorophyll region further south. We conclude that deep mixed layers alone cannot explain the HNLC area in the southern ACC.

Including a prognostic compartment for dissolved iron and considering possible iron limitation changes model results dramatically. Compared to the ambient regions, primary production and plankton biomass is enhanced in the vicinity of the front in all experiments including iron limitation. In contrast to Mitchell et al. (1991) who hypothesize that iron addition would not enhance phytoplankton growth in the Southern Ocean without increasing the strength of stratification, our results indicate that iron is the crucial factor limiting phytoplankton growth in the southern ACC. These findings agree with the hypotheses of several authors (e.g. Martin et al., 1990; Buma et al., 1991; de Baar et al., 1995), that the Southern

Ocean HNLC area is iron limited. Ignoring iron limitation leads to an overestimation of phytoplankton biomass in that area.

Due to the uptake of iron by phytoplankton, simulated iron concentration decreases in the southern ACC and agrees well with observations in that area. So, although the initial iron concentration in the simulation is horizontally uniform, the model is able to reproduce the regional distribution in the ACC, which indicates that ecosystem and frontal dynamics are the key mechanisms for iron redistribution in the Southern Ocean.

Our model results also indicate that the vertical transport linked to the meandering current and the cross front circulation is the prime source for iron in the ACC surface layer. In agreement with observations (Strass et al., 2001), minima and maxima of phytoplankton concentrations in the meander current coincide with up- and downwelling zones, respectively, which seems to contradict with the generally accepted idea that upwelling leads to increased phytoplankton biomass due to 'new nutrient input'. The reason for this unexpected result is that "newly" upwelled water is rich in nutrients (specifically iron) but poor in phytoplankton. This water spreads horizontally near the surface and phytoplankton grows until water is downwelled and the phytoplankton community is moved out of the euphotic zone. This process leads to the typical mesoscale phytoplankton distribution and to the formation of maximum chlorophyll concentrations directly south of the front.

The same argument applies for the larger scale, cross-frontal circulation: Two pronounced pairs of meridional overturning cells produce an intense upwelling near the front and strong downwelling north and south of it. Again, the upwelling areas are associated with high iron, low chlorophyll concentration while two maxima of plankton concentrations are found near the downwelling areas. It thus appears that maximum plankton concentrations are not only determined by the availability of nutrients but also by the individual residence time of the plankton community in the euphotic zone. North of these overturning cells, silicate limitation inhibits phytoplankton blooms, while iron limitation is responsible for the HNLC-area in the southern ACC.

Striking is the occurence of *two* phytoplankton maxima north and south of the front which also were found in observations from 1992 (Bathmann et al., 1997a) and 1995 (Hense, 1997; Bathmann et al., 1997b) in the same region. The two maxima are both associated with the APF; Sub-Antarctic Front and Southern Polar Front are located at roughly 45 and 55°S, respectively (Lutjeharms & Valentine, 1984; Veth et al., 1997), and thus out of the model domain. In the simulation, this double structure is caused by the formation of two pairs of overturning cells above the model representation of the northern slope of the Atlantic Indian Ridge. It cannot be found in experiments with a flat bottom where meridional overturning circulation is much less stationary. We conclude that large scale bottom topography strongly affects the cross-front circulation and may determine the meridional

position of local maxima and minima of phytoplankton biomass.

Sensitivity experiments with different Si/N-uptake ratios indicate that the boundary between silicate and iron limitation shifts southward when the Si/N-uptake ratio is increased. While phytoplankton growth is limited by iron in experiments with small Si/N-uptake ratios, a higher demand for silica (per nitrogen or iron unit) for uptake ratios larger than 2 leads to an early depletion of dissolved silicate and thus to silicate limitation in most of the APF region and iron limitation only in the southern ACC. The best agreement with observations was achieved in simulations with an Si:N-uptake ratio of 2, where during the summer the boundary between silicate limitation in the north and iron limitation in the south is close to the location of the Antarctic Polar Front. However, due to changes in the phytoplankton species composition, this might be subject to a large interannual variability. Some of the dominant diatom species are heavily silicified (e.g. Quéguiner et al., 1997; Hense et al., 1998); we expect that variaritions of their abundance influence the biogeochemical cycle and the boundary between different regimes.

While laboratory experiments with diatoms indicate that nitrogen uptake is reduced in the case of low iron concentrations, model simulations with a diagnostic Si:N-uptake ratio using the data of Takeda (1998) reveal only little sensitivity. Variations of iron concentration in the model domain are comparatively small so that the iron depending Si/N uptake ratio only varies from 2.2 to 2.4. Consequently, results of this experiments are very similar to the simulation with a fixed Si/N uptake ratio of 2. We conclude that in a natural environment variations of the Si:N-uptake ratio due to differences in iron concentrations are too small to have a significant effect on the distribution of phytoplankton biomass.

As measurements of iron dependent growth rates are scarce and apparently subject to large uncertainties, we conducted a series of experiments with different half saturation constants for iron. Not surprisingly, phytoplankton biomass strongly decreases for increasing iron half saturation constants. Best agreement with observations is achieved with an iron half saturation constant of 0.12 nmol/l; whereas using a half saturation constant of 1.2 nmol/l (Lancelot et al., 2000) leads to largely underestimated phytoplankton concentrations. We conclude that an iron half saturation constant of 1.2 nmol/l is too high for a natural (diatom dominated) phytoplankton community. However, reliable measurements of this parameter are still desirable.

Observation-based estimates of mesozooplankton grazing pressure range between 0.3...3.7 % (Dubischar & Bathmann, 1997) and 102 % (Pakhomov et al., 1997) of daily primary production. In our experiments, zooplankton grazing pressure was rather low, not exceeding 3 % of the primary production in the 10 day-mean. Thus, growth of larger phytoplankton is not primarily controlled by zooplankton grazing but rather by the occurence of downwelling events and the

deepening of the mixed layer in autumn.

In an experiment with an eliminated iron upwelling we find a decrease of annually integrated primary production in the order of 30% near the Polar Front. While this induces a reduction of vertically integrated phytoplankton biomass of only 20 %, zooplankton biomass is reduced by 33 %. Phytoplankton growth and zooplankton grazing are kept in a dynamic balance which compensates increased (decreased) primary production by increased (decreased) zooplankton grazing. This sensitivity has already been observed in other oceanic subsystems, e.g. in the California Current where reduced upwelling of cool, nutrient-rich water has coincided with a significant decline of zooplankton biomass (Weinheimer et al., 1999).

Given the high sensitivity of zooplankton concentrations to nutrient supply, it is reasonable to assume that carbon export and sedimentation of biogenic material is strongly affected by fluctuations in local iron upwelling. Observations from *in vitro* experiments in the Equatorial Pacific indicated a significant increase of carbon export in situations where upwelling leads to an even small increase of iron concentration in the surface layer (Coale et al., 1996), and we believe that the same holds true in the Southern Ocean.

On the other hand, the strength of upwelling might not only affect primary production and plankton stock but also upper trophic levels. Observations from Ghanian coastal waters indicate that upwelling events affect zooplankton concentration and the abundance and reproduction of fish in these regions (Quaatey & Maravelias, 1999). Thus, even the high abundance of fish and seabirds in the vicinity of the Antarctic Polar Front (Tate Regan, 1914; Norman, 1938, van Franeker, 1997) appears to be a results of increased upwelling of nutrient rich (iron rich) water in this region.

We therefore conclude that iron limitation is a crucial point for understanding the pelagic ecosystem in the Southern Ocean. Observed enhanced phytoplankton biomass in the region of the Antarctic Polar Front can be explained by mesoscale variability resulting in regional upwelling of iron and silicate. North and south of the front, silicate or iron limitation prevents phytoplankton blooms. Minima and maxima of phytoplankton biomass are linked with large scale bottom topography.

6 Outlook

Our simulations with BIMAP do not cover interannual variability of hydrography (e.g. location of the front, response to atmospheric forcing) or the ecosystem (e.g. species distribution, abundance of swarm organisms or top predators). From observations, it remains unclear whether shifts of phyto- and zooplankton species compositions can be attributed to variations in regional hydrography or represent

inherent variability of the ecosystem itself. So, the introduction of further phyto- and zooplankton compartments is desirable. However, in the region of the Polar Front the “typical” distinction between diatoms as large phytoplankton and autotrophic flagellates as small phytoplankton does not make much sense, as diatoms clearly dominate the phytoplankton biomass. Instead, different diatom species with different demand for nutrients and different nutrient uptake ratios should be considered but - as spatial resolution is to be kept eddy-resolving - would require further increase of computing resources. To achieve a realistic representation of the different plankton compartments and the fluxes between them, further measurements of nutrient uptake for the dominant phytoplankton species are required.

On a larger scale, investigations of ecosystem dynamics in a circumpolar model of the Southern Ocean could address questions of interannual varibility (e.g. effects of the Antarctic Circumpolar Wave) as well as the role of swarm organisms (e.g. salps) in this highly variable ecosystem.

Acknowledgements

Valuable discussions with R. Scharek are gratefully acknowlegded. Discussions within the AWI silica group, the BRIOS group, Ch. Dieterich, and V. Strass helped to improve the manuscript. The ECMWF analysis data were received via the German Weather Service.

References

Allanson & Parker (1983). Frontal zones, chlorophyll and primary production patterns in the surface waters of the Southern Ocean south of Cape Town. Reports from the 5th National Oceanographic Symposium, Afr. J. Sci./S.-Afr. Tydskr. Wet., 79/4, 153-154.

Antoine D., J.M. André & A. Morel (1996). Oceanic primary production: II. Estimation of global scale from satellite (coastal zone color scanner) chlorophyll. Global Biogeochemical Cycles, 10, 57-69.

Archer D.E. & K. Johnson (2000). A model of the iron cycle in the ocean. Global Biogeochemical Cycles, 14, 269-279.

Baretta J.W. W. Ebenhoeh & P. Ruardij (1995). The European Regional Seas Ecosystem Model, a complex marine ecosystem model. Neth. J. Sea Res. 33/3-4, 233-246.

Bathmann U.V., R. Scharek, C. Klaas, C.D. Dubischar & V. Smetacek (1997a) Spring development of phytoplankton biomass and composition in major water masses of the Atlantic Sector of the Southern Ocean. Deep-Sea Research, 44/1-2, 51-68.

Bathmann U. V., M. Lucas & V. Smetacek, with contributions of the participants (1997b) The expedition Antarktis XIII/1-2 of the research vessel "Polarstern" in 1995/96. Reports on Polar Research, 221, 1-136.

Beckmann A., H. H. Hellmer & R. Timmermann (1999). A numerical model of the Weddell Sea: large scale circulation and water mass distribution. Journal of Geophysical Research, 104/C10, 23375-23391.

Belkin I.M. & A.L. Gordon (1996). Southern Ocean fronts from the Greenwich meridian to Tasmania. Journal of Geophysical Research, 101/C2, 3675-3696.

Biddanda B.A. (1988). Microbial aggregation and degradation of phytoplankton-derived detritus in seawater. II. Microbial metabolism. Mar. Ecol. Prog. Ser., 42, 89-95.

Botnikov V.N. (1963). Geographic position of the Antarctic convergence zone in the Pacific Ocean. Soviet Antarctic Information Bulletin 4, 1827-1837.

Boyd P.W., A.J. Watson, C.S. Law, E.R. Abraham, T. Trull, R. Murdoch, D.C.E. Bakker, A.R. Bowie, K.O. Buesseler, Hoe Chang, M. Charette, P. Croot, K. Downing, J. Zeldis et al. (2000). A mesoscale phytoplankton bloom in the polar Southern Ocean stimulated by iron fertilization. Nature, 407/6805, 695-702.

Bracher A.U. & M.M. Tilzer (2001). Underwater light field and phytoplankton absorbance in different surface water masses of the Atlantic sector of the Southern Ocean. Polar Biology, 24/9, 687-696.

Bracher A.U., B.M.A. Kroon & M.I. Lucas (1999). Primary production, physiological state and composition of phytoplankton in the Atlantic sector of the Southern Ocean. Marine Ecology Progress Series, 190/1-16.

Bryden H.L. (1983). The southern Ocean, in Eddies in Marine Science, edited by A.R. Robinson, 265-277, Springer, New York.

Buma A.G.J., H.J.W. de Baar, R.F. Nolting, A.J. van Bennekom, (1991). Metal enrichment experiments in the Weddell-Scotia Seas: Effects of iron and manganese on various plankton communities. Limnology and Oceanography, 36/8, 1865-1878.

Burkov V.A. (1993). New features of the Southern Ocean hydrology. In: Pelagic ecosystems of the Southern Ocean, Voronina, N.M. (eds.). Nauka, Moskva, 5-19, SB. NAUCHN. TR. IOAN.

Chelton D.B., M.G. Schlax, D.L. Witter & J.G. Richman (1990). GEOSAT altimeter observations of the surface circulation of the Southern Ocean. Journal of Geophysical Research, 95/C10,17877-903.

Coale K.H., S.E. Fitzwater, R.M. Gordon, K.S. Johnson & R.T. Barber (1996). Control of community growth and export production by upwelled iron in the Equatorial Pacific Ocean. Nature, 379/6566, 621-624.

Cowles T.J., C.E. Wingard, J.A. Barth & S. D. Pierce (2000). Patterns of mesoscale variability in bio-optical properties in the Antarctic Polar Frontal zone in austral spring 1997 and summer 1998. Southern Ocean - JGOFS Symposium, Brest-F, 8-12 July 2000, P62.

Dafner E.V. & N.V. Mordasova (1994). Influence of biotic factors on the hydrochemical structure of surface water in the Polar Frontal Zone of the Atlantic Antarctic. Marine Chemistry, 45, 137-148.

de Baar H.J.W. (1994). von Liebig's Law of the minimum and plankton ecology (1899-1991). Progress in Oceanography, 33, 347-386.

de Baar H.J.W., J.T.M. de Jong, D.C.E. Bakker, B.M. Löscher, C.Veth, U. Bathmann & V. Smetacek (1995). Importance of iron for plankton blooms and carbon dioxide drawdown in the Southern Ocean. Nature, 373, 412-415.

de Jong J.T.M., J. den Das, K.R. Timmermans & H.J.W. de Baar (1997). Field distribution of iron in a section of the Antarctic Polar Frontal Zone. In: Reports on Polar Research: The expedition Antarktis XIII/1-2 of the research vessel "Polarstern" in 1995/96, Bathmann U. V., M. Lucas, V. Smetacek, with contributions of the participants (eds.), 44-52.

Dubischar C.D. & U.V. Bathmann (1997). Grazing impact of copepods and salps on phytoplankton in the Atlantic sector of the Southern Ocean. Deep-Sea Research, 44/1-2, 415-434.

Ebenhöh W., J.G. Bretta-Becker & J.W. Baretta (1995). The benthic biological submodel in the European Regional Seas Ecosystem Model. Neth. J. Sea Res. 33 (3/4), 423-452.

Eppley R.W. (1972). Temperature and phytoplankton growth in the sea. Fish. Bull., 70, 1063-1085.

Eriksen C.C., R.A. Weller, D.L. Rudnick, R.T. Pollard & L.A. Regier (1991). Ocean frontal variability in the Frontal Air-Sea Interaction Experiment. Special section: Frontal Air-Sea Interaction Experiment. Journal of Geophysical Research, 96/C5, 8569-8591.

Evans G.T. & J.S. Parslow (1985). A model of annual plankton cycles. Biol. Oceanogr., 3, 327-347.

Fasham M.J.R., H.W. Ducklow & S.M. McKelvie (1990). A nitrogen-based model of plankton dynamics in the oceanic mixed layer. Journal of Marine Research, 48: 591-639.

Flierl G.R. & C.S. Davis (1993). Biological effects of Gulf Stream meandering. Journal of Marine Research, 51/3, 529-560.

Fransz H.G. & S.R. Gonzalez (1997). Latitudanal metazoan plankton zones in the Antarctic Circumpolar Current along 6°W during austral spring 1992. Deep-Sea Research, 44/1-2, 395-414.

Froneman P.W., C.D. McQuaid & R.K. Laubscher (1999). Size-fractionated primary production studies in the vicinity of the Subtropical Front and an adjacent warm-core eddy south of Africa in austral winter. Journal of Plankton Research, 21/11, 2109-2035.

Gille S.T., D.P. Stevens, R.T. Tokmakian & K.J. Heywood (2001). Antarctic Circumpolar Current response to zonally averaged winds. Journal of Geophysical Research, 106/C2, 2743-2759.

Gille S.T. & K.A. Kelly (1996). Scales of spatial and temporal variability in the Southern Ocean. Journal of Geophysical Research, 101/C4, 8759-8773.

Gordon R.M., K.S. Johnson & K.H. Coale (1998). The behaviour of iron and other trace elements during the IronEx-I and PlumEx experiments in the Equatorial Pacific. Deep-Sea Research, 45/6, 995-1041.

Gouretski V.V., & A.I. Danilov (1994). Characteristics of warm rings in the African sector of the Antarctic Circumpolar Current. Deep-Sea Research, 41/8, 1131-1157.

Haidvogel D.B., J. L. Wilkin & R. E. Young (1991). A semi-spectral primitive equation ocean circulation model using vertical sigma and orthogonal curvilinear horizontal coordinates. J. Comput. Phys., 94, 151-185.

Haidvogel D.B. & A. Beckmann (1999). Numerical Ocean Circulation Modelling. Imperial College Press, 344 pp.

Hart T.J. (1934). On the phytoplankton of the South-West Atlantic and the Bellingshausen Sea, 1929-1931. Discovery Reports, 8, 1-268.

Hartmann C., B. Hollmann, G. Kattner, K.-U. Richter & A. Terbrüggen (1997). Nutrients, Dissolved and Particulate Matter. In: Reports on Polar Research: The expedition Antarktis XIII/1-2 of the research vessel ”Polarstern” in 1995/96, Bathmann U. V., M. Lucas, V. Smetacek, with contributions of the participants (eds.), 44-52.

Hense I. (1997). Chlorophyllverteilung und Phytoplanktonbiomasse in der antarktischen Polarfront. Diplomarbeit, Fachbereich Biologie/Chemie, University of Bremen, 72 pp.

Hense I., U. Bathmann, C. Hartmann, V. Strass & V. Smetacek (1998). Spiny phytoplankton-slowing down the carbon pump in the Southern Ocean? published as a supplement to EOS, Transactions, AGU, 79/1, OS31C-10.

Hense, I., U.V. Bathmann & R. Timmermannm (2000). Plankton dynamics in frontal systems of the Southern Ocean. Journal of Marine Systems, 27/1-3, 235-252.

Huntley M.E. & W. Nordhausen (1995). Ammonium cycling by Antarctic zooplankton in winter. Marine Biology, 121, 457-467.

Hutchins A. D. & K. W. Bruland (1998). Iron-limited diatom growth and Si:N uptake ratios in a coastal upwelling regime. Nature, 393, 561-564.

Hutchins D.A., V.M. Franck, M.A. Brzezinski & K.W. Bruland (1999). Inducing phytoplankton iron limitation in iron-replete coastal waters with a strong chelating ligand. Limnology and Oceanography, 44/4, 1009-1018.

Ikeda Y., G. Siedler & M. Zwierz, (1989). On the variability of Southern Ocean front locations between southern Brazil and the Antarctic Peninsula. Journal of Geophysical Research, 94/C4, 4757-4762.

Jerlov N.G. (1976). Marine Optics. Elsevier.

Jitts H.R., A. Morel & Y. Saijo (1976). The relation of oceanic primary production to available photosynthetic irradiance. Aust. J. Mar. Fresh. Res., 27, 441-454.

Klaas C., S. Kühn, S. Menden-Deuer, T. Reynarson & V. Smetacek (1997). Phytoplankton and heterotrophic protist counts. In: Reports on Polar Research: The expedition Antarktis XIII/1-2 of the research vessel ”Polarstern” in 1995/96, Bathmann U. V., M. Lucas, V. Smetacek, with contributions of the participants (eds.), 44-52.

Kumar N., R.F. Anderson, R.A. Mortlock, P.N. Froelich, P. Kubik, B. Dittrich-Hannen & M. Suter (1995). Increased biological productivity and export production in the glacial Southern Ocean. Nature, 378/6558, 675-680.

Laevastu T. (1960). Factors affecting the temperature of the surface layer of the sea. Comment. Phys. Math., 25/1.

Lancelot C., E. Hannon, S. Becquevort, C. Veth & H.J.W. de Baar (2000). Modeling phytoplankton blooms and carbon export production in the Southern Ocean: dominant controls by light and iron in the Atlantic sector in Austral spring 1992. Deep-Sea Research, 47/9, 1621-1662.

Landry M.R., R.T. Barber, R.R. Bidigare, F. Chai, K.H. Coale, H.G. Dam et al. (1997). Iron and grazing constraints on primary production in the central equatorial Pacific: An EqPac synthesis. Limnology and Oceanography, 42/3, 405-418.

Liebig von J. (1840). Organic chemistry and its application to agriculture and physiology. Taylor and Walton, London.

Longhurst A. (1995). Seasonal cycles of pelagic production and consumption. Progress in Oceanography, 36/2, 77-167.

Löscher B.M., H. J. W. de Baar, J. T. M. de Jong, C. Veth & F. Dehairs (1997). The distribution of Fe in the Antarctic Circumpolar Current. Deep-Sea Research, 44/1-2, 143-187.

Lorenzen C.J. (1972). Extiction of light in the ocean by phytoplankton. J. Cons., 34, 262-267.

Lutjeharms J.R.E. & H.R. Valentine (1984). Southern Ocean thermal fronts south of Africa. Deep-Sea Research, 31/12A, 1461-1475.

Martin J.H. (1990). Glacial-interglacial CO_2 change: The iron hypothesis. Paleoceanography, 5/1, 1-13.

Martin J.H., R.M. Gordon & S.E. Fitzwater (1990). Iron in Antarctic waters. Nature, 345, 156-158.

Mitchell B.G., E.A. Brody, O. Holm-Hansen, C. McClain & J. Bishop (1991). Light limitation of phytoplankton biomass and macronutrient utilization in the Southern Ocean. Limnology and Oceanography, 36/8, 1662-1677.

Moon C.H., S.R. Yang, H.S. Yang, H.J. Cho, S.Y. Lee & S.Y. Kim (1998). Regeneration processes of nutrients in the polar front area of the East Sea. 4. Chlorophyll alpha distribution, new production and the vertical diffusion of nitrate. Journal of the Korean Fisheries Society. 31/2, 259-266.

Morel F.M.M., R.J.M. Hudson & N.M. Price (1991). Limitation of productivity by trace metals in the sea. Limnology and Oceanography, 36/8, 1742-1755.

Nelson D.M. & P. Tréguer (1992). Role of silicon as a limiting nutrient to Antarctic diatoms: evidence from kinetic studies in the Ross Sea ice-edge zone. Mar. Ecol. Prog. Ser., 80, 255-264.

Nelson D. M., P. Tréguer, M.A. Brzezinski, A. Leynaert & B. Quéguiner (1995). Production and dissolution of biogenic silica in the ocean: Revised global estimates, comparison with regional data and relationship to biogenic sedimentation. Global Biogeochemical Cycle, 9/3, 359-372.

Norman J.R. (1938). Coast fishes, Part III, The Antarctic zone. Discovery Reports, 18/1-104.

Nowlin W.D. & J.M. Klinck (1986). The physics of the Antarctic Circumpolar Current. Reviews of Geophysics, 24/3, 469-491.

Onken R. (1992). Mesoscale upwelling and density finestructure in the seasonal thermocline–a dynamical model. Journal of Physical Oceanography, 22/11, 1257-1273.

Oschlies A. & V. Garçon (1998). Eddy-induced enhancement of primary production in a model of the North Atlantic Ocean. Nature, 394/6690, 266-269.

Oschlies A. & V. Garçon (1999). An eddy-permitting coupled physical-biological model of the North Atlantic. 1. Sensitivity to advection numerics and mixed layer physics. Global Biogeochemical Cycles, 13/1, 135-160.

Pacanowski R.C. & S.G.H. Philander (1986). A model of the seasonal cycle in the tropical Atlantic Ocean. Journal of Geophysical Research, 91, 14,192-14,206.

Parkinson C. L. & W. M. Washington (1979). A large-scale numerical model of sea ice. Journal of Geophysical Research, 84/C1, 311-337.

Pakhomov E.A., H.M. Verheye, A. Atkinson, R.K. Laubscher & J. Taunton-Clark (1997). Structure and grazing impact of the mesozooplankton community during late summer 1994 near South Georgia, Antarctica. Polar Biology, 18/3, 180-192.

Pingree R.D., P.M. Holligan & G.T. Mardell (1979). Phytoplankton growth and cyclonic eddies. Nature, 278, 245-247.

Pollard R.T. & L.A. Regier (1992). Vorticity and vertical circulation at an ocean front. Journal of Physical Oceanography, 22/6, 609-625.

Pondaven P., C. Fravalo, D. Ruiz-Pino, P. Tréguer, B. Quéguiner & C. Jeandel (1998). Modelling the silica pump in the Permanently Open Ocean Zone of the Southern Ocean. Journal of Marine Systems, 17, 587-619.

Pondaven P., D. Ruiz-Pino, J. N. Druon, C. Fravalo & P. Tréguer (1999). Factors controlling silicon and nitrogen biogeochemical cycles in high nutrient, low chlorophyll systems (the Southern Ocean and the North Pacific): Comparison with a mesotrophic system (the North Atlantic). Deep-Sea Research, 46, 1923-1968.

Quaatey S.N.K. & C.D. Maravelias (1999). Maturity and spawning pattern of Sardinella aurita in relation to water temperature and zooplankton abundance off Ghana, West Africa. Journal of Applied Ichthyology 15/2, 63-69.

Quéguiner B., P. Tréguer, I. Peeken & R. Scharek (1997). Biogeochemical Dynamics and the Silicon Cycle in the Atlantic Sector of the Southern Ocean During Austral Spring 1992. Deep-Sea Research, 44/2, 69-90.

Sakshaug E. & O. Holm-Hansen (1984). Factors governing pelagic production in polar oceans. In: Marine phytoplankton and productivity. Lecture notes on coastel and estuarine studies, 8, O. Holm-Hansen, L. Bolis, R. Gilles (eds.). Springer Verlag, 1-18.

Sarthou G., C. Jeandel, L.Brisset, D. Amouroux, T. Besson & O.F.X. Donard (1997). Fe and H_2O_2 distributions in the upper water column in the Indian sector of the Southern Ocean. Earth and Planetary Science Letters, 147, 83-92.

Scharek R., M.A. Van Leeuwe & H.J.W. De Baar (1997). Responses of Southern Ocean phytoplankton to the addition of trace metals. Deep-Sea Research, 44/1-2, 209-227.

Schnack S.B. (1985). Feeding by $Euphausia\ superba$ and copepod species in response to varying concentrations of phytoplankton. In: Antarctic nutrient cycles and food webs, W.R. Siegfried, P.R. Condy, R.M. Laws (eds.). Springer Verlag, 311-323.

Schülke M. (1998). Diatomeenverteilung und -biomasse im Bereich der antarktischen Polarfront. Diplomarbeit, Fachbereich Biologie/Chemie, University of Bremen, Germany, 101 pp.

Shiomoto A. & H. Ishii (1995). Distribution of biogenic silica and particulate organic matter in coastal and oceanic surface waters off the South Shetland Islands in summer. Polar Biol., 15, 105-113.

Six K.D. & E. Maier-Reimer (1996). Effects of plankton dynamics on seasonal carbon fluxes in an ocean general circulation model. Global Biogeochemical Cycles, 10/4, 559-583.

Smetacek V., H. J. W. de Baar, U. V. Bathmann, K. Lochte & M. M. Rutgers van der Loeff (1997). Ecology and biogeochemistry of the Antarctic Circumpolar Current during austral spring: a summary of Southern Ocean JGOFS cruise ANT X/6 of R.V. Polarstern. Deep-Sea Research, 44/1-2, 1-21.

Smith W.O. & D.M. Nelson (1985). Phytoplankton bloom produced by a receding ice edge in the Ross Sea: Spatial coherence with the density field. Science (Washington), 227,/4683, 163-166.

Smith N.R. & C.B. Fandry (1978). Combined effects of wind stress and topography in a two-layer model of the Southern Ocean. Deep-Sea Research, 25/4, 371-390.

Smith W.H.F. & D.T. Sandwell (1997). Global sea floor topography from satellite altimetry and ship depth soundings. Science, 277, 1956-1962.

Sommer U. (1986). Nitrate- and silicate-competition among antarctic phytoplankton. Marine Biology, 91, 345-351.

Spall S.A. & K.J. Richards (2000). A numerical model of mesoscale frontal instabilities and plankton dynamics–I. Model formulation and initial experiments. Deep-Sea Research, 47/7, 1261-1301.

Stramski D., R.A. Reynolds, M. Kahru & B.G. Mitchell (1999). Estimation of particulate organic carbon in the ocean from satellite remote sensing. Science (Washington), 285/5425, 239-242.

Strass V.H. (1994). Mesoscale instability and upwelling. Part 2: Testing the diagnostics of vertical motion with a three-dimensional ocean front model. Journal of Physical Oceanography, 24/8, 1759-1767.

Strass V.H., A.C. Naveira Garabato, R.T. Pollard, H.I. Fischer, I. Hense, J.T. Allen, J.F. Read, H. Leach & V. Smetacek (2001). Mesoscale Frontal Dynamics: Shaping the environment of primary production in the Antarctic Circumpolar Current. Deep-Sea Research, in press.

Sullivan C.W., K.R. Arrigo, C.R. McClain, J.C. Comiso & J. Firestone (1993). Distributions of phytoplankton blooms in the Southern Ocean. Science (Washington), 262/5141, 1832-1837.

Sverdrup H.U. (1953). On conditions for the vernal blooming of phytoplankton. J. Cons. Cons. Int. Explo. Mer., 18, 287-295.

Takeda S. (1998). Influence of iron variability on nutrient consumption ratio of diatoms in oceanic waters. Nature, 393, 774-777.

Tate Regan C. (1914). British Antarctic (Terra Nova) Expedition 1910, fishes. Terra Nova Reports Zoology, 1, 125-156.

Timmermann R., A. Beckmann & H.H. Hellmer (2000). Simulation of ice-ocean dynamics in the Weddell Sea. Part I: Model description and validation. Journal of Geophysical Research, in press.

Trathan P.N., M.A. Brandon & E.J. Murphy (1997). Characterization of the Antarctic Polar Frontal Zone to the north of South Georgia in summer 1994. Journal of Geophysical Research, 102/C5, 10483-10497.

Tréguer J. & G. Jacques, (1992). Dynamics of nutrients and phytoplankton, and fluxes of carbon, nitrogen and silicon in the Antarctic Ocean. Polar Biology, 12, 149-162.

van Franeker J.A. & N. W. van den Brink (1997). Censuses of marine birds and mammals. In: Reports on Polar Research: The expedition Antarktis XIII/1-2 of the research vessel "Polarstern" in 1995/96, Bathmann U. V., M. Lucas, V. Smetacek, with contributions of the participants (eds.), 116-121.

Veth C., I. Peeken & R. Scharek (1997). Physical anatomy of fronts and surface waters in the ACC near the 6°W meridian during austral spring 1992. Deep-Sea Research, 44/1-2, 23-50.

Wearn R.B. & J. Baker (1981). Relation of ocean currents to wind in the Southern Hemisphere. Climate Diagnostics Workshop. Proceedings, Mar. 1981; 5th, p.264-267.

Wefer G. & G. Fischer (1991). Annual primary production and export flux in the Southern Ocean from sediment trap data. Marine Chemistry, 35/1-4, 597-613.

Weinheimer A.L., J.P. Kennett & D.R. Cayan (1999) Recent increase in surface-water stability during warming off California as recorded in marine sediments. Geology, 27/11, 1019-1022.

Williams P.J. (1990). The importance of losses during microbial growth: commentary on the physiology, measurement and ecology of the release of dissolved organic material. Marine Microbial Food Webs, 4, 175-206.

WOCE Hydrographic Program Office, $http://oceanic.cms.udel.edu/woce/$, $http://www.dkrz.de/u241046/SACserver/SACHome.htm$

Wyrtki K. (1960). The Antarctic convergence and divergence. Nature, 187/4737, 581-582.

Zettler E.R., R.J. Olsen, B.J. Binder, S.W. Chisholm, S.E. Fitzwater & R.M. Gordon (1996). Iron-enrichment bottle experiments in the Equatorial Pacific: Responses of individual phytoplankton cells. Deep-Sea Research, 43/4-6, 1017-1029.

Zhuang G., Y. Zhen, R.A. Duce & P.R. Brown (1992). Link between iron and sulphur cycles suggested by detection of Fe(II) in remote marine aerosols. Nature, 355/6360, 537-539.

Zillmann J. W. (1981). A study of some aspects of the radiation and heat budgets of the southern hemisphere oceans. In: Meteorological study, 26, Bureau of Meteorology, Dept. of the Interior, Canberra, Australia, 526pp.

Of more general interest [than hydrography alone] are perhaps the [inter]annual variations in the currents....

Helland-Hansen und Nansen 1909

Teil IV

Regional and Interannual Variability of Ecosystem Dynamics in the Southern Ocean

Inga Hense, Ralph Timmermann, Aike Beckmann and Ulrich V. Bathmann

Alfred-Wegener-Institut für Polar- und Meeresforschung, Bremerhaven, Germany

submitted December, 4, 2001 to Ocean Dynamics

Abstract

To investigate regional and interannual variability of the ecosystem in the Southern Ocean, a coupled circumpolar ice-ocean-plankton model has been developed. The ice-ocean component (known as BRIOS-2) is based on a modified version of the s-Coordinate Primitive Equation Model (SPEM) coupled to a dynamic-thermodynamic sea ice-model. The biological model (BIMAP) comprises two biogeochemical cycles - silica and nitrogen - and a prognostic iron compartment to include possible effects of micronutrient limitation. Simulations with the coupled ice-ocean-plankton model indicate that the physical-biological interaction is not limited to the effect of a varying surface mixed layer depth. In the Pacific sector, large anomalies in winter mixed layer depth cause an increased iron supply and enhanced primary production and plankton biomass in the following summer, whereas in the Atlantic sector variability in primary production is caused mainly by fluctuations of oceanic upwelling. Thus, the ACW induces regional oscillations of phytoplankton biomass in both sectors, but not a propagating signal. Furthermore, interannual variability in plankton biomass and primary production is strong in the Coastal and Continental Shelf Zone and the Seasonal Ice Zone around the Antarctic continent. Interannual variability induced by the ACW has large effects on the regional scale, but the associated variability in vertical carbon fluxes is negligible compared to the long-term carbon sequestration of the Southern Ocean.

keywords: ACW, Southern Ocean, plankton biomass, primary production, interannual variability

1 Introduction

One of the prominent signals of interannual variability in the Southern Ocean is the Antarctic Circumpolar Wave (ACW) [*White and Peterson*, 1996]. Based on ECMWF reanalysis data along 56°S and on remote sensing sea ice concentration data, the ACW has been described as a set of closely connected anomalies of sea surface pressure and temperature, meridional wind stress and sea ice extent. These patterns propagate around Antarctica with a predominantly four-year period, typically featuring a quadrupole structure of positive and negative anomalies. They are linked to regional oscillations; quasiperiodic fluctuations of meridional wind stress in the Weddell Sea drive interannual variations of ice export and sea ice formation (Timmermann et al., 2001b).

Oscillations in air-sea CO_2 fluxes related to the ACW have been deduced from the interannual variability of the mixed layer depth in a global OGCM (Le Quéré et al., 2000). However, a systematic investigation of the ecosystem's response to quasi-periodic fluctuations in physical boundary conditions has not yet been performed.

To investigate the mechanims relevant for regional interannual variability of primary production and plankton bloom development, a biological model of intermediate complexity (BIMAP, Hense et al. 2001) has been coupled to a circumpolar ice-ocean model (Timmermann et al., 2001a). After a description of the model setup, we present results from the coupled simulations. It turns out that regional and interannual variations in physical boundary conditions like wind, heat fluxes and ice coverage strongly influence the occurence of phytoplankton blooms and that the mechanisms relevant for this interaction are not confined to the effects of a varying mixed layer depth.

2 Model Setup

The coupled ice-ocean-ecosystem model presented here is based on the circumpolar ice-ocean model BRIOS-2 (Timmermann et al., 2001a) which consists of a modified version of the *s-coordinate Primitive Equation Model* (SPEM; Haidvogel et al., 1991) and a dynamic-thermodynamic sea ice-model (Hibler, 1979; Lemke et al., 1990) and has been used succesfully in a number of regional climate-modeling and process study applications (Timmermann et al., 2001b; Beckmann et al., 2001).

The ecosystem model (BIMAP; Hense et al, 2001) includes two biogeochemical cycles - silica and nitrogen - and considers possible micronutrient limitation. It comprises compartments for phyto- and zooplankton, the nutrients nitrate, ammonium, silicate and iron and two compartments for nitrogen- and silica-based

detritus. Silica, nitrogen and iron uptake are linked by constant factors. Parameterizations are derived from measurements mainly from Antarctic diatom and copepod species. The model considers advection and diffusion using velocities and diffusivities from the ocean model and does not explicitly assume a homogeneous surface mixed layer. Coupled to an eddy-resolving implementation of SPEM, it has been used and validated in an idealized domain representing a section of the Antarctic Circumpolar Current (Hense et al., 2001) and shows good quantitative agreement with observations.

The presence of sea ice influences the marine ecosystem mainly by the absorption of light which reduces or prohibits primary production. In the coupled model, sea ice is assumed to absorb short-wave radiation in the photosynthetically active band with an extinction coefficient of 3 m^{-1}; total solar irradiance at the ocean surface is a weighted average over the ice-covered and open water parts of each grid cell using the ice concentration A as a measure of fractional coverage.

The ocean model is initialized using data from the Hydrographic Atlas of the Southern Ocean (Olbers et al., 1992) and with zero ice volume. Initial silicate and nitrate fields are derived from the WOCE data set (WOCE, 1997); for ammonium, phyto- and zooplankton we chose typical winter concentrations. Dissolved iron is initialized with no horizontal gradients and a concentration increasing linearly with depth (Löscher et al., 1997; Sohrin et al., 2000). Initial concentrations in the detritus pools are zero. The model is forced using 6-hourly wind fields, air and dew point temperatures, and cloudiness from the ECMWF-reanalysis of 1985 -1993 and the analysis of 1994-1999.

3 Results

3.1 Climatology

Climatological monthly means of phytoplankton distribution agree well with findings from observations and satellite images (Tréguer and Jacques, 1992; Moore and Abbott, 2000). During the period of maximum phytoplankton concentrations, in January (Fig. 1), areas with enhanced phytoplankton biomass are found in the coastal and continental shelf zones, at the northern tip of the Antarctic Peninsula, east of South America, and at some locations within the Seasonal Ice Zone, especially in the Ross Sea. High phytoplankton concentrations along the northern boundary resemble the increased biomass along the Antarctic Polar Front (APF). In the southern ACC, iron limitation causes a band with low chlorophyll concentrations, known as the high nutrient low chlorophyll (HNLC) area. We will return to the mechanisms relevant for the regional distribution of productive areas along with the discussion of their variability.

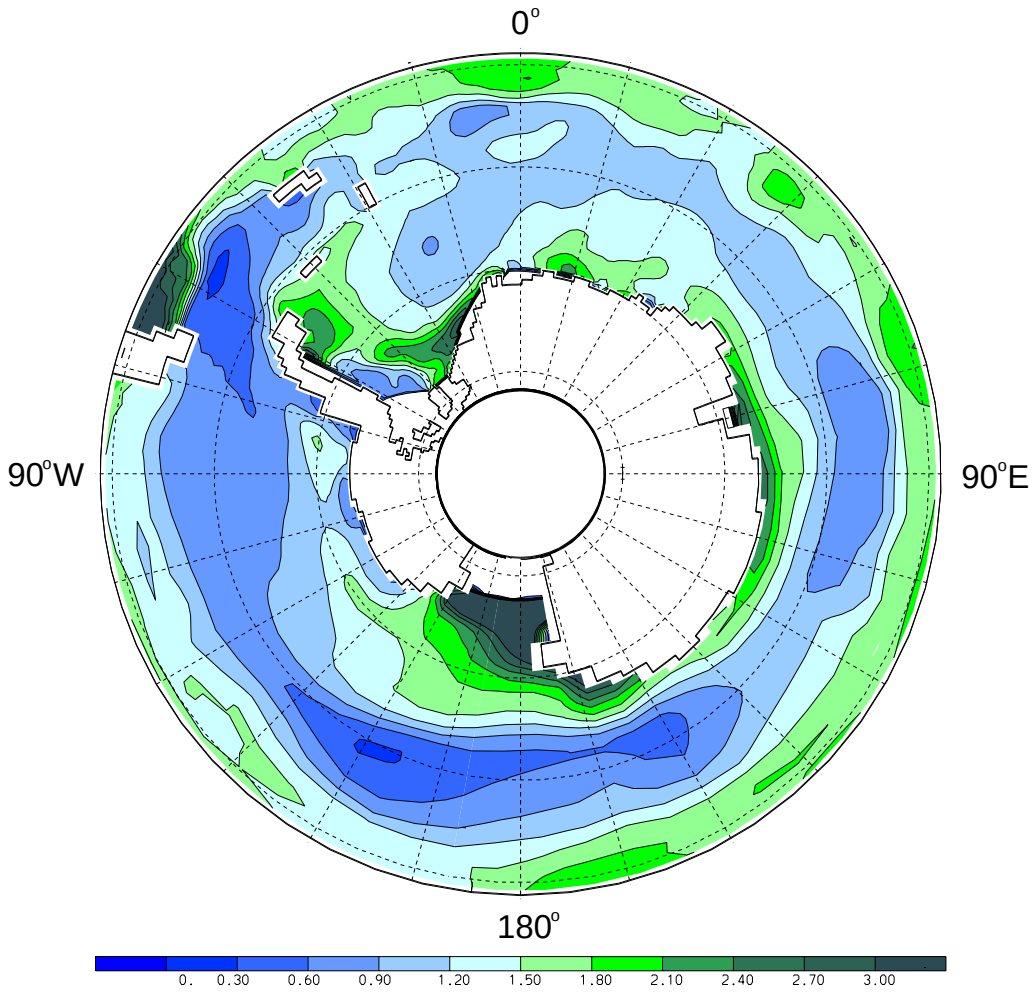

Figure 1: Climatological monthly mean surface phytoplankton concentration [μg Chl a/l] for January from a simulation with the coupled ice-ocean-ecosystem model.

3.2 Interannual variability in the southern ACC

Howmoeller diagrams of simulated sea surface temperature (SST) averaged between 53 and 61°S (Fig. 2, left panel) show propagating anomalies consistent with the analyses of White and Peterson (1996) and the simulations of Beckmann and Timmermann (2001). Maximum amplitudes (± 0.08°C) are found in the Pacific Sector at roughly 140 °W. Along with the SST, anomalies of mixed layer depth feature a local period of about 3-4 years (Fig. 2, rigth panel), propagating eastward around the globe within 5-8 years, which is consistent with simulations of Le Quéré et al. (2000) who used a 1.5 order turbulent closure scheme with an explicit formulation of the mixed layer. Propagating cold SST anomalies are generally associated with an anomalously deep mixed layer, but the highest amplitudes of mixed layer depth ($\pm$ 36 m) are found further west (155°W) in the Ross Sea sector and feature a pronounced local oscillation. This is the region where the largest ampliutdes of wind speed and heat flux variability are found; fluctuations of turbulent kinetic energy input caused by varying wind speed together with the interannual variability of surface heat fluxes create strong anomalies of mixed layer depth.

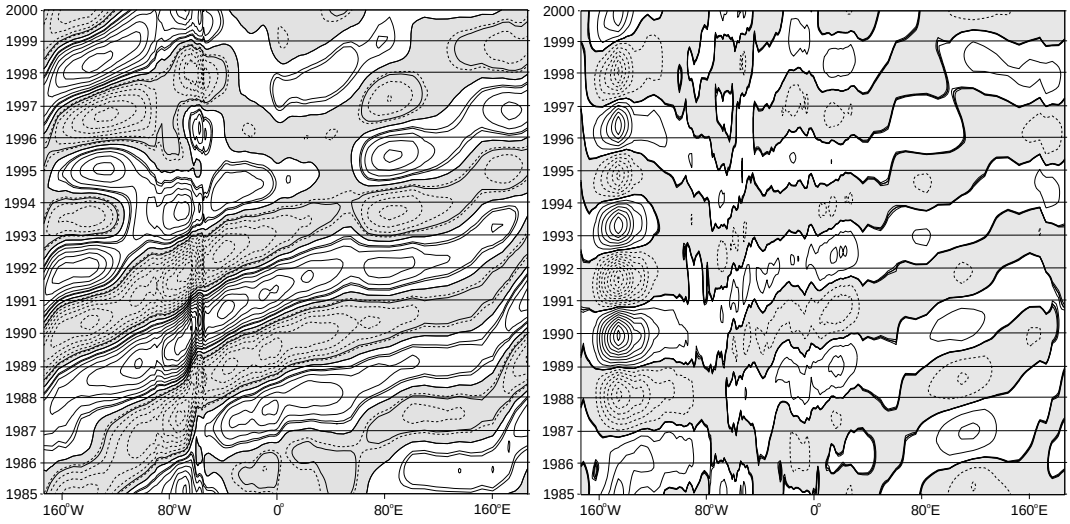

Figure 2: Filtered anomalies (averaged over 53 - 61°S) of SST (left) and mixed layer depth (right). Contour interval is 0.08°C for SST and 4 m for mixed layer depth. Negative values are grey-shaded. Data were filtered using a 3-7 yr bandpass filter, as in the analysis of White and Peterson (1996)

The ecosystem's response to the interannual variability of physical boundary conditions is at first sight surprising: A propagating signal in phytoplankton concentrations cannot be seen (Fig. 3, left panel). Along with the variability of mixed

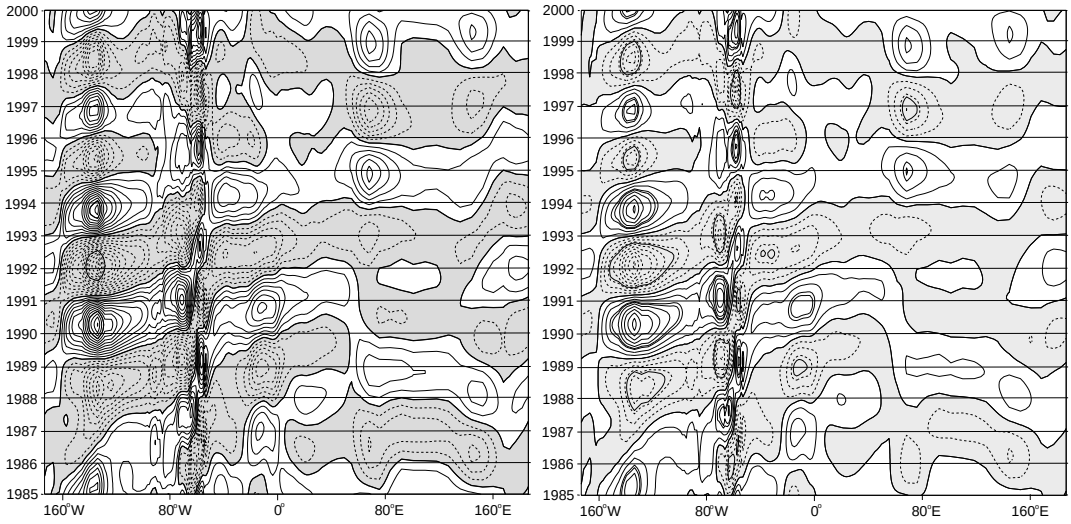

Figure 3: Filtered anomalies (averaged over 53 - 61°S) of phytoplankton (left) and zooplankton (right) concentrations. Contour interval is 0.01 μg Chl a / l for phytoplankton and 0.03 μg C / l for zooplankton. Negative values are grey-shaded.

layer depth, the largest anomalies of phytoplankton concentrations occur in the Pacific sector. Positive anomalies of phytoplankton concentrations are linked to positive anomalies of mixed layer depth.

Time series of regionally averaged iron concentration and mixed layer depth (Fig. 4, top panel) reveal that - while the variability of summer mixed layer depth is small - anomalously deep winter mixed layers cause a higher input of iron. This additional supply of iron enhances phytoplankton growth in the subsequent spring and summer. Thus, we find a time lag between the anomalies of mixed layer depth and iron concentrations on the one hand and phytoplankton concentrations on the other hand.

The characteristics of this interaction change at the Antarctic Peninsula. While maxima of winter mixed layer depth in the Pacific sector of the ACC cause positive anomalies of phytoplankton concentrations, this relation cannot be found in the Atlantic Sector of the ACC (including the Scotia Sea), where interannual variability of winter mixed layer depth is considerably smaller. Again, phytoplankton concentrations are enhanced following increased iron concentrations (Fig. 4, bottom panel). However, as the vertical velocity in the Atlantic sector of the ACC is considerably higher (mean: 0.038 m/d) than in the Pacific (0.018 m/d), iron supply in the Atlantic Sector of the ACC occurs mainly due to upwelling. Thus, the variations of surface concentrations of dissolved iron and thus the variations of primary production are mainly determined by anomalies of vertical velocity.

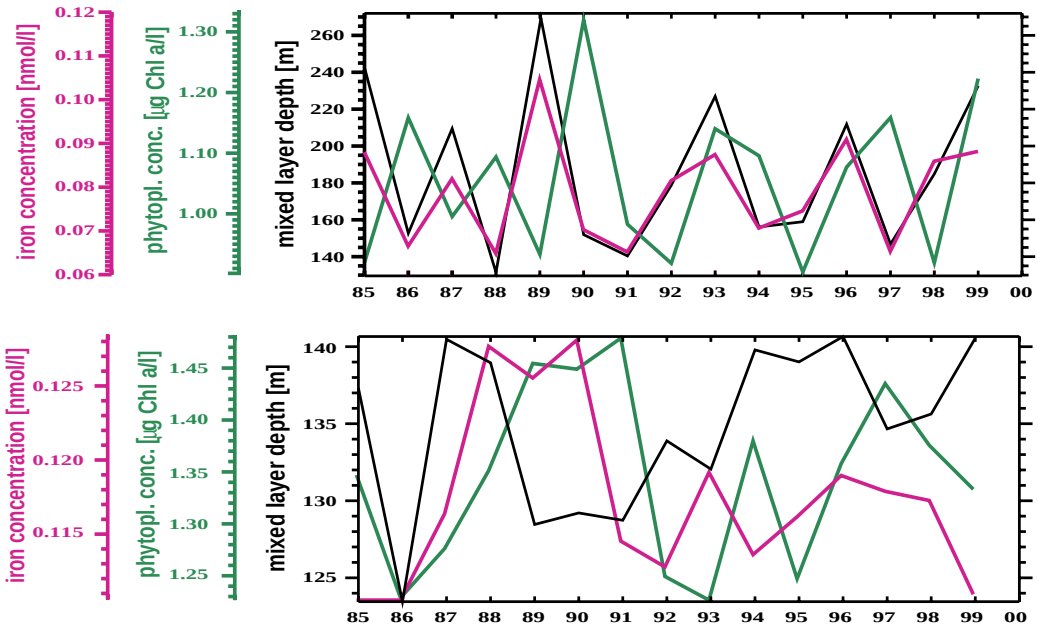

Figure 4: Time series of the simulated winter mixed layer depth (black), winter surface concentrations of iron (magenta), and summer surface concentrations of phytoplankton (green) for regions in the Pacific (53-61° S, 143-150° W; top) and in the Atlantic (53-61° S, 18-24° W; bottom) sector of the ACC.

Occasional exceptions occur in years with anomalously weak vertical velocity but strong positive anomalies in mixed layer depth, e.g. 1987 or 1996, where an increased iron supply results from entrainment at the mixed layer base.

Variations of zooplankton concentrations are closely related to the anomalies of phytoplankton concentration. Positive anomalies in phytoplankton concentration are associated with an enhanced growth of zooplankton. The maxima, however, are delayed by a few weeks.

3.3 Impact of sea ice - The Ronne Polynya

Oscillations associated with the ACW are not only visible in the ACC. Timmermann et al. (2001b) have shown that anomalies of the meridional wind stress in the inner Weddell Sea create an interannual variability of sea ice export. In austral summer 1997/1998, extraordinarily strong winds from southwest led to the development of a polynya in the southern Weddell Sea which is called “Ronne-Polynya” (Hunke und Ackley, 2001). In our simulation, the formation of a large area of open water in early summer leads to a large phytoplankton bloom in this usually ice-covered region (Fig. 5), which is consistent with remote sensing data

from the SeaWiFS (Moore and Abbott, 2000). Zooplankton quickly responds to the enhanced primary production and phytoplankton biomass, leading to an anomalously high standing stock of zooplankton biomass (not shown).

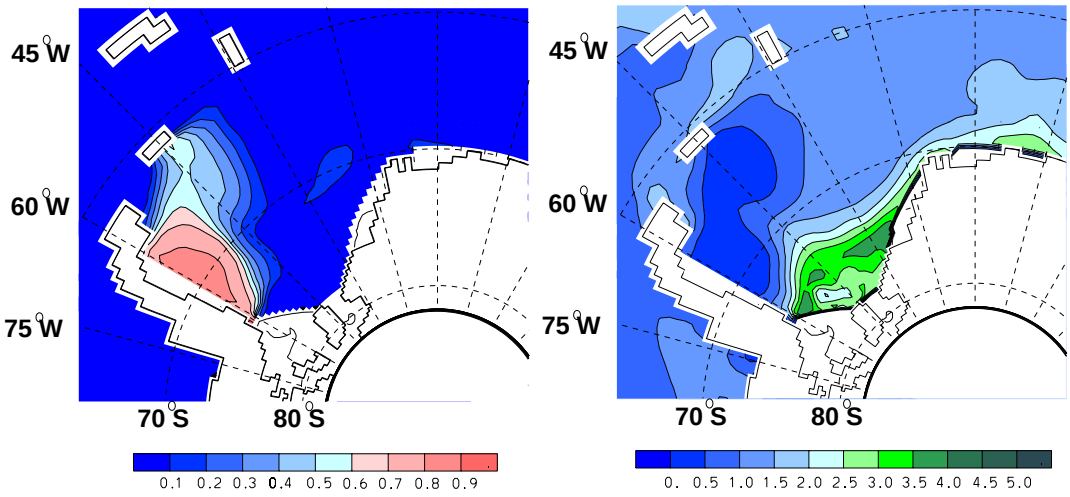

Figure 5: Simulated sea ice extent (left) and surface chlorophyll concentration [μg/l] (right) in the Weddell Sea for January 1998.

The spontaneous occurence of a phytoplankton bloom in the Ronne Polynya indicates that ecosystem dynamics in the Southern Ocean is strongly influenced by the ice coverage. Strong signals of interannual variability are found in the continental shelf zones and in regions which are seasonally ice-covered (Fig. 6). While the maximum of solar irradiance occurs in December, sea ice extent during early summer is still high. Phytoplankton blooms can only develop in regions of open water; as the location of early sea ice breakup varies considerably from year to year, so does the location of plankton blooms in the inner Weddell Sea. Due to the corresponding absorption of light, interannual variations of sea ice coverage cause significantly stronger fluctuations than the mixed layer anomalies in the Pacific sector of the ACC or others regions north of the seasonally ice-covered zone (SIZ).

Another region of increased phytoplankton variability is found near Maud Rise, in the eastern Weddell Sea. Regional upwelling induced by passing cyclones is locally enhanced due to the presence of the seamount. Here, atmospheric variability on a synoptic scale creates local anomalies of phytoplankton biomass.[4]

[4]In the real ocean, tidal rectification at the seamount (Beckmann et al., 2001) may further contribute to an enhanced productivity near Maud Rise.

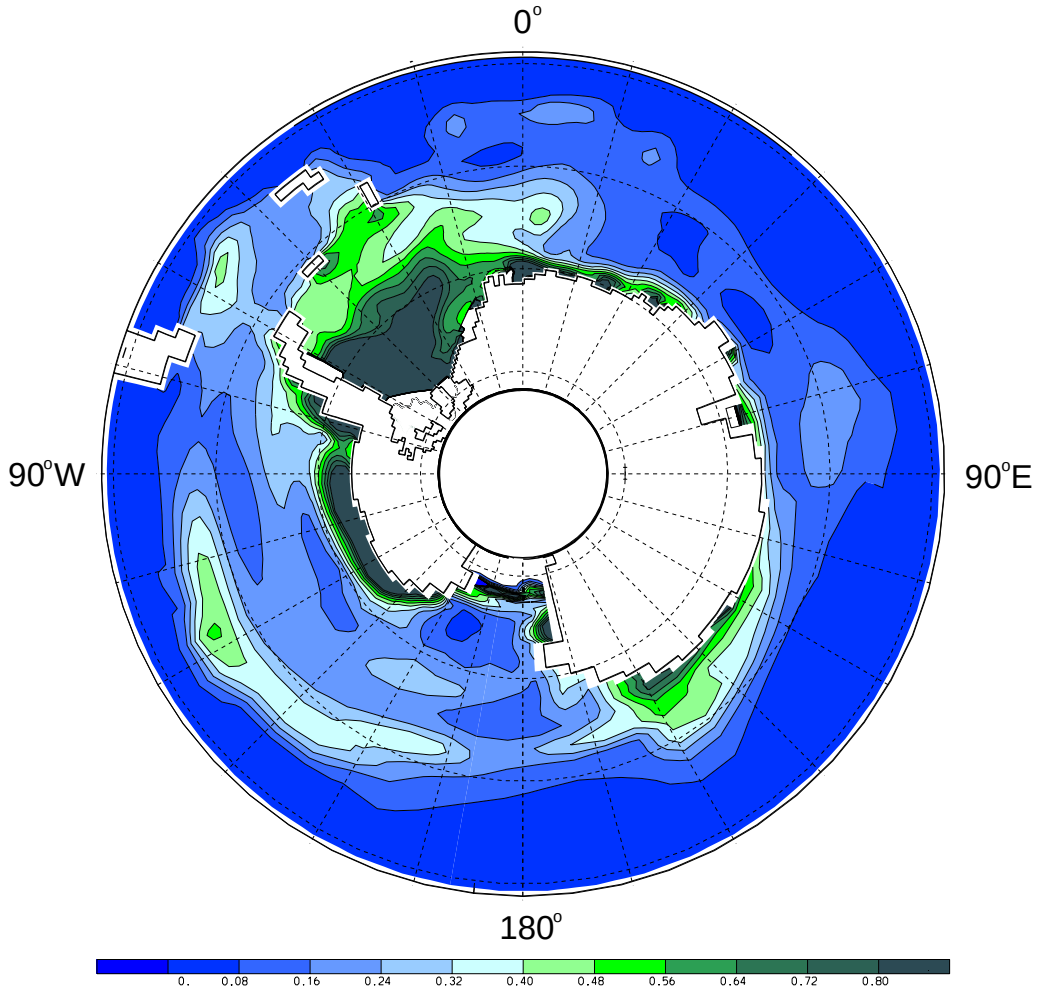

Figure 6: Relative standard deviation of summer surface concentrations of phytoplankton [μg Chl a/l] in January 1985-2000.

3.4 Regional and interannual variability of primary production

Area-averaged primary production in the different sectors of the Southern Ocean (Tab. 1) ranges from 32 to 43 g C m^{-2} y^{-1}, agreeing well with calculations derived from carbon requirements of top predators which are between 30 and 40 g C m^{-2} y^{-1} (Priddle et al., 1998). Regional differences in the productivity are coherent with estimates derived from satellite images and observations (Tréguer and Jaques, 1992; Rubin et al., 1998; Arrigo et al., 1998): Due to low iron concentrations, productivity in the Pacific sector is comparatively small. High simulated

phytoplankton concentration in the Ross Sea is caused by (a) an early start of phytoplankton bloom in the regularly occuring Ross Polynya, (b) a shallow surface mixed layer in summer (due to high input of sea ice melt water), and (c) persistent oceanic upwelling (0.6 m/d in 100 m depth in the April-September mean) in winter which ensures nutrient supply. In the Atlantic and Indian sectors, high productivity is confined to the Coastal and Continental Shelf Zone (CCSZ) and parts of the SIZ. It is partly counterbalanced by the low productivity in the iron limited permanent open ocean zone (POOZ), but as large parts of the CCSZ and SIZ in these sectors are ice-free for 3-4 months during austral summer, annual mean productivity amounts to values equal to or even greater than the rates from the Ross Sea sector.

Atlantic sector	36.9±1.5
Pacific sector	32.2±1.1
Ross Sea sector	37.9±1.5
Indian sector	43.3±1.6
Southern Ocean	38.1±0.8

Table 1: Area-averaged primary production [g C $m^{-2}y^{-1}$] south of 50°S of the Atlantic sector (63°W - 20°E), Pacific sector (150°W - 71°W), Ross Sea sector (150°W - 150°E), Indian sector (20°E - 150°E) and of the whole Southern Ocean.

The effect of local interannual variability on basin scale primary production is rather small. Total simulated primary production in the whole Southern Ocean is 1.7 GT C yr^{-1} with a standard deviation of only 0.037 GT C yr^{-1} (referring to an ensemble of annual means). Assuming that a total of 2.0±0.6 GT C yr^{-1} is sequestered by the ocean (by both the physical and the biological carbon pump; Battle et al., 2000) and assuming that maximum 4% of primary production is exported into the deep ocean (Fischer et al., 2000), interannual variability of simulated primary production converts into fluctuations of carbon sequestration of less than 1%.

4 Summary

We have presented a newly developed circumpolar coupled ice-ocean-ecosystem model that includes biogeochemical cycles of nitrogen and silica and considers possible iron limitation. It is configured in a circumpolar domain surrounding the Antarctic continent up to $50°$S. Consisting of a primitive-equation ocean model with a terrain-following vertical coordinate and a dynamic-thermodynamic sea ice-model, the physical component provides realistic boundary conditions for the modeled ecosystem. The use of high-frequency forcing data ensures an adequate

representation of atmospheric variability on seasonal and interannual time scales.

Model results indicate that interannual variability of primary production is negligible compared to the long-term carbon sequestration of the Southern Ocean. However, on regional (and local) scales atmospheric anomalies associated with the Antarctic Circumpolar Wave (ACW) strongly influence the ecosystem in the southern ACC and in parts of the Seasonal Ice Zone (SIZ). In the Pacific sector of the Southern Ocean, strongly varying winds and heat fluxes cause large anomalies of winter mixed layer depth. Increased iron supply due to vigorous entrainment at the mixed layer base stimulates primary production in the subsequent summer, so that high phytoplankton concentrations are found after a deep winter mixed layer. In the Atlantic sector, however, interannual variability of primary production is mainly caused by fluctuations of oceanic upwelling. Again, an increased iron supply triggers positive anomalies of phytoplankton biomass. However, as the mechanisms for the enhancements of primary production differ between the Pacific and the Atlantic Sector of the ACC, the ACW induces regional oscillations of phytoplankton biomass in both sectors, but not a propagating signal.

Regional productivity in the individual sectors of the Southern Ocean differs due to characteristic differences in the physical regime: Persistent oceanic upwelling mainly during the winter season, an early sea-ice breakup in the Ross-Polynya and a shallow mixed layer in summer cause a high productivity and high phytoplankton concentrations in the Ross Sea. Outside the Ross Sea, high productivity is confined to the Coastal and Continental Shelf Zone (CCSZ) and those parts of the SIZ where an early breakup of sea ice allows for the develepment of a phytoplankton bloom in a shallow mixed layer. Light limitation due to the presence of sea ice prohibits phytoplankton blooms in large parts of the SIZ; ACW-related sea ice anomalies like the Ronne Polynya of 1997/98 may thus induce spontaneous phytoplankton blooms even very far south.

A relatively simple ecosystem model like BIMAP cannot cover all ascpect of variability. Long-term obervations from Elephant Island indicate that krill populations increase in years with a large ice extent, while in “warm” years krill abundance is low and salps dominate the community of swarm organisms (Loeb et al. 1997; Siegel et al., 1998). Given the large impact of atmospheric variability on sea ice coverage, this would imply that fluctuations related to the ACW not only affect primary production and phytoplankton biomass but also induce shifts in species composition at higher trophical levels.

Acknowledgements

Data of the ECMWF analysis and reanalysis were recieved via the DWD.

References

Arrigo, K. R., Worthen, D., Schnell, A. & Lizotte, M. P.: Primary production in Southern Ocean waters. *J. Geophys. Res.*, **103(C8)**, 15,587-15,600 (1998).

Battle, M. et al.: Global carbon sinks and their variability inferred from atmospheric O_2 and delta ^{1}3C. *Science Wash.*, **287(5462)**, 2467-2470 (2000).

Beckmann, A. & Timmermann R.: Circumpolar Influences on the Weddell Sea: Indication of an Antarctic Circumpolar Coastal Wave. J. Climate, *14*, 3785-3792 (2001).

Beckmann, A., R. Timmermann, A. F. Pereira & C. Mohn: The effect of flow at Maud Rise on the sea ice cover - Numerical experiments. *Ocean Dynamics*, **52**, 11-25, 2001.

Fischer, G., Ratmeyer, V. & Wefer, G.: Organic carbon fluxes in the Atlantic and the Southern Ocean: relationship to primary production compiled from satellite radiometer data. *Deep-Sea Res. II*, **47(9-11)**, 1961-1997 (2000).

Haidvogel, D. B., Wilkin J. L. & Young R. E.: A semi-spectral primitive equation ocean circulation model using vertical sigma and orthogonal curvilinear horizontal coordinates. *J. Comput. Phys.*, **94**, 151-185 (1991).

Hense, I., Timmermannm R., A. Beckmann & Bathmann, U. V.: Regional ecosystem dynamics in the ACC: Simulations with a three-dimensional oceanplankton model. *Progress in Oceanography*, submitted (2001).

Hibler III, W. D.: A dynamic thermodynamic sea ice model. *J. Phys. Oceanography*, **9(4)**, 815-846 (1979).

Hunke, E. C. & Ackley S. F.: A numerical investigation of the 1997-1998 Ronne Polynya. *J. Geophys. Res.*, **106(C10)**, 22,373-22,382 (2001.)

Lemke P., Owens, W. B. & Hibler III, W. D.: A coupled sea ice - mixed layer - pycnocline model for the Weddell Sea. *J. Geophys. Res.*, **95(C6)**, 9513-9525 (1990).

Le Quéré, C., Orr, J. C., Monfray, P. & Aumont, O.: Interannual variability of the oceanic sink of CO2 from 1979 through 1997. *Global Biogeochem. Cycles*, **14**, 1247-1265 (2000).

Löscher, B. M., de Baar, H. J. W., de Jong, J. T. M. & Veth C.: The distribution of Fe in the Antarctic Circumpolar Current. *Deep-Sea Res. II*, **44(1-2)**, 143-187 (1997).

Moore, J. K. & Abbott, M. R.: Phytoplankton chlorophyll distributions and primary production in the Southern Ocean. *J. Geophys. Res.*, **105(C12)**, 28,709-28,722 (2000).

Olbers, D., Gouretski, V., Seiss, G. & Schröter, J.: Hydrographic atlas of the Southern Ocean. *Alfred Wegener-Institut für Polar- und Meeresforschung*, Bremerhaven (1992).

Priddle, J., Boyd,I. L., Whitehouse, M. J., Murphy, E. J. & Croxall, J. P.: Estimates of Southern Ocean primary production–constraints from predator carbon demand and nutrient drawdown. *J. Mar. Systems* **17(1-4)**, 275-288 (1998).

Rubin, S. I., Takahashi, T., Chipman, D. W. & Goddard, J. G.: Primary productivity and nutrient utilization ratios in the Pacific sector of the Southern Ocean based on seasonal changes in seawater chemistry.*Deep-Sea Res. I*, **45(8)**, 1211-1234 (1998).

Sohrin, Y. et al.: The distribution of Fe in the Australian sector of the Southern Ocean. *Deep-Sea Res. I* **47**, 55-84 (2000).

Timmermann, R., Beckmann, A. & Hellmer H. H.: Simulation of ice-ocean dynamics in the Weddell Sea. Part I: Model description and validation. *J. Geophys. Res.*, in press (2001a).

Timmermann, R., Hellmer, H. H. & Beckmann, A.: Simulation of ice-ocean dynamics in the Weddell Sea. Part II: Interannual variability 1985 — 1993. *J. Geophys. Res.*, in press (2001b).

Tréguer, J. & Jacques G.: Dynamics of nutrients and phytoplankton, and fluxes of carbon, nitrogen and silicon in the Antarctic Ocean. *Polar Biology*, **12**, 149-162 (1992).

White, B. W. & Peterson, R. G. An Antarctic circumpolar wave in surface pressure, wind, temperature and sea ice extent. *Nature*, **380(6576)**, 699-702 (1996).

WOCE Hydrographic Program Office Special Analysis Center,*http://www.dkrz.de/ u241046/SACserver/SACHome.htm* (1997).

To be sure, I have never pretended that [models] are truly realistic. My only defense has been that they help us to think.... They frequently yield results that are not intuitively obvious, and they teach us caution about drawing conclusions that seem to violate mathematical logic. That is the way physics and astronomy have grown. Biological oceanography, messy though it may be, needs the same kind of disciplined thinking.

G.A. Riley, 1984

Teil V

Schlußbetrachtung und Ausblick

Zur Untersuchung der Planktondynamik im Südpolarmeer wurde ein gekoppeltes biologisch-physikalisches Modell entwickelt, das die Charakteristika des pelagischen Ökosystems dieser Region widerspiegelt. Das biologische Modell (BIMAP) enthält miteinander gekoppelte Kreisläufe von Silizium, Stickstoff und Eisen; Parametrisierungen der Flüsse zwischen den verschiedenen Kompartimenten orientieren sich eng an Feldmessungen und Laborexperimenten mit antarktischen Diatomeen und den das Mesozooplankton dominierenden Copepoden. Primärproduktion ist eine Funktion des Licht- und Nährstoffangebots; der Fraßdruck durch Zooplankton wird als nichtlineare Funktion der Phytoplankton-Konzentration parametrisiert. Simulationen werden mit Nährstoffverteilungen aus dem WOCE-Datensatz initialisiert.

Dieses Modell wurde in verschiedenen Konfigurationen angewendet. In vertikal integrierten Studien mit vorgegebenen Bedingungen wurde die Sensitivität des Modells gegenüber unterschiedlichen Wachstumsraten, Halbsättigungskonstanten und Si:N-Aufnahmeverhältnissen untersucht. Eine mögliche Limitierung der Wachsumsrate durch Mikronährstoffe wurde hier zunächst vernachlässigt. Es stellte sich heraus, daß die maximale Planktonkonzentration zwar stark von der Wahl des Si:N-Aufnahmeverhältnisses und dem vorgegebenen Jahresgang der Deckschichttiefe abhängt, daß dieser einfache Ansatz aber nicht in der Lage ist, die beobachteten regionalen Unterschiede in der Planktonkonzentration im Antarktischen Zirkumpolarstrom zu reproduzieren.

Für Untersuchungen zur Planktondynamik in der Region um die Antarktische Polarfront wurde dieses Modell an eine wirbelauflösende, in einem periodischen Kanal konfigurierte Version des *s-coordinate Primitive Equation Models* (SPEM) gekoppelt. Mit einer horizontalen Auflösung von rund 6 km liefert das Modell eine realistische Beschreibung der mesoskaligen Dynamik an der Antarktischen Polarfront; die vertikale Diskretisierung auf 24 Schichten, von denen neun in den oberen 80 m liegen, erlaubt eine realitätsnahe Simulation der oberflächennahen Prozesse. In einer weiteren, zirkumpolaren Konfiguration mit gröberer Auflösung

umfaßt das Modellgebiet das gesamte Südpolarmeer südlich von 50°S.

Die Simulationsresultate weisen darauf hin, daß die Planktonverteilung im Südpolarmeer nicht nur durch die Verteilung der Makronährstoffe, sondern in ganz erheblichem Maße vom physikalischen Regime geprägt wird. Im Bereich der Antarktischen Polarfront (APF) führt barokline Instabilität zu mäandrierenden Strömungen und zur Ausbildung mesoskaliger Auf- und Abtriebsgebiete, die die Planktonverteilung auf mehrfache Weise beeinflussen. Maßgebend ist hierbei nicht allein die Variation der Deckschichttiefe: Die beobachteten flachen Deckschichten an der Polarfront und tiefere Deckschichten südlich davon werden zwar vom Modell realistisch wiedergegeben; sie können die regionalen Konzentrationsunterschiede aber nicht erklären. Stattdessen führen mäandrierende Strömungen und mesoskalige Auf- und Abtriebsgebiete zu einer lokalen, advektiven Umverteilung von Nährstoffen und Plankton, die sich in charakteristischen, mäander-ähnlichen Mustern widerspiegelt. So hebt sich die Polarfront als eine Region erhöhter Primärproduktion von der Umgebung ab: Während niedrige Silikatkonzentrationen nördlich der APF die Bildung reicher Phytoplanktonblüten verhindern, sorgt Eisenlimitierung im südlichen ACC für die Entstehung des aus Beobachtungen bekannten HNLC-Gebietes. Im Bereich der APF dagegen wird durch mesoskalige upwelling-Gebiete Eisen aus tieferen Schichten des Ozeans in die euphotische Zone transportiert, wobei sich die größten Vertikalgeschwindigkeiten (20 m/d) und damit die größten Transporte nicht innerhalb geschlossener Wirbel (*eddies*) finden, sondern an den Rücken der Mäander. Dieses Wasser ist naturgemäß arm an Phytoplankton, so daß sich die Auftriebsregionen als lokale Minima der Phytoplanktonkonzentration darstellen. Erst während sich das Wasser der horizontalen Divergenz folgend ausbreitet, kann Phytoplankton unter dem Einfluß der solaren Einstrahlung *so* lange wachsen, bis es in einer konvergenten Strömung (d.h. in einem *downwelling*-Gebiet) wieder in lichtärmere Schichten verfrachtet wird. Die maximalen Planktonkonzentrationen findet man daher in den *downwelling*-Gebieten.

Neben den mesoskaligen Prozessen im Bereich der mäandrierenden Front führt auch die Querfrontzirkulation, die im zonalen Mittel die Form einer meridionalen Umwälzbewegung hat, zu einer Umverteilung von Nährstoffen. Am Nordhang des im wirbelauflösenden Modell dargestellten Atlantisch-Indischen Rückens bildet sich in dieser Zirkulation eine Doppelzellenstruktur aus, die zur Entstehung von zwei Auftriebsgebieten führt. Diese bilden wieder relative Minima der zonal integrierten Planktonkonzentration, während sich das *downwelling*-Gebiet dazwischen durch erhöhten Phytoplanktonbestand auszeichnet. Die Doppelstruktur und die Ausbildung *zweier* Plankton-Minima sind an die Existenz dieses Rückens gebunden; offenbar haben also großskalige Merkmale der Bodentopographie einen Einfluß auf die Verteilung der Planktonbiomasse.

Nur unter Berücksichtigung möglicher Eisenlimitierung führen diese Prozes-

se zu einer realitätsnahen Wiedergabe der Planktonverteilung im ACC: Wird die Eisenlimitierung vernachlässigt, bildet sich unter dem Einfluß der großen Silikatkonzentrationen südlich der APF eine ausgedehnte Phytoplanktonblüte, die mit Beobachtungen nicht in Einklang steht. Die Konzentration von Eisen ist in den Simulationen horizontal homogen initialisiert; die erhöhte Biomasse im Bereich der Polarfront ist also kein Artefakt willkürlich gewählter Anfangs- oder Randbedingungen, sondern wird vom Modell als Teil der inhärenten Dynamik produziert. Nach etwa einem Jahr Integration stellt sich eine realistische horizontale Verteilung mit geringen Eisenkonzentrationen im südlichen ACC ein.[5]

Diese Resultate sind relativ robust gegenüber der Wahl der Halbsättigungskonstanten für die Eisenaufnahme. Da aus dem Südpolarmeer keine quantitativ auswertbaren Datensätze verfügbar waren, wurde die Referenzsimulation mit der aus Messungen im äquatorialen Pazifik (Landry et al., 1997) abgeleiteten Halbsättigungskonstanten von 0.12 nmol/l durchgeführt.

Sensitivitätsexperimente mit 0.6 nmol/l ergaben eine geringere Konzentration von Phyto- und Zooplankton, aber keine qualitativen Änderungen. Experimente mit einer Halbsättigungskonstanten von 1.2 nmol/l, wie sie von Lancelot et al. (2000) benutzt wurde, unterschätzen die Planktonkonzentration dagegen deutlich.

Die Modellresultate weisen auch darauf hin, daß Änderungen des Eiseneintrags in die Deckschicht den Bestand an Zooplankton stärker beeinflussen als den des Phytoplanktons. Obwohl der Fraßdruck der in BIMAP beschriebenen Mesozooplankter einen Anteil von 3 % der Primärproduktion im Zehntagesmittel nicht übersteigt, stellt er doch eine wichtige Senke für den Bestand von Phytoplankton dar. Bei steigender Nährstoffzufuhr steigt zwar die Primärproduktion an, der ebenfalls steigende Fraßdruck sorgt aber für eine nur moderate Erhöhung der Phytoplanktonkonzentration. Wird andererseits das upwelling von Eisen unterbunden, sinkt die Konzentration von Phytoplankton nahe der APF nur um 20%, während der Zooplanktonbestand um rund ein Drittel reduziert wird.

Der Einfluß von Schwarmorganismen auf die Horizontalverteilung des Phytoplanktons ist im Rahmen der bisher publizierten Studien nicht untersucht worden. Schwarmorganismen wie Salpen oder Krill können durch sehr effiziente Beweidung den Phytoplanktonbestand deutlich dezimieren (Dubischar und Bathmann, 1997; Perissinotto und Pakhomov, 1998); ihr Auftreten südlich der APF wurde in der Vergangenheit als mögliche Erklärung für das Entstehen des HNLC-Gebietes im südlichen ACC betrachtet. Um eine Abschätzung über die Größe dieses Effektes zu erhalten, wurde eine Simulation mit der zirkumpolaren Version des gekoppelten Modells durchgeführt, in der der Fraßdruck alle 5 Tage für 36 Stunden um den Faktor 10 erhöht wurde (Anhang C). In diesen Experimenten wird zwar

[5] Null- und ein-dimensionale Modelle können solche transienten Vorgänge nicht adäquat beschreiben. Ihre Ergebnisse hängen stark von der Wahl der Randbedingungen ab; ihre Eigendynamik ist stark reduziert.

ein reduzierter Bestand von Phytoplankton prognostiziert; der Effekt ist jedoch zu klein, um diese alternative Hypothese zu stützen.

Obwohl sie nicht zu einer qualitativen Veränderung der Phytoplanktonverteilung führen, beeinflussen Änderungen im Aufnahmeverhältnis von Si:N die Phytoplanktonbiomasse und die Nährstoffzusammensetzung des Meerwassers erheblich. Als Folge der stärkeren Silikatzehrung führen hohe Si:N-Aufnahmeverhältnisse in den Simulationen zu geringen Konzentrationen von gelöstem Silikat und zu Silikatlimitierung in weiten Teilen des Modellgebiets, während ein Si:N-Verhältnis von 1 zu einer Überschätzung der Planktonkonzentration im Bereich der Polafront führt. Für eine antarktische Planktongemeinschaft mit einem hohen Anteil von Diatomeen liefern Si:N-Aufnahmeverhältnisse zwischen 2 und 4 realistische Resultate - was konsistent mit Analysen der natürlichen Planktongemeinschaft in dieser Region (Nelson und Smith, 1986; Shiomoto und Ishii, 1995; Quéguiner et al., 1997; Hense, 1997) ist. Als Ursache für diese Verschiebung der Stöchiometrie werden u.a. physiologische Effekte der Eisenlimitierung (Takeda, 1998; Hutchins und Bruland, 1998) vermutet. Es ist naheliegend, daß Veränderungen der Elementzusammensetzung innerhalb des Phytoplanktons und der Aufbau der dicken Silikatschalen (Nelson und Smith, 1986; Shiomoto und Ishii, 1995; Quéguiner et al., 1997; Schülke, 1998) die Exportflüsse von Silizium und Kohlenstoff beeinflussen können. Jedoch sind in BIMAP die biogeochemischen Prozesse außerhalb der euphotischen Zone stark vereinfacht dargestellt, so daß Aussagen über die Exportflüsse gegenwärtig nicht möglich sind.

Daß sich die komplexen Wechselwirkungen zwischen Hydrographie und Ökosystem nicht durch die simple Annahme eines erhöhten Wachstums bei flacher Deckschicht beschreiben lassen, wird auch in Simulationen in der zirkumpolaren Konfiguration deutlich. Bei Untersuchungen der zwischenjährlichen Variabilität des Ökosystems im Südpolarmeer zeigen sich große regionale Unterschiede in den grundlegenden Wechselwirkungen zwischen physikalischen Randbedingungen und der Reaktion des Ökosystems: Im pazifischen Sektor (nördliches Amundsen-/Bellingshausenmeer) führen positive Anomalien der winterlichen Deckschichttiefe zu signifikant erhöhtem Eiseneintrag und damit zu erhöhten Phytoplanktonkonzentrationen im folgenden Sommer. Im atlantischen Sektor dagegen, wo Anomalien des atmosphärischen Antriebs weniger ausgeprägt sind, ist die zwischenjährliche Variabilität der Deckschichttiefe gering. Hier bilden Anomalien der Vertikalgeschwindigkeit die primäre Ursache für zwischenjährliche Variationen des Planktonwachstums. In beiden Sektoren haben mit der Antarktischen Zirkumpolarwelle verknüpfte atmosphärische Anomalien signifikanten Einfluß auf den Aufbau einer Phytoplanktonblüte, jedoch verhindert die Verschiedenheit der hierfür relevanten Mechanismen die Ausbildung eines zirkumpolar fortschreitenden Signals.

Eine Schlüsselrolle in diesen Mechanismen spielt stets die Limitierung des

Wachstums durch die Verfügbarkeit von gelöstem Silikat, oder - häufiger - von gelöstem Eisen.[6] Auf den ersten Blick stützt dies die von Martin (1990) aufgestellte Eisenhypothese: Die Modellergebnisse weisen darauf hin, daß die Primärproduktion in großen Teilen des Südpolarmeeres eisenlimitiert ist. Es ist anzunehmen, daß erhöhte Konzentrationen von Phyto- und Zooplankton durch vermehrte Produktion von (i.a. schnell absinkenden) Kotballen einen erhöhten Export von Kohlenstoff hervorrufen, doch weisen Untersuchungen von González und Smetacek (1994) darauf hin, daß viele der Kotballen von kleineren Copepoden aufgenommen werden und so nicht mehr zu einem erhöhten Export beitragen können (Dubischar und Bathmann, 2001). Zudem legt die enge Verknüpfung von Primärproduktion/Planktonbiomasse mit den physikalischen Bedingungen den Schluß nahe, daß Veränderungen der Hydrographie beim Übergang zum Glazial vergleichbar große Änderungen der Primärproduktion und damit der CO_2-Fixierung verursacht haben könnten. Ob sich diese Effekte addieren oder (mindestens teilweise) kompensieren, ist zur Zeit unklar.

Die Untersuchung zwischenjährlicher Variabilität führte zur Identifikation biologischer *centers of action*. Gebiete mit hoher zwischenjährlicher Variabilität der sommerlichen Planktonblüte liegen im Pazifischen Sektor des Südpolarmeeres, wo starke, wahrscheinlich mit der *El Niño*-Oszillation assoziierte atmosphärische Anomalien große Variationen der sommerlichen Planktonkonzentration verursachen, sowie im saisonal eisbedeckten Bereich. Variationen der sommerlichen Eisausdehnung, verursacht durch die Antarktische Zirkumpolarwelle (ACW; vgl. Timmermann et al., 2001b), spiegeln sich in wechselnden Verteilungen der sommerlichen Planktonblüte in den antarktischen Randmeeren wieder. Hohe Planktonkonzentrationen im Rossmeer konnten auf anhaltendes *upwelling* vor allem während der Wintermonate, ein frühes Aufbrechen des Meereises in der Ross-Polynya und flache Deckschichten im Sommer zurückgeführt werden. Singuläre Ereignisse wie die Ronne-Polynya im Jahre 1998 führen zu ausgeprägten Anomalien; da diese aber regional und zeitlich eng begrenzt sind, bleibt ihr Einfluß auf die zirkumpolar integrierte Primärproduktion und damit den globalen Kohlenstoffkreislauf gering.

Über die hier beschriebene, überwiegend durch physikalische Gegebenheiten verursachte, zwischenjährliche Variabilität hinaus weisen Beobachtungen insbesondere im ACC und in der Eisrandzone darauf hin, daß die Artenzusammensetzung des marinen Ökosystems erheblichen Schwankungen unterworfen sein kann. So zeigen Untersuchungen von Loeb et al. (1997) und Siegel et al. (1998), daß in Jahren mit viel Meereis die Population von Krill deutlich anwächst, Salpen hingegen nur einen geringen Anteil der Biomasse stellen, während in Jahren mit geringer Meereisausdehnung die Salpen dominieren. BIMAP enthält gegenwärtig nur

[6] Um die Verläßlichkeit künftiger Modelluntersuchungen zu erhöhen, wäre eine Verbesserung der Datenbasis für die regionale Verteilung von gelöstem Eisen wünschenswert.

je ein Phyto- und Zooplankton-Kompartiment; Verschiebungen in der Artenzusammensetzung können also nicht beschrieben werden. Ein möglicher Schritt zur Verbesserung des Modells wäre die Erweiterung um zusätzliche Kompartimente. Da die dominierenden blütenbildenden Phytoplanktonarten hauptsächlich Diatomeen, lokal aber auch *Phaeocystis sp.* sind, erscheint es sinnvoll, verschiedene Diatomeenarten mit unterschiedlichem Nährstoffbedarf, vor allem aber auch eine prognostische Beschreibung von Phaeocystis, dessen Wachtstum ohne Silikataufnahme erfolgt, zu implementieren. Zusätzliche Zooplanktonkompartimente könnten die kleinen Copepoden sowie verschiedene Schwarmorganismen umfassen. In Verbindung mit einer Erweiterung des Modells um eine einfache Beschreibung des Exportes von organischem Material aus der oberflächennahen Deckschicht würde dies eine umfassende Beschreibung der Biogeochemie, insbesondere der Flüsse von Silizium und Kohlenstoff im Südpolarmeer erlauben.

A Struktur des biologischen Modells

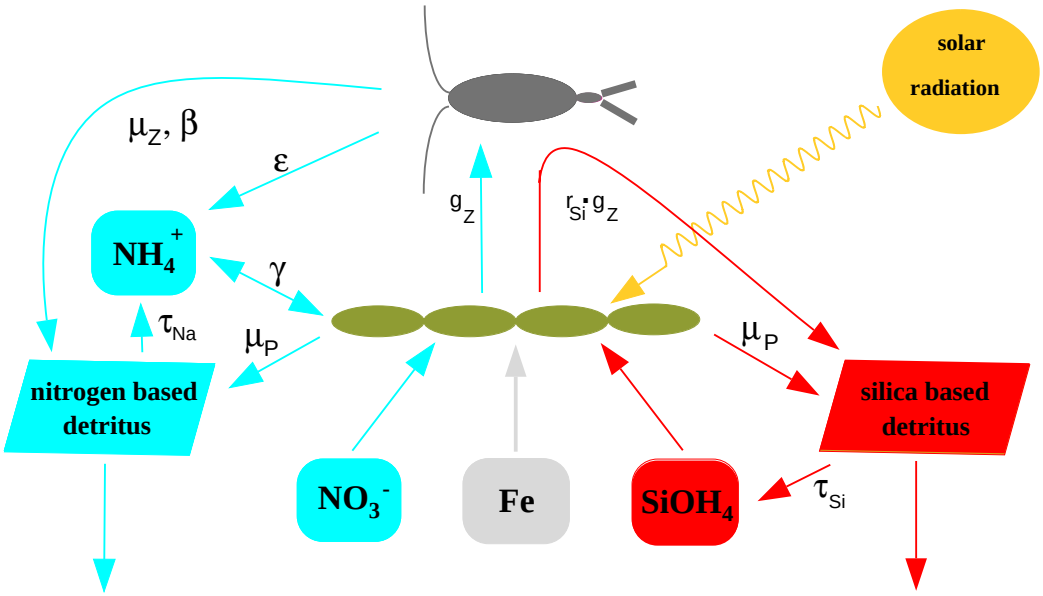

Abbildung A.1: Struktur des Ökosystemmodells BIMAP. Dargestellt sind die Kreisläufe von Silizium (rot) und Stickstoff (orange) und die Aufnahme von Eisen (braun).

Das biologische Modell (BIMAP) enthält miteinander gekoppelte Kreisläufe von Silizium, Stickstoff und Eisen (Abb. A.1). Die Aufnahmeraten der Nährstoffe sind durch feste Verhältnisse r_{Si}, r_{Fe} miteinander verknüpft. Primärproduktion ist eine Funktion des Licht- und Nährstoffangebots; wobei jeder der Nährstoffe Nitrat, Silikat und Eisen das Phytoplanktonwachstum limitieren kann. Bei der Exudation (γ) frei gewordener Stickstoff wird direkt dem Ammoniumkompartiment zugeführt. Der Fraßdruck durch Zooplankton (g_Z) wird als nichtlineare Funktion der Phytoplankton-Konzentration parametrisiert. Der Stickstoffanteil wird vom Zooplankton aufgenommen und in Biomasse umgesetzt; der Siliziumanteil geht direkt in den entsprechen Detritus-pool. Der bei der Exkretion (ϵ) frei gewordene Stickstoff wird dem Ammonium-Kompartiment hinzugefügt. Ausscheidungen von Zooplanktern (”faecal pellets”; β) bilden zusammen mit der abgestorbenen Phyto- und Zooplanktonbiomasse (μ_P, μ_Z) die Quellen des stickstoffbasierten Detritus-Kompartiments. Remineralisierung (τ_N, τ_{Si}) und Verluste durch Absinken stellen die Senken der Detritus-Kompartimente dar. Die Gleichungen und Parameter sind in Teil III ausführlich erläutert.

B Artikel in der UNESCO-Zeitschrift WIND$_O$W

DEVELOPMENT OF A PLANKTON-MODEL FOR THE SOUTHERN OCEAN

Although the Southern Ocean is rich in nutrients, phytoplankton biomass is generally low. Hence the Southern Ocean is one of the three large high nutrient low chlorophyll (HNLC) areas.

However, cruise data and satellite images show a high variability in the distribution of phytoplankton biomass. The Antarctic Polar Front is characterized by high phytoplankton biomass which highlight this region as an exceptional zone with frequent plankton blooms in the ambient HNLC area.

The question that has been raised is why the phytoplankton biomass is higher in the Polar Front than in the ambient area - or why the phytoplankton biomass is low outside the Polar Front.

Different explanations for the factors controlling the occurrence of phytoplankton blooms are given as follows:-

- Frontal dynamics lead to areas of intense upwelling. This is linked to a shallow mixed layer and a higher supply of nutrients in the euphotic zone.
- Swarm organisms like salps and krill which are not present in the Antarctic Polar Front may limit the development of phytoplankton biomass in the southern area.
- Lower iron concentration in the southern area may limit the development of a phytoplankton bloom. In a 1992 Joint Global Ocean Flux Studies (JGOFS) cruise, a higher concentration of iron in the Polar Front coincided with a phytoplankton bloom.

Modelling Approach

Our model, called the Biological Model for the Antarctic Polar Front (BIMAP), is meant to be an instrument to study the processes stimulating and controlling phytoplankton blooms in the Southern Ocean.

The model is based on the paper by Fasham *et.al.* (1990). The concept of the model is to divide the marine biosphere into several compartments and to compute fluxes of biomass between them. Biomass and fluxes are calculated in nitrogen units. We decided to confine ourselves to phytoplankton and of course their main predator the zooplankton represented by herbivorous copepods and the nutrients nitrate, ammonium and silicate.

The phytoplankton in the Polar Front is dominated by large diatoms which have a great demand for silicate. Therefore, silicate is the most limiting macronutrient in some regions of the Southern Ocean especially in the region of the Polar Front. Although nitrate and ammonium are not in limiting concentrations in that region, we decided to take them into account because:

- The reasonable dataset on nutrient concentrations available gives a good chance for validation;
- There is discussion about the Si:N uptake-ratio of phytoplankton in the Southern Ocean. Generally, the uptake ratio of these two nutrients was regarded as 1:1. Nevertheless, numerous authors have recorded a higher uptake ratio or "disappearance ratio" of up to 4.0 in the Southern Ocean. With the help of the model we are testing different uptake ratios;
- Later on, we intend to implement an iron compartment which has an effect on the uptake of nitrate.

We decided to disregard the compartments of dissolved organic nitrogen (DON), bacteria and the non-living organic matter (detritus). There is still some uncertainty about the role of DON. Only the labile substances are known and these are remineralized rapidly, thus we directly lead the DON exuded by phytoplankton into the ammonium pool. We disregard bacteria and detritus because we only care for processes in the upper ocean and we assume that remineralization is quite low there.

Different versions of the model are being constructed and these are:

- a vertically integrated model, so called 0-dimensional model (0d-model);
- a 1d-model;
- a coupled 3d-ocean-plankton-model to record the influence of frontal systems.

0d- and 1d-model runs will always accompany 3d model runs. The 0d- and 1d-model are able to run on a workstation or on a PC. They are forced by annual cycles of the mixed layer depth and by solar radiation considering the daily and annual cycles, the latitude and a mean cloud cover after the standard astronomical formulae (Brock, 1981). The mixed layer depth is derived from a 1-dimensional mixed layer model.

A difficulty of this kind of modelling is that data for that area are quite sparse. Cruises in that area take place mainly in summer and only for short times, mostly 6 weeks. Neither annual cycles of mixed layer depth to force the model nor seasonal cycles of phytoplankton biomass for validation are available. Only "snapshots" of the concentrations of phytoplankton and zooplankton in summer and winter and a reasonable dataset of nutrient concentrations are available. The parameters to calculate the fluxes between phytoplankton, zooplankton and nutrients - growth rate, the initial slope of the photosynthetic irradiance curve, exudation, mortality, grazing pressure, half saturation constants for nutrients etc. - were partly difficult to find in literature but even for the Southern Ocean these data were measured in some cruises. We aspire to keep the number of free parameters as low as possible. That means we tend to

confine ourselves to rather few compartments and stick to those fluxes where measured parameters are available.

Some Model Results and Future Work

We ran the model at two positions in the Polar Front at 50°S and south of it at 59°S without changing parameters except the concentration of nutrients, which are higher south of the Polar Front, the solar radiation and the annual cycle of the mixed layer depth.

Although very simple, the vertically integrated model is able to reproduce regional differences. The concentrations of phytoplankton and zooplankton at 50°S are reproduced quite realistically. Silicate is low for about 6 months and limits the growth of phytoplankton. It is often recorded that silicate is depleted in the Polar Front but it might be unrealistical over such a long period. Thus our first approach to disregard remineralization and dissolution of biogenic silicate might be wrong. Model runs with a detritus compartment considering remineralization and dissolution shall test the influence of these processes. According to observations, south of the Polar Front the phytoplankton biomass is lower than in the Polar Front, however the model fails to reproduce the concentrations of phytoplankton zooplankton and nutrients. Thus other processes may limit the growth of phytoplankton.

The development of the 1d model is finished but model runs have to be analysed. It seems that remineralization of nutrients and dissolution of silicate is important for the reflection of the vertical structure of these nutrients.

Furthermore, we have added a new compartment of small phytoplankton (flagellates) which have almost no demand on silicate, and another new compartment with small zooplankton but this version is not ready yet. Last but not least the development of the coupled biological and physical 3d-model goes on...

References

Brock, T.D. 1981. Calculating solar radiation for ecological studies. Ecological Modelling, 14: 1-19.

Fasham, M.J.R., Ducklow, H.W., McKelvie, S.M. 1990. A nitrogen-based model of plankton dynamics in the oceanic mixed layer. Journal of Marine Research, 48: 591-639.

Inga Hense
Alfred Wegener Institute for Polar and Marine Research
D-27515 Bremerhaven
GERMANY
Email: ihense@awi-bremerhaven.de

The author is attending a PhD-programme in the groups of Biological Oceanography and Ocean Modelling. The AWI research programme is sponsored by the German Federal Ministry of Science and Technology.

WINDOW
WESTERN INDIAN OCEAN WATERS

C Eisenlimitierung und Schwarmorganismen im zirkumpolaren biologisch-physikalischen Modell

In Simulationen mit der wirbelauflösenden Konfiguration des gekoppelten Plankton-Ozean-Modells (Teil III) hat sich gezeigt, daß Eisenlimitierung im südlichen ACC die Entstehung von Planktonblüten verhindert und zu den niedrigen Phytoplanktonkonzentrationen führt, wie sie in der Region beobachtet werden können. Eine Vernachlässigung möglicher Eisenlimitierung führt in diesen Experimenten zu einer qualitativ unrealistischen Planktonverteilung mit einer deutlichen Überschätzung der Biomasse im südlichen ACC.

Um zu überprüfen, ob dies auch im zirkumpolaren gekoppelten Plankton-Meereis-Ozean-Modell gilt, wurde neben den in Teil IV beschriebenen Simulationen ein Experiment durchgeführt, in dem der Effekt der Eisenlimitierung ignoriert wird. Es stellt sich heraus, daß auch in dieser Konfiguration die Phytoplanktonkonzentration im südlichen ACC durch die Verfügbarkeit von gelöstem Eisen bestimmt wird. Das HNLC-Gebiet im südlichen ACC wird in Experimenten ohne Eisenlimitierung nicht reproduziert (Abb. C.1, links).

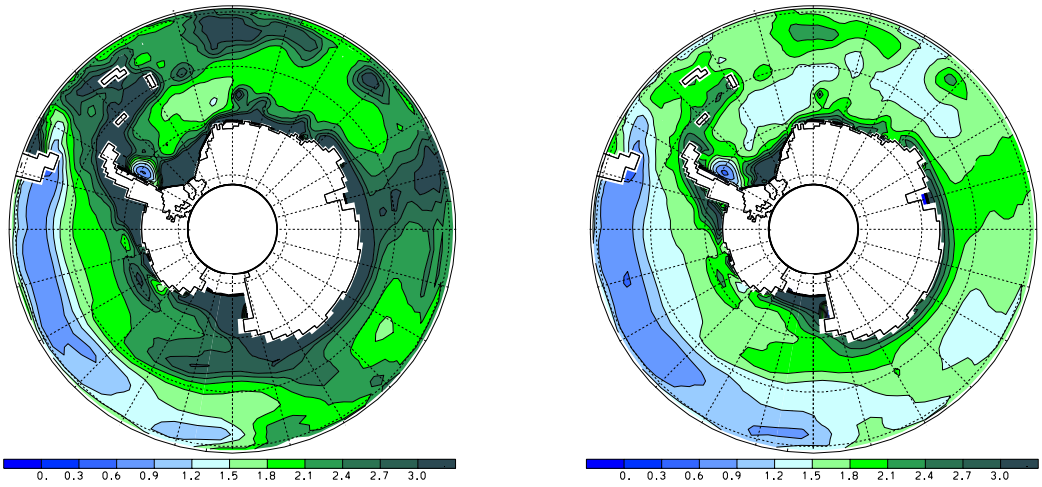

Abbildung C.1: Klimatologisches Januar-Mittel der Phytoplanktonkonzentration [μg Chl a/l] in Experimenten ohne Eisenlimitierung (links), und mit Schwarmorganismen (rechts). Das entsprechende Feld aus der Referenzsimulation ist in Teil IV, Fig. 1 abgebildet.

Schwarmorganismen haben im Vergleich zum Mesozooplankton eine 10-20fach höhere Fraßrate, so daß sie über 100% der täglichen Primärproduktion verzehren können (Dubischar und Bathmann, 1997). Wie in der Einführung beschrieben, bezieht sich eine Alternativhypothese für das Entstehen des HNLC-

Gebietes auf das Vorkommen von Schwarmorganismen (Salpen, Krill) in dieser Region. Um eine Abschätzung des möglichen Effektes zu erhalten, wurde in einem Experiment ohne Eisenlimitierung die Fraßrate des Mesozooplanktons alle 5 Tage für 36 Stunden um den Faktor 10 erhöht. In diesem Experiment werden zwar deutlich geringere Phytoplanktonkonzentrationen produziert, doch wird die Phytoplanktonbiomasse im südlichen ACC weiterhin überschätzt (Abb. C.1, rechts). Fraßdruck durch Schwarmorganismen kann daher im Gegensatz zu Eisenlimitierung nicht die sehr niedrigen Phytoplanktonkonzentrationen im südlichen ACC erklären.

Literaturverzeichnis

Abrams, R. W. und J. R. E. Lutjeharms (1986). Relationships between seabirds and meso-scale hydrographic features in the Agulhas Current Retroflection region. In: *Acta XIX Congressus Internationalis Ornithologici*, **I**, Ottawa, Canada, 22-29.VI.1986, 991-996.

Ban, S. et al. (2001). The paradox of diatom-copepod interactions. *Mar. Ecol. Prog. Ser.*, **157**, 287-293.

Bathmann, U.V., R. Scharek, C. Klaas, C. D. Dubischar und V. Smetacek (1997) Spring development of phytoplankton biomass and composition in major water masses of the Atlantic Sector of the Southern Ocean. *Deep-Sea Res.*, **44/1-2**, 51-68.

Beckmann, A., H. H. Hellmer und R. Timmermann (1999). A numerical model of the Weddell Sea: large scale circulation and water mass distribution. *J. Geophys. Res.*, **104/C10**, 23375-23391.

Brussard, C. P. M. (1997). Phytoplankton cell lysis and its ecological implications. *Annu. Rep. Neth. Inst. Sea Res.*, 1997.

de Baar, H. J. W., J. T. M. de Jong, D. C. E. Bakker, B. M. Löscher, C. Veth, U. Bathmann und V. Smetacek (1995). Importance of iron for plankton blooms and carbon dioxide drawdown in the Southern Ocean. *Nature*, **373**, 412-415.

Boyd, P. W. et al. (2000). A mesoscale phytoplankton bloom in the polar Southern Ocean stimulated by iron fertilization. *Nature*, **407**, 695-702.

Coale, K. H. et al. (1996). A massive phytoplankton bloom induced by an ecosystem-scale iron fertilization experiment in the Equatorial Pacific Ocean. *Nature*, **383/6600**, 495-501.

Defelice, D. und S. W. Wise (1981). Surafce lithofacies, biofacies and diatom diversity patterns as models for delineation of climatic change in the southeast Atlantic Ocean. *Marine Micropaleontology*, **6**, 29-70.

Drebes, G., S. F. Kühn, A. Gmelch und E. Schnepf (1996). *Cryothecomonas aestivalis sp. nov.*, a colourless nanoflagellate feeding on the marine centric diatom *Guinardia delicatula* (Cleve.) Hasle. *Helgol. Meeresunters.*, **50/4**, 497-515.

Dubischar, C. D. und U. V. Bathmann (1997). Grazing impact of copepods and salps on phytoplankton in the Atlantic sector of the Southern Ocean. *Deep-Sea Res.*, **44/1-2**, 415-434.

Dubischar, C. D. (2000). Mesozooplankton an der Polarfront des Südlichen Ozeans: Artenzusammensetzung, Verteilung und Rolle im Pelagial. Dissertation, Fachbereich Biologie/Chemie, University of Bremen, 199 pp.

Emery, W. J. und J. Meincke (1986). Global water masses: summary and review. *Oceanol. Acta*, **9/4**, 383-391.

Eppley, R. W. (1972). Temperature and phytoplankton growth in the sea. *Fish. Bull.*, **70**, 1063-1085.

Fanning, K. A. (1992). Nutrient provinces in the sea: Concentration ratios, reaction rate ratios, and ideal covariation. *J. Geophys. Res.*, **97/C4**, 5693-5712.

Volk, T. und M. I. Hoffert (1985). Ocean carbon pumps: analysis of relative strengths and efficiencies in ocean-driven atmospheric CO_2 changes. In: *The Carbon Cycle and Atmospheric CO_2: Natural Variations Archean to Present*, Hrsg. E. T. Sundquist und W. S. Broecker, Geophysical Monograph **32**, AGU, Washington, D.C., 99-110.

Foster, T. D. und E. C. Carmack (1976). Frontal zone mixing and Antarctic Bottom Water formation in the southern Weddell Sea. *Deep-Sea Res.*, **23/4**, 301-317.

Gonzalez, H. E. und V. Smetacek (1994). The possible role of the cyclopoid copepod *Oithona* in retarding vertical flux of zooplankton faecal material. *Mar. Ecol. Porg. Ser.*, **113/3**, 233-246.

Jones, I.S. und H. E. Young (2000). Reducing greenhouse gas by ocean nourishment. *Offshore Technology Conference*, Houston, Texas (May 1-4, 2000).

Haidvogel D. B., J. L. Wilkin und R. E. Young (1991). A semi-spectral primitive equation ocean circulation model using vertical sigma and orthogonal curvilinear horizontal coordinates. *J. Comput. Phys.*, **94**, 151-185.

Hartmann, C., B. Hollmann, G. Kattner, K.-U. Richter und A. Terbrüggen (1997). Nutrients, Dissolved and Particulate Matter. In: *Reports on Polar Research: The expedition Antarktis XIII/1-2 of the research vessel "Polarstern" in 1995/96*, Hrsg. U. V. Bathmann, M. Lucas, V. Smetacek, with contributions of the participants, **221**, 44-52.

Hense, I. (1997). Chlorophyllverteilung und Phytoplanktonbiomasse in der antarktischen Polarfront. Diplomarbeit, Fachbereich Biologie/Chemie, University of Bremen, 72 pp.

Hunke, E. C. und S. F. Ackley (2001). A numerical investigation of the 1997-1998 Ronne Polynya. *J. Geophys. Res.*, **106/C10**, 22,373-22,382.

Hutchins, A. D. und K. W. Bruland (1998). Iron-limited diatom growth and Si:N uptake ratios in a coastal upwelling regime. *Nature*, **393**, 561-564.

Klaas, C., S. Kühn, S. Menden-Deuer, T. Reynarson und V. Smetacek (1997). Phytoplankton and Heterotrophic Protist Counts. In: *Reports on Polar Research: The expedition Antarktis XIII/1-2 of the research vessel "Polarstern" in 1995/96*, Hrsg. U. V. Bathmann, M. Lucas, V. Smetacek, with contributions of the participants, **221**, 68-71.

Kühn, S., G. Drebes und E. Schnepf (1996). Five species of the nanoflagellate *Pirsonia* in the German Bight, North Sea, feeding on planktic diatoms. *Helgol. Meeresunters.*, **50**, 205-222.

Lancelot, C., E. Hannon, S. Becquevort, C. Veth und H. J. W. de Baar (2000). Modeling phytoplankton blooms and carbon export production in the Southern Ocean: dominant controls by light and iron in the Atlantic sector in Austral spring 1992. *Deep-Sea Res.*, **47/9**, 1621-1662.

Landry, M. R. et al. (1997). Iron and grazing constraints on primary production in the central equatorial Pacific: An EqPac synthesis. *Limnology and Oceanography*, **42/3**, 405-418.

Le Fèvre, J. (1986). Aspects of the Biology of Frontal systems. *Advances in Marine Biology*, **23**, 163-299.

Le Quéré, C., J. C. Orr, P. Monfray und O. Aumont (2000). Interannual variability of the oceanic sink of CO2 from 1979 through 1997. *Global Biogeochem. Cycles*, **14**, 1247-1265.

Loeb, V., V. Siegel, O. Holm-Hansen, R. Hewitt, W. Fraser, W. Trivelpiece und S. Trivelpiece (1997). Effects of sea-ice extent and krill or salp dominance on the Antarctic food web. *Nature*, **387/6636**, 897-900.

Longhurst, A. (1995). Seasonal cycles of pelagic production and consumption. *Progress in Oceanography*, **36/2**, 77-167.

Lutjeharms J. R. E., N. M. Walter und B. R. Allanson (1985) Oceanic frontal systems and biological enhancement. In: *Antarctic nutrient cycles and food webs*, Hrsg.: W. R. Siegfried, P. R. Condy, R. M. Laws, Springer Verlag, 11-21.

Lutjeharms, J. R. E., B. R. Allanson und L. Parker (1986). Frontal zones, chlorophyll and primary production patterns in the surface waters of the Southern Ocean of Cape Town. Marine interfaces Ecohydrodynamics, 1986. In: *Elsevier Oceanography Series,* Hrsg. J. C. J. Nihoul, **42**, 105-118.

Machu, E., B. Ferret und V. Garcon (1999). Phytoplankton pigment distribution from SeaWiFS data in the subtropical convergence zone south of Africa: a wavelet analysis. *Geophys. Res. Letters*, **26/10**, 1469-1472.

Marchant, H., A. Davidson, S. Wright und J. Glazebrook (2000). The distribution and abundance of viruses in the Southern Ocean during spring. *Antarctic Science*, **12/4**, 414-417.

Markels, M. und R. T. Barber (2000) The sequestration of carbon to the deep ocean by fertilization. *ACS Symposium on CO_2 Capture, Utilization, and Sequestration*, August 20-24, 2000.

Martin, J. H. (1990). Glacial-interglacial CO_2 change: The iron hypothesis. *Paleoceanography*, **5/1**, 1-13.

Martin, J. H., R. M. Gordon und S. E. Fitzwater (1990). Iron in Antarctic waters. *Nature*, **345**, 156-158.

McGillicuddy, D. J., R. Johnson, D. A. Siegel, A. F. Michaels, N. R. Bates, und A. H. Knap (1999). Mesoscale variations of biogeochemical properties in the Sargasso Sea. *J. Geophys. Res.*, **104/C6**, 13,381-13,394.

Mitchell, B. G., E. A. Brody, O. Holm-Hansen, C. McClain und J. Bishop (1991). Light limitation of phytoplankton biomass and macronutrient utilization in the Southern Ocean. *Limnology and Oceanography*, **36/8**, 1662-1677.

Monod, J. (1950). La technique de culture continue; theorie et applications. *Annales Institute Pasteur*, **79**, 390-410.

Moore, J. K. und M. R. Abbott (2000) Phytoplankton chlorophyll distributions and primary production in the Southern Ocean. *J. Geophys. Res.*, **105/C12**, 28,709-28,722.

Naveira Garabato, A. C., J. T. Allen, H. Leach, V.H. Strass und R. T. Pollard (2001). Mesoscale subduction at the Antarctic Polar Front driven by baroclinic instability. *J. Phys. Oceanogr.*, **31**, 2087-2107.

Nelson, D. M. und W. O. Smith Jr. (1986). Phytoplankton bloom dynamics of the western Ross Sea ice edge, II, Mesoscale cycling of nitrogen and silicon. *Deep-Sea Res.*, **33/1**, 1389-1412.

Nowlin, W. D. und J. M. Klinck (1986). The physics of the Antarctic Circumpolar Current. *Reviews of Geophysics*, **24/3**, 469-491.

Onji, M., T. Sawabe und Y. Ezura (2000). Characteristics of virus-like growth suppression agents against phytoplankton obtained from seawater at the mouth of Funka Bay, Hokkaido, Japan. *Fisheries science*, **66/1**, 38-43.

Orsi, A. H., T. Whitworth und W. D. Nowlin (1995). On the meridional extent and fronts of the Antarctic Circumpolar Current, *Deep-Sea Res.*, **42/5**, 641-673.

Oschlies, A. und V. Garçon (1998). Eddy-induced enhancement of primary production in a model of the North Atlantic Ocean. *Nature*, **394/6690**, 266-269.

Quéguiner, B., P. Tréguer, I. Peeken und R. Scharek (1997). Biogeochemical Dynamics and the Silicon Cycle in the Atlantic Sector of the Southern Ocean During Austral Spring 1992. *Deep-Sea Res.*, **44/2**, 69-90.

Pahlow, M. und U. Riebesell (2000). Temporal trends in deep ocean Redfield ratios. *Science (Washington)*, **287/5454**, 831-833.

Pearce, F. (2000). A cool trick: how Chile could help save the world and get credits for it. *New Scientist*, **18**.

Perissinotto, R. und E. A. Pakhomov (1998). Contribution of salps to carbon flux of marginal ice zone of the Lazarev Sea, Southern Ocean. *Marine Biology*, **131/1**, 25-32.

Peters, E. und D. N. Thomas (1996). Prolonged darkness and diatom mortality I: Marine Antarctic species. *J. Exp. Mar. Biol. Ecol.*, **207**, 25-41.

Pichon, J. J., M. Labracherie, L. Labeyrie und J. Duprat (1987). Transfer functions between diatom assemblages and surface hydrology in the Southern Ocean. *Palaeogeography, Palaeoclimatology, Palaeoecology*, **61**, 79-95.

Read, J. F., M. I. Lucas, S. E. Holley und R. T. Pollard (2000). Phytoplankton, nutrients and hydrography in the frontal zone between the Southwest Indian Subtropical gyre and the Southern Ocean. *Deep-Sea Res.*, **47/12**, 2341-2367.

Redfield, A. B., B. H. Ketchum und F. A. Richards (1963). The influence of organisms on the composition of seawater. In: *The Sea*, **2/2**, Hrsg. M. N. Hill, Wiley Interscience, New York, 26-77.

Rodhouse, P. G. et al. (1996). Cephalopods and mesoscale oceanography at the Antarctic Polar Front: Satellite tracked predators locate pelagic trophic interactions *Mar. Ecol. Prog. Ser.*, **136/1-3**, 37-50.

Romero, O. E., G. Fischer, C. B. Lange und G. Wefer (2000). Siliceous phytoplankton of the western equatorial Atlantic: sediment traps and surface sediments. *Deep-Sea Res.*, **47/9-11**, 1939-1959.

Saravanane, N., K. Nandakumar, G. Durairaj und K. V. K. Nair (2000). Plankton as indicators of coastal water bodies during south-west to north-east monsoon transition at Kalpakkam. *Current Science*, **78/2**, 173-176.

Sakshaug, E. und O. Holm-Hansen (1984). Factors governing pelagic production in polar oceans. In: *Marine phytoplankton and productivity. Lecture notes on coastal and estuarine studies*, **8**, Hrsg. O. Holm-Hansen, L. Bolis und R. Gilles, Springer Verlag, 1-18.

Schülke, M. (1998). Diatomeenverteilung und -biomasse im Bereich der antarktischen Polarfront. Diplomarbeit, Fachbereich Biologie/Chemie, University of Bremen, Germany, 101 pp.

Schütt, F. (1892) aus: *Biological Oceanography, An Early History, 1870-1960*, p. 124, Hrsg. Eric L. Mills, Cornell University Press, 378 pp.

Shiomoto, A., und H. Ishii (1995). Distribution of biogenic silica and particulate organic matter in coastal and oceanic surface waters off the South Shetland Islands in summer. *Polar Biol.*, **15**, 105-113.

Siegel, V., V. Loeb und J.Groeger (1998). Krill (*Euphausia superba*) density, proportional and absolute recruitment and biomass in the Elephant Island region (Antarctic Peninsula) during the period 1977 to 1997. *Polar Biol.*, **19/6**, 393-398.

Smetacek, V., R. Scharek und E. M. Nöthig (1990). Seasonal and regional variations in the pelagial and its relationship to the life history cycle of krill. In: *Antarctic Ecosystems. Ecological Change and Conservation*, Hrsg. K. R. Kerry und G. Hempel, Springer, Berlin, 103-114.

Smetacek V., U. Passow (1990) Spring bloom initiation and Sverdrup' s critical-depth model. *Limnology and Oceanography*, **35/1**, 228-234.

Smetacek, V., U. V. Bathmann und S. El Naggar with contributions of the participants (2001). In: *Reports on Polar Research: The expedition Antarktis XVIII/1-2 of the research vessel "Polarstern" in 2001*, **400**, 232 pp.

Stiasny, G. (1913). Das Plankton des Meeres. *Sammlung Göschen*, **675**, G. J. Göschen'sche Verlagshandlung G.m.b.H., Berlin, 160 pp.

Stramski, D., R. A. Reynolds, M. Kahru und B. G. Mitchell (1999). Estimation of particulate organic carbon in the ocean from satellite remote sensing. *Science (Washington)*, **285/5425**, 239-242.

Strass, V. H., A. C. Naveira Garabato, R. T. Pollard, H. I. Fischer, I. Hense, J.T. Allen, J.F. Read, H. Leach und V. Smetacek (2001). Mesoscale Frontal Dynamics: Shaping the environment of primary production in the Antarctic Circumpolar Current. *Deep-Sea Res.*, in press.

Sverdrup, H. U. (1953). On conditions for the vernal blooming of phytoplankton. *J. Cons. Cons. Int. Explor. Mer.*, **18**, 287-295.

Takeda, S. (1998). Influence of iron variability on nutrient consumption ratio of diatoms in oceanic waters. *Nature*, **393**, 774-777.

Timmermann, R., A. Beckmann, A. und H. H. Hellmer (2001a). Simulation of ice-ocean dynamics in the Weddell Sea. Part I: Model description and validation. *J. Geophys. Res.*, in press.

Timmermann, R., H. H. Hellmer und A. Beckmann (2001b) Simulation of ice-ocean dynamics in the Weddell Sea. Part II: Interannual variability 1985 — 1993. *J. Geophys. Res.*, in press.

Trathan, P. N., M. A. Brandon und E. J. Murphy (1997). Characterization of the Antarctic Polar Frontal Zone to the north of South Georgia in summer 1994. *J. of Geophys. Res.*, **102/C5**, 10,483-10,497.

Tréguer, J. und G. Jacques (1992). Dynamics of nutrients and phytoplankton, and fluxes of carbon, nitrogen and silicon in the Antarctic Ocean. *Polar Biol.*, **12**, 149-162.

van Couwelaar, M. (1997). Zooplankton and micronekton biomass off Somalia and in the southern Red Sea during the SW monsoon of 1992 and the NE monsoon of 1993. *Deep-Sea Res.*, **44/6-7**, 1213-1234.

van Franeker J. A. und N. W. van den Brink (1997). Censuses of marine birds and mammals. n: *Reports on Polar Research: The expedition Antarktis XIII/1-2 of the research vessel "Polarstern" in 1995/96*, Hrsg. U. V. Bathmann, M. Lucas, V. Smetacek, with contributions of the participants, **221**, 116-121.

Veth, C., I. Peeken und R. Scharek (1997). Physical anatomy of fronts and surface waters in the ACC near the 6°W meridian during austral spring 1992. *Deep-Sea Res.*, **44/1-2**, 23-50.

White, B. W. und R. G. Peterson (1996) An Antarctic circumpolar wave in surface pressure, wind, temperature and sea ice extent. *Nature*, **380/6576**, 699-702.

Wyrtki, K. (1960). The Antarctic convergence and divergence. *Nature*, **187/4737**, 581-582.

Zielinski, U. und R. Gersonde (1997). Diatom distribution in Southern Ocean surface sediments (Atlantic Sector): Implications for palaeoenvironmental reconstructions. *Palaeogeography, Palaeoclimatology, Palaeoecology*, **129**, 213-250.

Eigenleistung bei den Veröffentlichungen

Plankton dynamics in frontal systems of the Southern Ocean
Inga Hense, Ulrich V. Bathmann, Ralph Timmermann

Eigenständige Entwicklung des Konzeptes, des biologischen Modells sowie Durchführung, Auswertung und Interpretation der Experimente. Erstellung des Manuskriptes unter Mitarbeit der Co-Autoren.

Regional ecosystem dynamics in the ACC: Simulations with a three-dimensional ocean-plankton model.
Inga Hense, Ralph Timmermann, Aike Beckmann und Ulrich V. Bathmann

Eigenständige Entwicklung des Konzeptes und Erweiterung des biologischen Modells. Das physikalische Modell wurde von Aike Beckmann zur Verfügung gestellt; Kopplung des physikalischen Modells mit dem biologischen Modell sowie Validierung des physikalischen Modells erfolgte in Zusammenarbeit mit Ralph Timmermann. Eigenständige Durchführung, Auswertung und Interpretation der Experimente. Erstellung des Manuskriptes unter Mitarbeit der Co-Autoren.

Regional and Interannual Variablity of Ecosystem Dynamics in the Southern Ocean
Inga Hense, Ralph Timmermann, Aike Beckmann und Ulrich V. Bathmann

Eigenständige Entwicklung des Konzeptes sowie eigenständige Durchführung der Experimente. Modellkopplung, Numerik und Interpretation der Resultate der Eis-Ozeankomponente des Modells in Zusammenarbeit mit Ralph Timmermann. Erstellung des Manuskriptes unter Mitarbeit der Co-Autoren.